

NATIONAL LIBRARY
OTTAWA



BIBLIOTHÈQUE NATIONALE
OTTAWA

8097

NAME OF AUTHOR... RANDY KEITH LOMNES.....
TITLE OF THESIS... USING ULTRASONIC ATTENUATION.....
 TO STUDY PHOTOCONDUCTION IN CADMIUM SULFIDE

UNIVERSITY... UNIVERSITY OF ALBERTA.....
DEGREE FOR WHICH THESIS WAS PRESENTED... Ph.D.....
YEAR THIS DEGREE GRANTED... 1971.....

Permission is hereby granted to THE NATIONAL LIBRARY
OF CANADA to microfilm this thesis and to lend or sell copies
of the film.

The author reserves other publication rights, and
neither the thesis nor extensive extracts from it may be
printed or otherwise reproduced without the author's
written permission.

(Signed) Randy Lomnes

PERMANENT ADDRESS:

Dept. of Physics.....
SIMON FRAZER UNIVERSITY
BURNABY B.C......

DATED Feb 9.....1971

NL-91 (10-68)

THE UNIVERSITY OF ALBERTA

USING ULTRASONIC ATTENUATION TO STUDY
PHOTOCONDUCTION IN CADMIUM SULFIDE

BY



RANDY KEITH LOMNES

A THESIS

SUBMITTED TO THE FACULTY OF GRADUATE STUDIES
IN PARTIAL FULFILMENT OF THE REQUIREMENTS FOR THE
DEGREE OF DOCTOR OF PHILOSOPHY

DEPARTMENT OF PHYSICS

EDMONTON, ALBERTA

SPRING, 1971

UNIVERSITY OF ALBERTA
FACULTY OF GRADUATE STUDIES

The undersigned certify that they have read, and recommend to the Faculty of Graduate Studies for acceptance, a thesis entitled "USING ULTRASONIC ATTENUATION TO STUDY PHOTOCONDUCTION IN CADMIUM SULFIDE", submitted by Randy Keith Lomnes in partial fulfilment of the requirements for the degree of Doctor of Philosophy.

F. L. Weirh
Supervisor

B. J. (S. J. S. J.)

Paul A. Goud

J. H. (S. J. S. J.)

W. R. (S. J. S. J.)
External Examiner

Date Feb 4/1971

ABSTRACT

In this thesis, the photosensitive ultrasonic attenuation observed in cadmium sulfide is examined as a possible tool for studying photoconduction and optical properties in piezoelectric semiconductors. Experiments were carried out on large single crystals of CdS by measuring the change in ultrasonic attenuation when light is incident normal to the surface at which the acoustic wave is reflected.

The theory put forward by Hutson and White (1962) (describing the attenuation of ultrasound due to the interaction between lattice vibrations and mobile charge carriers) is adapted to fit the geometry of the experiment. The equations that are developed indicate that by measuring the photosensitive ultrasonic attenuation at different ultrasonic frequencies, calculations can be carried out to yield values for both the conductivity and the optical absorption coefficient.

When calculations are performed on the experimental data, numerical values for the optical absorption coefficient are obtained that agree

within experimental error with results obtained by direct optical attenuation measurements. The ultrasonic attenuation method yields values for the optical absorption coefficient up to about $5 \times 10^3 \text{ cm}^{-1}$. For absorption coefficients greater than 10^3 cm^{-1} the model starts to break down. However it is suggested that with a better model the possibility exists for extracting data on the absorption coefficient up to 10^5 cm^{-1} from the measurements.

Most of the measurements were done at room temperature, although some low temperature observations are reported. For most of the crystals that were available, the signal levels of the photosensitive ultrasonic attenuation at low temperatures become quite small and noise levels are then a problem.

ACKNOWLEDGEMENTS

I would like very much to express my appreciation to Dr. F. L. Weichman for having suggested the research problem and for his assistance during the course of the work.

It is a great pleasure to thank the technical staff of the physics department and, in particular Mr. H. McClung and Mr. N. Riebeck for their assistance during all stages of the work.

Discussions with Max B. Burbank in relation to lapping and polishing CdS crystals were a great help to me and for this I would like to express my thanks.

Also my thanks are due to W. A. Roger for discussions relating to the bonding of quartz transducers to CdS samples.

It is also a sincere pleasure to thank Dr. John C. W. Taylor for the many discussions we had in connection with this work.

I wish also to thank Dr. D. C. Reynolds for supplying several crystals of CdS for use in some of the experiments.

The financial assistance provided by the University of Alberta and the National Research Council is gratefully acknowledged.

Finally, I would like to express my sincere thanks to my wife, Karen, for her patience with me during the course of this work and for her help with typing and proof reading the final draft of this manuscript.

R. K. L.

TABLE OF CONTENTS

	PAGE
Chapter 1 : Introduction	1
Chapter 2 : Theory	5
Chapter 3 : Analysis of the Experiment	19
Chapter 4 : Experimental Details	42
Chapter 5 : Experimental Results	73
Chapter 6 : Calculations and Discussion	119
Chapter 7 : Conclusion	156
Appendix A : General wave motion in a piezoelectric medium	160
Appendix B : Tensor properties of CdS	165
Appendix C : Derivation of complex elastic stiffness constant	168
Appendix D : Miscellaneous properties of CdS	174
Appendix E : A.P.L. computer programs	176
Bibliography	183

LIST OF FIGURES

	<u>PAGE</u>
Figure 3.a : Block diagram for experiment	20
Figure 3.b : Decay of light in sample ($\kappa d \gg 1$)	27
Figure 3.c : Theoretical Plots of reduced attenuation versus modified absorption parameter	29
Figure 3.d : Theoretical Plot of reduced attenuation versus conductivity parameter	31
Figure 3.e : Decay of light in sample ($\kappa d < 1$)	37
Figure 4.a : Cross-section of cryostat	43
Figure 4.b : Monochromator output profile	46
Figure 4.c : Automatic attenuation measure- ment system	48
Figure 4.d : Sample holder	53
Figure 4.e : Echo trains in sample SR-1	56
Figure 4.f : X-ray orientation with polishing jig	64
Figure 4.g : Etch pit orientation with polishing jig	67
Figure 5.a : Time response in sample SE-1	74

	<u>PAGE</u>
Figure 5.b : Time response in sample SB-3	77
Figure 5.c : Attenuation in sample SB-3 versus wavelength of light	81
Figure 5.d : Attenuation at blue edge in sample SB-3	86
Figure 5.e : Attenuation versus optical wavelength in SB-3	91
Figure 5.f : Attenuation versus optical wavelength at different light intensities	96
Figure 5.g : Attenuation at blue edge at different temperatures	101
Figure 5.h : Attenuation versus wavelength at 77°K	104
Figure 5.i : Attenuation in sample SE-1	107
Figure 5.j : Attenuation in weak photo- conductors	110
Figure 5.k : Attenuation in sample SB-00	113
Figure 5.l : Monochromator output profile	116
Figure 6.a : Calculated absorption co- efficients versus photon energy	125
Figure 6.b : Calculated conductivity para- meter versus optical wave- length	131

LIST OF TABLES

	<u>PAGE</u>
Table I : Samples used in experiments	72
Table II : Attenuation in SB-3 at different optical wavelengths	83
Table III : Reduced attenuation corresponding to table II	84
Table IV : Attenuation at blue edge in SB-3	88
Table V : Reduced attenuation corresponding to table IV	89
Table VI : Attenuation in SB-3 at different optical wavelengths	93
Table VII : Reduced attenuation corresponding to table VI	94
Table VIII : Attenuation in SB-3 at different optical wavelengths	98
Table IX : Reduced attenuation corresponding to table VIII	99
Table X : Intensity normalization factors	118
Table XI : Calculated optical absorption coefficient	121
Table XII : Calculated optical absorption coefficient	122

	<u>PAGE</u>
Table XIII : Calculated optical absorption coefficient	123
Table XIV : Calculated conductivity parameter	128
Table XV : Calculated conductivity parameter	129
Table XVI : Calculated conductivity parameter	130
Table XVII : Calculated optical absorption coefficient	139

CHAPTER 1

Introduction

Interest in the ultrasonic properties of Cadmium sulfide arose when Nine (1960) reported that the ultrasonic attenuation could be altered by illumination in photosensitive CdS. This phenomenon was recognized by Hutson and White (1962) to result from the strong coupling that can occur in a piezoelectric semiconductor between lattice vibrations and free carriers. Hutson, White and McFee (1961), White (1962) and McFee (1963) went on to show that the ultrasonic attenuation relative to the attenuation under conditions of no illumination could be made either positive or negative with the application of an external electric field. The observation of negative attenuation or ultrasonic gain encouraged others to carry on research in this area. For example theoretical papers by Pippard (1962), Paranjape (1963), Kikuchi (1967), and Spector (1962 and 1964) provided greater understanding of the ultrasonic gain effect. Further experimental work along these lines was provided by Southgate and Spector (1965), Uchida

(1964), Astrov (1965), and Kikuchi (1967).

Nearly all work in the area of ultrasonics in CdS since 1960 has been related in one way or another to the acoustic amplification effects. The work to be reported here, however, deviates from this trend and is concerned only with the case when no external field is applied. The photosensitive attenuation is then considered as a possible tool for studying photoconduction in CdS. Nine (1960) in his original paper had briefly suggested this possibility but it appears that little work has followed along these lines. In this respect the present work is in reality a follow up of the work reported in 1960 by Nine.

In the thesis an attempt is made to treat the general subject area of ultrasonic attenuation in piezoelectric semiconductors in a manner that is both applicable to the thesis and logical in its development. Accordingly, the contents of Chapter 2 deals with the subject of wave motion in piezoelectric materials and then go on to develop briefly the theory of Hutson and White (1962) describing the ultrasonic attenuation in piezoelectric semiconductors under

conditions where $ql \ll 1$ (i.e. the acoustic wavelength is much greater than the electron mean free path).

Chapter 3 describes the sample geometry used for the experiments and a discussion is given of the approach taken to adapt the theory of Hutson and White to this geometry. Equations are derived that show how information can be obtained on the photoconduction and optical absorption from experimental data on the ultrasonic attenuation.

The discussion in Chapter 4 goes into the details connected with the experiments from the point of view of equipment used, methods employed to measure the ultrasonic attenuation and techniques utilized for preparing CdS samples for ultrasonic work. The procedures that were used in performing the actual experiments are given in Chapter 5 and the data acquired from these experiments is also shown.

In the final chapter, attempts are made to relate the observed data with the equations developed in Chapter 3. Values for the optical absorption coefficient as a function of the wavelength of light are calculated from the ultrasonic data

and a comparison is made with published data. The development as presented in Chapter 3 tends to break down in certain regions and an explanatory discussion is presented.

The amount of work done on CdS that can be related either directly or indirectly to the work done in this thesis is quite extensive. Many of the papers having only an indirect relation are not referenced directly in the text. It was felt therefore, that an extensive bibliography should be included to give a complete picture.

CHAPTER 2.

Theory1) Wave motion in piezoelectric crystals

A piezoelectric crystal under adiabatic conditions can be described by the equations of state

$$T_{ij} = c_{ijkl} S_{kl} - e_{lij} E_l \quad (1.1)$$

$$D_k = e_{klm} S_{lm} + \epsilon_{ik} E_i \quad (1.2)$$

where T is the stress tensor, S is the strain tensor, E is the electric field and D is the electric displacement. The coefficients in equations (1.1) and (1.2) represent the following: c is the rank four tensor of the elastic stiffness constants at constant E , ϵ is the rank two tensor of the permittivity at constant strain and e is the rank three piezoelectric tensor. Summation over repeated indices is assumed throughout.

Equations (1.1) and (1.2) suggest that the equations of motion for the lattice will contain terms involving the electric field and that the Maxwell equations will contain terms involving the strain of the crystal. Therefore, the piezoelectric

nature of the medium provides a coupling between the three acoustic modes and the two transverse electromagnetic modes that can propagate in the crystal. This leads to the case of propagation in the crystal of five electromagnetic-mechanical waves. An electromagnetic wave propagating in a piezoelectric crystal will have accompanying it an acoustic wave (travelling at the electromagnetic phase velocity) and conversely an acoustic wave will have an electromagnetic wave (travelling at the acoustic velocity) which is produced by the displacement current resulting from the piezoelectric polarization.

The general problem of wave motion in piezoelectric crystals was first dealt with by Kyame (1948 and 1954) and later reviewed by Hutson (1962). Following the approach of Kyame, Appendix A gives a brief outline of the derivation of the 5×5 determinant which gives the dispersion relations for the five modes of wave propagation. It is further shown in Appendix A that the amount of energy carried by the electromagnetic wave in the acoustic mode is smaller than that of the acoustic wave by a factor $v/c \sim 10^{-5}$ where v is the acoustic velocity and c is the electromagnetic

velocity in the crystal. Similarly the acoustic energy carried by the electromagnetic wave travelling with speed c is negligible compared to that of the electromagnetic wave.

Of importance in the piezoelectric crystal, as far as acoustic waves are concerned, is not the small transverse e.m. wave travelling with the acoustic wave but, rather, the longitudinal electric field of non-negligible magnitude that can accompany the acoustic wave. The piezoelectric property in a crystal can thus be taken into account as far as the acoustic waves are concerned by solving the appropriate acoustic problem and including the proper longitudinal electric field.

Equation (A.14) of Appendix A gives an expression for the longitudinal electric field as

$$E_3 = - (ike_{3j3} u_j + \epsilon_{p3} E_p) / \epsilon_{33}$$

where $p = 1, 2$ and $j = 1, 2, 3$ and the equation is written for wave propagation in the x_3 direction and arbitrary orientation in the crystal.

The contribution of the transverse field E_p is small for the acoustic waves and

$$E_3 \approx - (ike_{3j3} u_j) / \epsilon_{33}$$

Acoustic waves which have a longitudinal electric field associated with them are said to be piezoelectrically active.

2) Piezoelectric properties in CdS

CdS normally exists in the Wurtzite structure, which is a member of crystal class 6mm. Since class 6mm lacks a center of inversion symmetry, crystals of the Wurtzite structure are permitted to have rank three tensor properties.

The piezoelectric properties of CdS were first reported by Hutson (1960) and it was shown that the magnitude of this effect in CdS was considerably greater than for quartz. Values for the components of the piezoelectric tensor are given in Appendix D for CdS.

3) Ultrasonic Attenuation in CdS

Ultrasonic waves that are usually of interest are either purely longitudinal or purely transverse. In CdS these waves can propagate only in a direction parallel to the c-axis or parallel to the basal plane. The equation of motion for a piezoelectric lattice is given in Appendix A as

$$\rho \ddot{u}_i = c_{ijkl} u_{l,kj} - e_{lij} E_{l,j} \quad (A.6)$$

where ρ is the mass density and u is the particle displacement. If the crystal is oriented such that the x_3 direction is parallel to the c-axis, the equation of motion can be written for a wave propagating in the x_3 direction as

$$\rho \ddot{u}_i = c_{i33j} u_{j,33} - e_{ji3} E_{1,3}. \quad (1.3)$$

The three equations of (1.3) can be written out explicitly for a CdS crystal using the components of the tensors given in Appendix B

$$\rho \ddot{u}_1 = c_{44} u_{1,33} - e_{113} E_{1,3}$$

$$\rho \ddot{u}_2 = c_{44} u_{2,33} - e_{113} E_{2,3}$$

$$\rho \ddot{u}_3 = c_{33} u_{3,33} - e_{333} E_{3,3}. \quad (1.4)$$

For waves propagating in the basal plane (e.g. the x_1 direction) the equation of motion becomes

$$\rho \ddot{u}_i = c_{i11j} u_{j,11} - e_{ji1} E_{j,1} \quad (1.5)$$

The three equations of (1.5) when written out explicitly become

$$\rho \ddot{u}_1 = c_{11} u_{1,11} - e_{311} E_{3,1}$$

$$\rho \ddot{u}_2 = \frac{1}{2} (c_{11} - c_{12}) u_{2,11}$$

$$\rho \ddot{u}_3 = c_{44} u_{3,11} - e_{113} E_{1,1} \quad (1.6)$$

It is seen that only equations (1.4) and (1.6) are of interest since they have a longitudinal electric field associated with the acoustic wave. That is to say the two piezoelectrically active waves are the longitudinal acoustic wave propagating parallel to the c -axis and the transverse waves propagating perpendicular to the c -axis with particle direction parallel to the c -axis.

Equations (1.4) and (1.6) contain only terms pertaining to one direction and therefore it is possible to treat the propagation of piezoelectrically active acoustic waves in CdS as essentially a one dimensional problem. The equation is then simply

$$\frac{\partial^2 u}{\partial t^2} = \frac{c}{\rho} \frac{\partial^2 u}{\partial z^2} - \frac{e}{\rho} \frac{\partial E}{\partial z} \quad (1.7)$$

where $c = c_{33}$ and $e = e_{333}$ for longitudinal acoustic waves and $c = c_{44}$ and $e = e_{113}$ for transverse waves and propagation is in the z direction.

The one dimensional problem of acoustic propagation in a piezoelectric semiconductor was first solved by Hutson and White (1962). They showed that the longitudinal piezoelectric field will couple the acoustic wave to the free charge carriers in such a way as to give rise to an attenuation of the acoustic wave. An outline of their derivation will be given here.

The necessary equations that must be considered are a) the equation of motion (1.7), b) the one dimensional form of equation (1.2)

$$D = e \frac{\partial u}{\partial z} + \epsilon E \quad (1.8)$$

c) the Gauss equation

$$\frac{\partial D}{\partial z} = Q \quad (1.9)$$

where Q is the space charge, and d) the continuity equation

$$\frac{\partial Q}{\partial t} + \frac{\partial J}{\partial z} = 0 \quad (1.10)$$

where J is the current density.

Expressions for J and Q must then be provided to include the contribution of the free

charge carriers to the problem. The passage of a piezoelectrically active acoustic wave will locally destroy the neutrality that exists in the semiconductor and thus give rise to a space charge Q . The motion of carriers in creating the space charge will result in the current J . The explicit expressions of Q and J will depend on the model taken to describe the semiconductor.

Extrinsic semiconductor

Consider the case of an extrinsic semiconductor in which only electrons are present. The space charge and current can then be written as

$$Q = - qn \quad (1.11)$$

$$J = q(n_0 + fn) \mu E$$

where q is the electron charge and n_0 is the equilibrium density of electrons in the conduction band, n is the disturbance of n_0 which gives rise to the space charge, μ is the electron mobility and the number f is included to take care of any local disturbance in the equilibrium that exists between electrons in the conduction band and electrons residing at trapping levels. That is to say space charge can arise from bound states as

well as from the conduction band, but only the fraction f of the space charge is mobile and is able to contribute to the current.

The perturbation of the electron density in the conduction band due to the presence of an acoustic wave can also give rise to electron density gradients which in turn will result in a diffusion current such that the complete electron current will become

$$J = q(n_0 + fn) \mu E + qD f \frac{dn}{dz} \quad (1.12)$$

where D is the diffusion constant for the electrons.

Equations (1.7), (1.8), (1.9), (1.10), (1.11), and (1.12) can now be manipulated to give a complex elastic constant c' such that the wave equation becomes

$$\frac{\partial^2 u}{\partial t^2} = \frac{c'}{\rho} \frac{\partial^2 u}{\partial z^2} \quad .$$

Small amplitude strains and wave solutions of the form $D = D_0 \exp(ikz - i\omega t)$ and $E = E_0 \exp(ikz - i\omega t)$ are assumed in the derivation. The phase velocity and attenuation of the acoustic wave are the given by the relations

$$v = v_0 \text{ Real } \sqrt{c'/c} \quad (1.13)$$

$$\alpha = \frac{\omega}{v_0} \operatorname{Im} \sqrt{c'/c} \quad (1.14)$$

where $v_0 = \sqrt{c/\rho}$ is the velocity of sound where no charge carriers are present.

The details of the derivation of c' are given in Appendix C. The result is given as

$$c' = c \left\{ 1 + \frac{e^2}{c\epsilon} \left[\frac{1 + (\omega_c/\omega_D) + (\omega/\omega_D)^2 - i(\omega_c/\omega)}{1 + 2(\omega_c/\omega_D) + (\omega/\omega_D)^2 + (\omega_c/\omega)^2} \right] \right\} \quad (1.15)$$

where $\omega_c = \sigma/\epsilon$ is called the dielectric relaxation frequency and $\omega_D = v_0^2/fD$ is the diffusion frequency. This expression for the effective elastic stiffness coefficient gives the following expressions for the phase velocity and attenuation.

$$v = v_0 \left\{ 1 + \frac{e^2}{2c\epsilon} \left[\frac{1 + (\omega_c/\omega_D) + (\omega/\omega_D)}{1 + 2(\omega_c/\omega_D) + (\omega/\omega_D)^2 + (\omega_c/\omega)^2} \right] \right\} \quad (1.16)$$

$$\alpha = \frac{\omega}{v_0} \left(\frac{e^2}{2c\epsilon} \right) \left[\frac{\omega_c/\omega}{1 + 2(\omega_c/\omega_D) + (\omega/\omega_D)^2 + (\omega_c/\omega)^2} \right] \quad (1.17)$$

For the case where $\omega_c, \omega \ll \omega_D$ then the above expressions for v and α reduce to the simpler forms

$$v = v_0 \left[1 + \frac{B}{1 + (\omega_c/\omega)^2} \right] \quad (1.18)$$

$$\alpha = B \frac{\omega}{v_0} \left[\frac{\omega_c/\omega}{1 + (\omega_c/\omega)^2} \right] \quad (1.19)$$

where $B = e^2/2c\epsilon$.

Intrinsic semiconductor

Two limiting cases for an intrinsic semiconductor were considered by Hutson (1962) which will be briefly mentioned here to illustrate the effect that two types of charge carriers would have on the ultrasonic attenuation. Taking the case where the times for recombination between electrons and holes is long compared with the period of the acoustic wave, the electrons and holes then will act independently and separately satisfy continuity equations. Thus

$$\frac{\partial J_p}{\partial z} + \frac{\partial Q_p}{\partial t} = 0 \quad (1.20)$$

$$\frac{\partial J_n}{\partial z} + \frac{\partial Q_n}{\partial t} = 0 \quad (1.21)$$

where

$$Q_p = qp \quad (1.22)$$

$$Q_n = -qn \quad (1.23)$$

$$J_p = q (p_0 + p) \mu_p E - q D_p \frac{dp}{dz} \quad (1.24)$$

$$J_n = q (n_0 + n) \mu_n E + q D_n \frac{dn}{dz} \quad (1.25)$$

and the total current density is given by

$$J = J_p + J_n$$

The complex elastic stiffness constant c' is derived in Appendix C where the result is given as

$$\frac{c'}{c} = 1 + \frac{e^2/c\epsilon}{1 + i \left[\frac{\omega_c p/\omega}{1 + i(\omega/\omega_{D_p})} + \frac{\omega_c n/\omega}{1 + i(\omega/\omega_{D_n})} \right]}$$

The diffusion frequencies for the electrons and holes are given by

$$\omega_{D_n} = v_0^2 / D_n$$

$$\omega_{D_p} = v_0^2 / D_p$$

In the simple case where $\omega \ll \omega_{D_p}, \omega_{D_n}$ the elastic stiffness constant reduces to

$$c' = c \left\{ 1 + \frac{e^2}{c\epsilon} \left[\frac{1 - i(\omega_c/\omega)}{1 + (\omega_c/\omega)^2} \right] \right\}$$

which is the same in the extrinsic case except

that the dielectric relaxation frequency contains contributions from both holes and electrons

$$\omega_c = \frac{\sigma}{\epsilon} = \frac{q}{\epsilon} (\mu_n n_0 + \mu_p p_0)$$

The other limiting case occurs where the recombination times for the holes and electrons are much faster than the acoustic wave period. In this case the electrons and holes satisfy a single continuity equation

$$\frac{\partial J}{\partial z} + \frac{\partial Q}{\partial t} = 0$$

where $Q = -2qn$ and the electron density $= n_0 + n$ and the hole density $= p_0 - n$. The current then becomes

$$J = q \{ (n_0 + n)\mu_n + (p_0 - n)\mu_p \} E + q(D_n + D_p) \frac{dn}{dz}$$

The details for the derivation of the complex elastic constant c' are given in Appendix C where the result is shown to be exactly the same as in the extrinsic case (i.e. equation 1.15) with the requirements that the dielectric relaxation frequency and the diffusion frequency are given by

$$\omega_c = \frac{\sigma}{\epsilon} = \frac{q}{\epsilon} (\mu_n n_0 + \mu_p p_0)$$

$$\omega_D = v_0^2 / (D_n + D_p)$$

In the simple case where diffusion effects are unimportant (i.e. $\omega \ll \omega_D$) the acoustic attenuation is identical in both the extrinsic and intrinsic case. That is attenuation is only a function of the conductivity of the crystal and of the acoustic frequency.

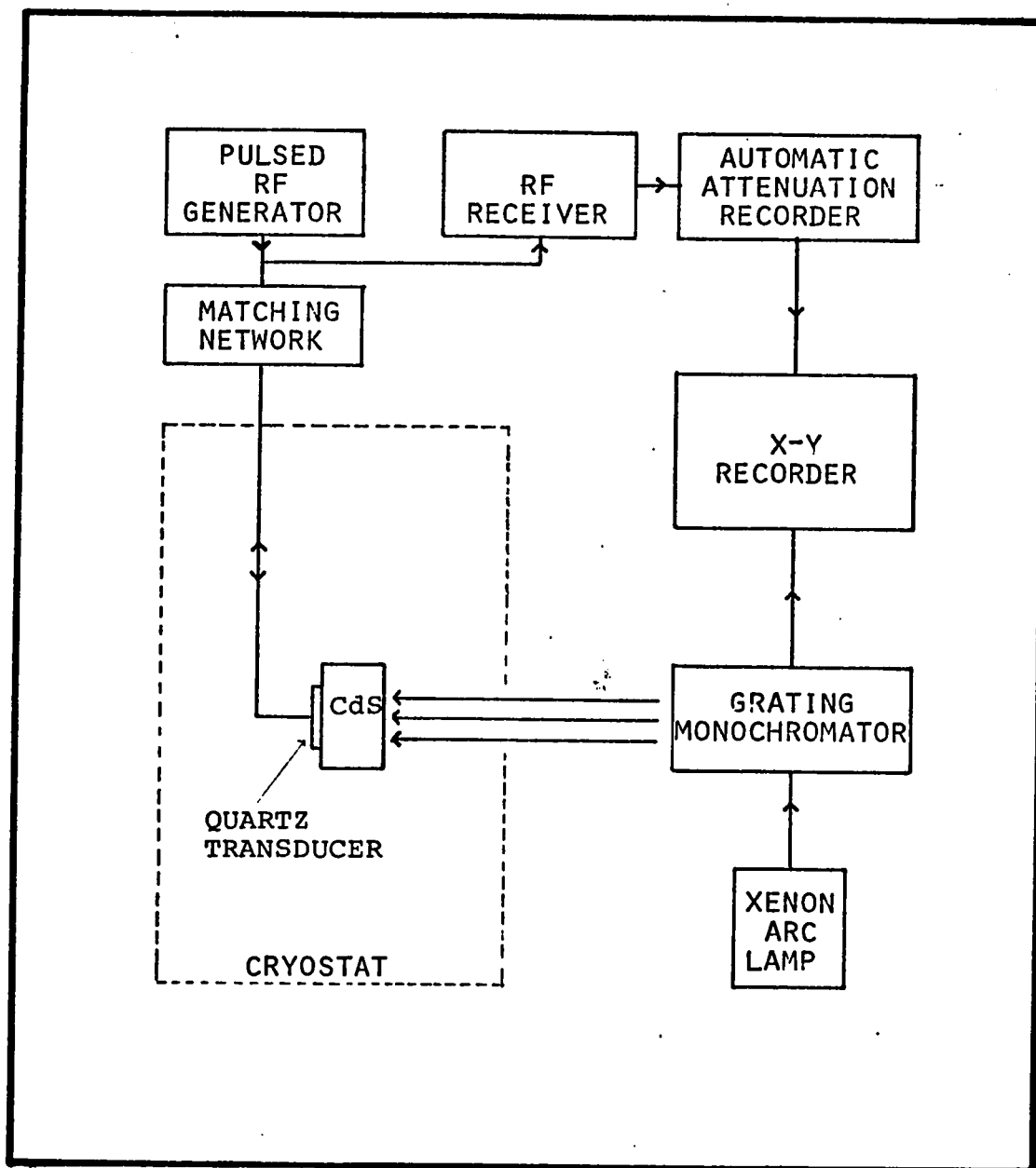
CHAPTER 3

Analysis of the Experiment

Experimentally, the ultrasonic attenuation is measured in samples of CdS where the carrier concentration is introduced by the absorption of light. Samples used in the experiments normally have a low conductivity in the absence of illumination and under optical excitation of the appropriate wavelength, show a photoconduction effect.

The experimental arrangement is illustrated in figure (3.a). A CdS sample is cut and polished with two surfaces flat and parallel. The orientation is such that the c-axis is perpendicular to the surfaces. Longitudinal ultrasonic waves are introduced into the sample by bonding a X-cut quartz transducer to one surface. The sample is positioned in an optical cryostat in such a way that the illumination is directed toward the surface opposite the transducer and is parallel to the direction of ultrasonic propagation. In this way the ultrasonic wave will always see a uniform cross section of illumination for all values of the optical absorption coefficient.

FIGURE 3.A



BLOCK DIAGRAM FOR EXPERIMENT

Measurements of the ultrasonic attenuation are made using the pulse echo technique. The attenuation is measured as a function of the wavelength of the incident illumination in the region of the band edge of CdS. Attenuation versus wavelength curves were made for different intensities of light and for different ultrasonic frequencies. Most of the measurements were made at room temperature but some results are reported at temperatures down to liquid helium.

Experiments of this kind are similar in some respects to photoconductivity studies in that it is the electrical conductivity of the crystal that gives rise to the effect that is measured. The attenuation measurements are unique however, in the fact that all problems associated with making electrical contacts to the sample are avoided. Also for light that is highly absorbed, the surface region of the sample, where this absorption takes place, can be probed from within the bulk of the sample rather than externally as would be the case for a regular photoconductivity measurement. The acoustic wavelength acts as a basic unit of length. Information can be obtained from a region below the

surface of thickness $\geq \lambda/10$. In this respect, the ultrasonic frequency provides a variable in ultrasonic studies of photoconductivity for which there is no analogy in a simple conduction experiment. The frequency is shown later to be an important parameter for obtaining information about the solid.

For the optical arrangement used, the attenuation due to carriers will be inhomogeneous in the propagation direction because of the exponential decay of the illumination within the sample. A method must therefore be derived to take care of this fact. The attenuation as measured for one round trip of the sample will be the net accumulation of each infinitesimal attenuation at points within the sample. That is to say for a sample of thickness d , the attenuation measured for one trip will be

$$\alpha_t = 2 \int_0^d \alpha(z) dz$$

where $\alpha(z) dz$ is the attenuation of the acoustic wave in the cross section of the sample between z and $z + dz$.

An expression for the attenuation between z and $z + dz$ due to piezoelectric coupling

to the charge carriers can be obtained from equation (1.17). This equation is however, simplified considerably in the case where ω_c , $\omega \ll \omega_D$ can be used. Since the work is being done in CdS samples it is instructive to look at the numerical value of ω_D in CdS. The Einstein relation

$$qD = \mu kT$$

can be used to get a value of D from the electron mobility and hence

$$\omega_D = q v_0^2 / \mu kT.$$

Using the values $\mu = 300 \text{ cm}^2/\text{volt sec}$

$$v_0 = 4.3 \times 10^5 \text{ cm/sec}$$

$$T = 300^\circ \text{K}$$

$$q = 1.6 \times 10^{-19} \text{ coul}$$

$$k = 1.38 \times 10^{-23} \text{ coul volt}/^\circ \text{K}$$

the diffusion frequency is found to be

$$\omega_D \sim 10^{10} \text{ sec}^{-1}.$$

For the case of lower temperatures or if holes were considered (which have a much lower mobility in CdS than electrons) the diffusion frequency would be even larger.

From the experimental point of view the

maximum ultrasonic frequency that was used in this work is around 200 MHz which gives $\omega \lesssim 10^9 \text{ sec}^{-1}$. It should therefore be reasonable to consider the case where $\omega \ll \omega_D$ in which case equation (1.19) can be used for the attenuation between z and $z + dz$, thus

$$\alpha(z) dz = \frac{B\omega}{v_0} \left\{ \frac{(\omega_C(z)/\omega)}{1 + (\omega_C(z)/\omega)^2} \right\} dz$$

The ultrasonic attenuation measured for one round trip of the sample is then

$$\alpha_T = \frac{2B\omega}{v_0} \int_0^d \frac{dz}{[(\omega_C(z)/\omega) + (\omega/\omega_C(z))]} \quad (3.2)$$

Since $\omega_C(z) = \sigma(z)/\epsilon$, an expression giving the dependence of the conductivity on z must be found in order to solve (3.2). The expression for $\sigma(z)$ will depend on the decay of illumination with depth in the sample and on the model that is chosen to describe the photoconduction.

The decay of light intensity within the crystal can be described by the equation

$$I = I_0 e^{-\kappa z}$$

where κ , the optical absorption coefficient, will be a function of the wavelength of the illumination. I_0 is the intensity of the light transmitted into

the crystal at $z = 0$.

Under steady state conditions, the conductivity of the crystal can be written as

$$\sigma(z) = \sigma_0 + \Delta\sigma(z)$$

where σ_0 is the conductivity when no illumination is present and $\Delta\sigma$ is the contribution to the conductivity from the non-equilibrium carriers created by the light. The non-equilibrium conductivity can be written for steady state conditions as

$$\Delta\sigma(z) = \Delta\sigma_n + \Delta\sigma_p = q\beta (\mu_n\tau_n + \mu_p\tau_p) \frac{dI}{dz}$$

where μ_n and μ_p are the electron and hole mobilities, τ_n and τ_p are the electron and hole lifetimes in their respective conduction bands. The coefficient β represents the number of pairs of electrons and holes created for each photon absorbed.

Of interest here is the case where σ_0 is very small and insignificant compared with $\Delta\sigma(z)$ so that $\sigma(z) = \Delta\sigma(z)$. Consider now the special case where the electron and hole lifetimes are constant and independent of I and hence z (i.e. the so called linear case). Thus an

expression for the dielectric relaxation frequency can be written as

$$\omega_c(z) = \frac{\sigma(z)}{\epsilon} = \frac{q\beta}{\epsilon} (\mu_n \tau_n + \mu_p \tau_p) \frac{dI}{dz} \quad (3.3)$$

Consider figure (3.b) which shows the sample in relationship to the light for the case where $\kappa d > 1$. This is the situation where any light reflected into the sample from surface (2) can be neglected. Under these conditions

$$\frac{dI}{dz} = \kappa I_0 e^{-\kappa z} \quad (3.4)$$

and substitution of (3.4) and (3.3) into (3.2) gives

$$\alpha_T = \frac{2B\omega d}{v_0} \left\{ \frac{1}{x} \int_0^x \frac{d\xi}{f(\xi) + f^{-1}(\xi)} \right\}$$

where $f(\xi) = x\zeta e^{-\xi}$

$x = \kappa d$ = modified absorption parameter

$\xi = \kappa z$

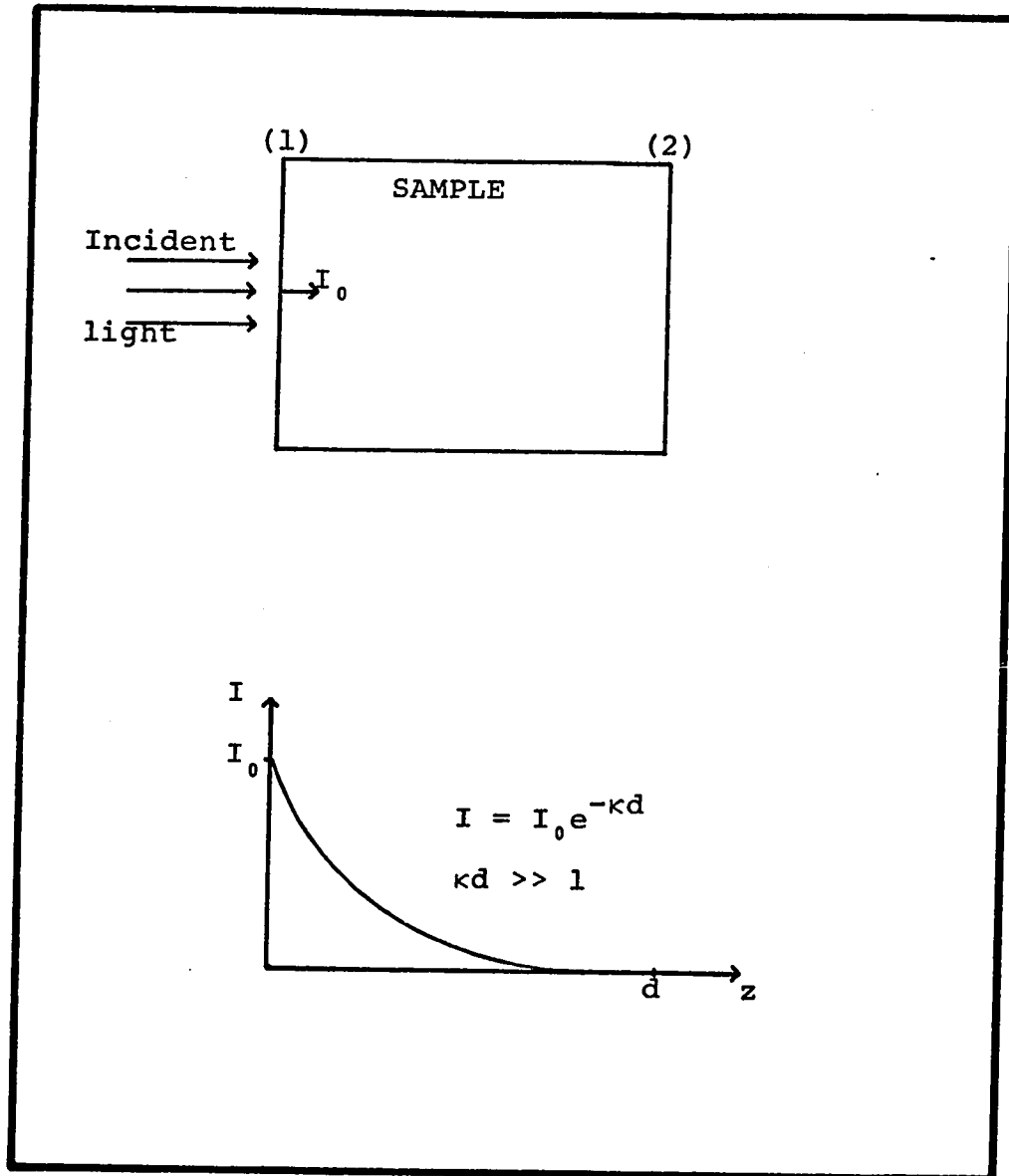
$\zeta = \frac{q\beta I_0}{\epsilon \omega d} (\mu_n \tau_n + \mu_p \tau_p)$ = conductivity parameter

The quantity $(x\omega\zeta)$ then represents the dielectric relaxation frequency at the surface of the crystal.

It is convenient to define the reduced ultrasonic attenuation as

$$y = \alpha_T \left(\frac{v_0}{2B\omega d} \right) \quad (3.5)$$

FIGURE 3.B

DECAY OF LIGHT IN SAMPLE ($\kappa d \gg 1$)

so that

$$y = \frac{1}{x} \int_0^x \frac{d\xi}{f(\xi) + f^{-1}(\xi)} \quad (3.6)$$

Since $f(\xi) = x\zeta e^{-\xi}$ equation (3.6) can be solved exactly to give the reduced attenuation as

$$y = \frac{1}{x} \tan^{-1} \left\{ \frac{x\zeta (1-e^{-x})}{1 + (x\zeta)^2 e^{-x}} \right\} \quad (3.7)$$

where $x > 1$.

Computer calculated plots of the function (3.7) are shown in figures (3.c) and (3.d). The solid line of figure (3.c) shows the dependence of y on x for different values of ζ while figure (3.d) gives the dependence of y on ζ for different values of x . The curves of figures (3.c) and (3.d) show clearly the asymptotes to this function. For example when $x\zeta \ll 1$ the reduced attenuation becomes

$$y \approx \frac{1}{x} \tan^{-1} \{ x\zeta(1-e^{-x}) \} \approx \zeta(1-e^{-x})$$

and when x is restricted such that $1 \ll x \ll \zeta^{-1}$

then

$$y \approx \zeta \quad (3.8)$$

This region is shown in figure (3.c) by the flat top on the curves for small ζ .

Figure 3.c : Computer calculated plots of the reduced attenuation as a function of the modified absorption parameter x .

The solid line is valid for the case where $x \gg 1$. The dashed line represents the case where reflections at the surfaces are taken into account and is thus valid for all x .

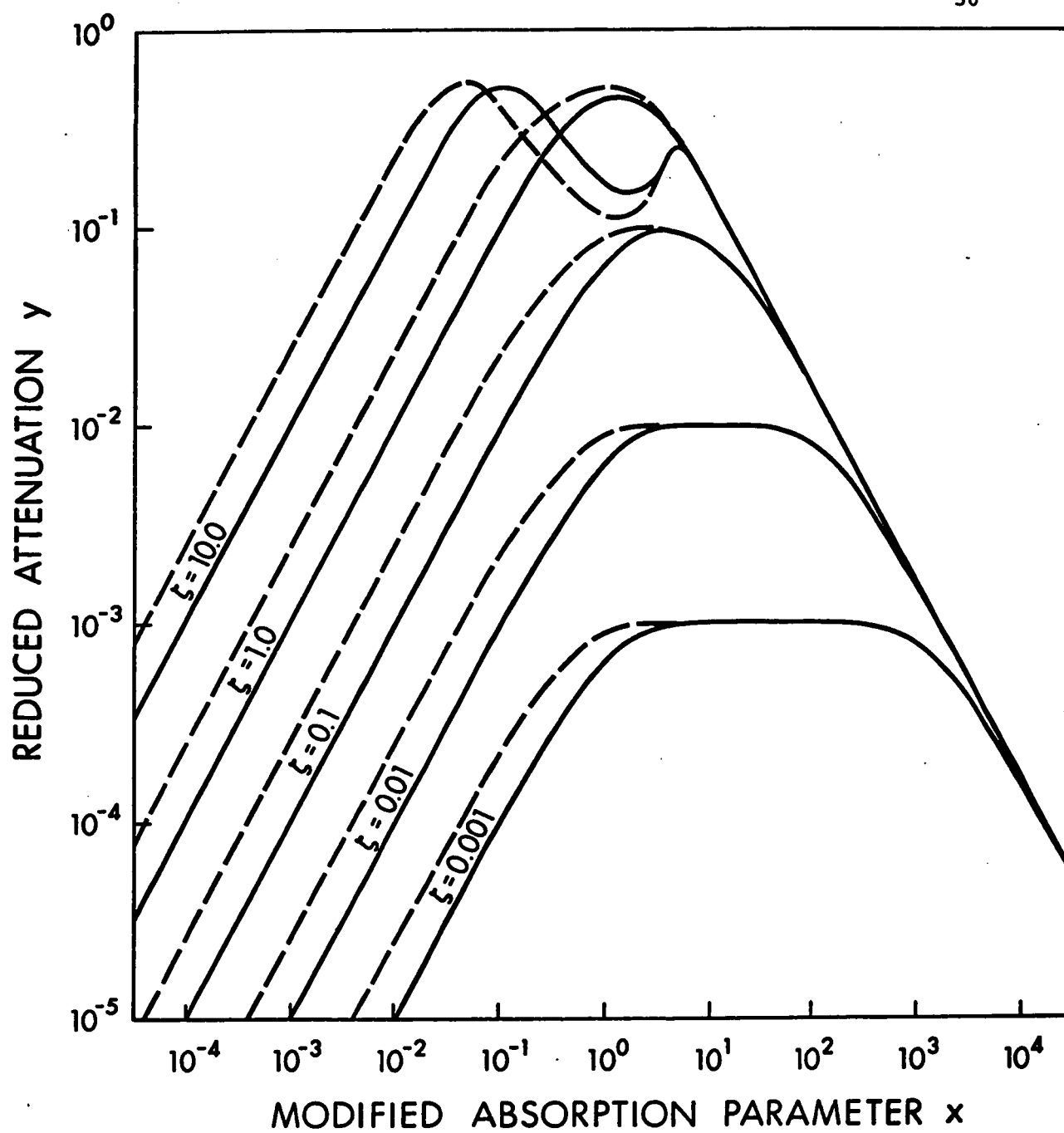
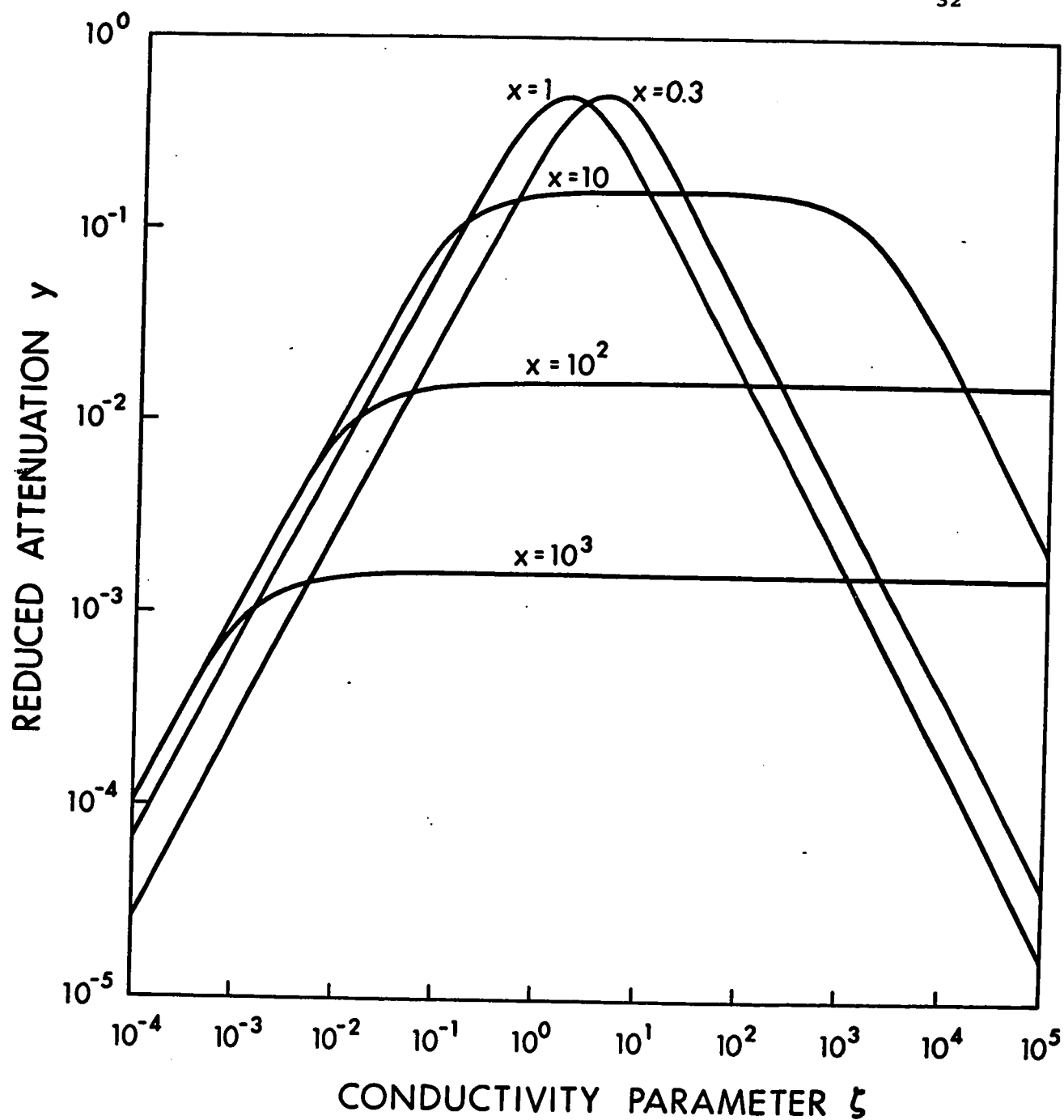


Figure 3.d : Computer calculated plots
of the reduced attenuation as a function of the
conductivity parameter ζ .



The actual attenuation for one round trip can be found by using equation (3.8) with (3.5) which gives

$$\begin{aligned}\alpha_T &= 2B\omega d\zeta/v_0 \\ &= \frac{2Bq}{\epsilon v_0} (\mu_n \tau_n + \mu_p \tau_p) \beta I_0 .\end{aligned}$$

Hence the attenuation of the acoustic wave (in the region where $1 \ll x \ll \zeta^{-1}$) is proportional to the conductivity in the surface layer of the crystal and is independent of the ultrasonic frequency, the thickness of the crystal, and the optical absorption coefficient.

Another asymptote to function (3.7) occurs when $e^{2x} \gg (x\zeta) \gg 1$. In this case (3.7) reduces to

$$y \approx \frac{1}{x} \tan^{-1} \{ x\zeta(1-e^{-x}) \} \approx \frac{\pi}{2x}$$

which shows that y is independent of ζ and is determined only by x . The actual attenuation for this case is then

$$\alpha_T = \pi B/v_0 \kappa$$

Therefore when the conductivity is large enough in the surface region, the acoustic attenuation is independent of this conductivity and is only determined by the optical absorption coefficient.

This region for the function (3.7) shows up clearly on figure (3.c) as the common asymptote for all curves at high values of x . In figure (3.d) this region shows up as the flat top on the curves for high values of x .

For other regions of x and ζ the reduced attenuation y is dependent on both x and ζ . It is in these regions that it should be possible under certain cases to obtain values of both x and ζ from experimental determination of y . By performing the experiment at two different ultrasonic frequencies we get

$$y_1 = f(x, \zeta_1)$$

$$y_2 = f(x, \zeta_2)$$

But $\zeta_2/\zeta_1 = \omega_1/\omega_2 = \gamma$

so that
$$\begin{aligned} y_1 &= f(x, \zeta) \\ y_2 &= f(x, \gamma\zeta) \end{aligned} \tag{3.9}$$

where $\zeta = \zeta_1$. Experimental determination of y_1 , y_2 and γ thus gives two equations in two unknowns which can be simultaneously solved to yield value for both z and ζ under certain conditions.

The curves of figure (3.d) are helpful

to see where solutions to equations (3.9) are possible. The two values of the reduced attenuation in (3.9) must be separated by the amount γ on the logarithmic ζ axis of figure (3.d). Hence the problem becomes one of finding a value of x which makes the curve pass through these two values of y separated by γ . It is seen that if the two values of y lie on the graph where the curves take on their asymptotic values, that no unique solution for x and ζ is possible. For example, in the case where $(x\zeta) \ll 1$ equation (3.7) reduces to

$$y \approx \zeta(1-e^{-x}).$$

Therefore measuring α at two different frequencies will give

$$y_1 = \zeta(1-e^{-x})$$

$$y_2 = \gamma\zeta(1-e^{-x})$$

which only gives $\gamma = y_2/y_1$ and no information about x and ζ is obtained. If however, x is large such that $e^{-x} \ll 1$ then $\zeta = y_1$ as mentioned before.

The curves of figures (3.c) and (3.d) in the region of $x < 1$ are only valid for the case where all of the light that passes through the

crystal to surface (2) escapes. In reality this will not be the case. The maximum amount of light that will pass through surface (2) is given by

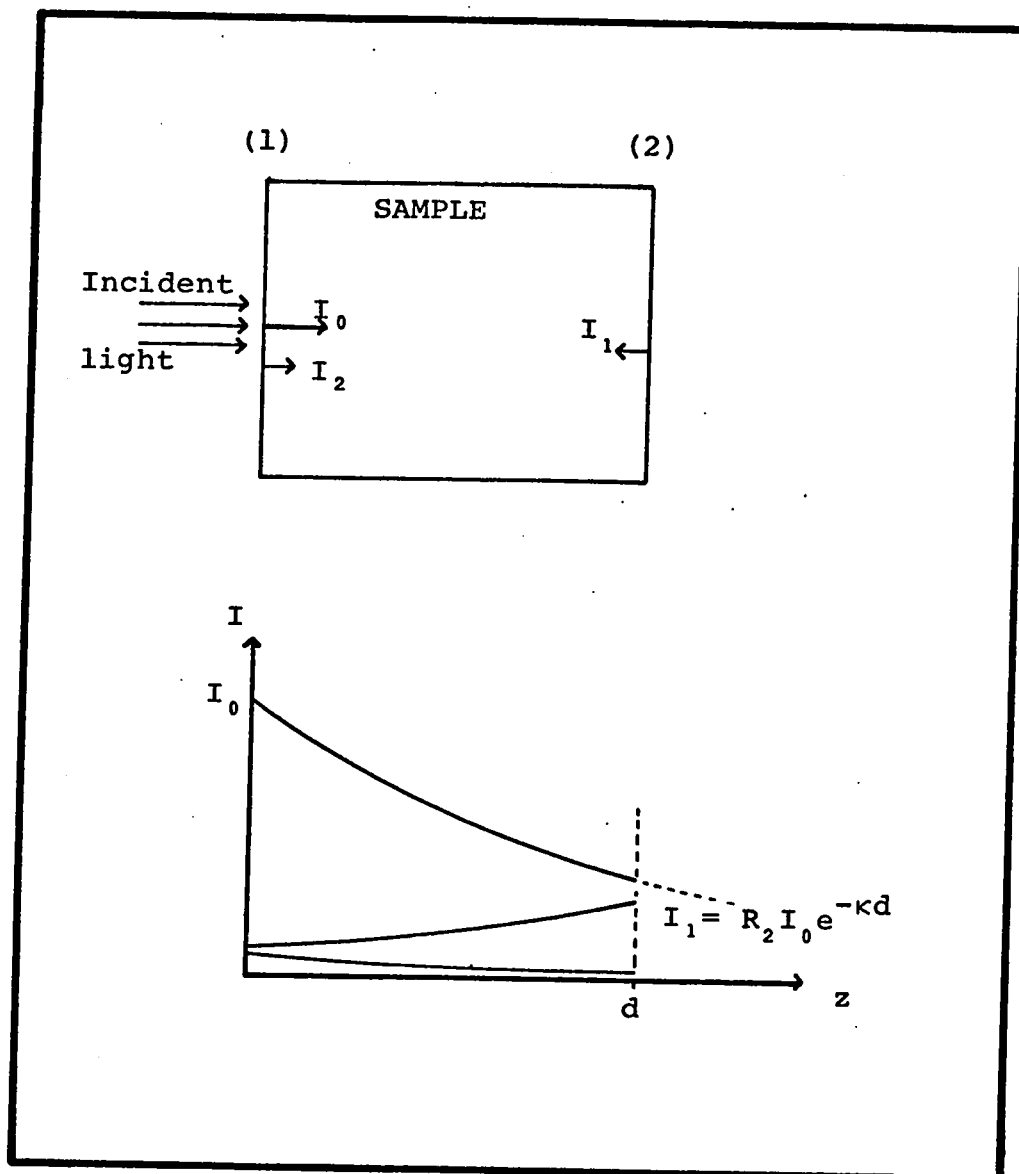
$$\frac{4n^2}{(n+1)^2 + (\kappa\lambda/4)^2} \approx \left[\frac{2n}{n+1}\right]^2 \approx .84$$

where n is the refractive index and has a value of about 2.3 for CdS, and λ is the wavelength of the light. In the arrangement used experimentally surface (2) had an evaporated film of indium for electrical contact to the transducer. Therefore, the amount of light that would be reflected back into the sample at surface (2) is nearly 100%.

Any light passing through the crystal back to surface (1) will experience a 16% reflection back into the crystal for a third transit. Therefore, in the region of $x < 1$, a more complex model is needed to take account of the increased optical absorption due to reflections.

Figure (3.e) shows the case for multiple reflections from the sample boundaries. In this diagram the light at the point $z = 0$, traveling in the positive direction in the crystal, is $I_0 + I_2 + I_4 + \dots$ and the light at the point $z = d$

FIGURE 3.E

DECAY OF LIGHT IN SAMPLE ($\kappa d < 1$)

travelling to the left in the crystal is

$I_1 + I_3 + I_5 + \dots$. In general, the intensity at a point z in the crystal is

$$\begin{aligned} I(z) &= I_0 e^{-\kappa z} + I_1 e^{-\kappa(d-z)} + I_2 e^{-\kappa z} + \dots \\ &= e^{-\kappa z} (I_0 + I_2 + I_4 + \dots) + e^{-\kappa(d-z)} (I_1 + I_3 + I_5 + \dots) \\ &= e^{-\kappa z} \sum_{n=0}^{\infty} I_{2n} + e^{-\kappa(d-z)} \sum_{n=1}^{\infty} I_{2n-1} \end{aligned}$$

where

$$\begin{aligned} I_{2n} &= I_0 (R_1 R_2 e^{-2\kappa d})^n \\ I_{2n-1} &= I_0 R_2 e^{-\kappa d} (R_1 R_2 e^{-2\kappa d})^{n-1} \end{aligned} \quad n = 1, 2, 3, 4, \dots$$

Define $G = R_1 R_2 \exp(-2\kappa d)$ and therefore the intensity at a point z becomes

$$\begin{aligned} I(z) &= I_0 (e^{-\kappa z} + R_2 e^{-2\kappa d} e^{+\kappa z}) \sum_{n=0}^{\infty} G^n \\ &= I_0 (e^{-\kappa z} + R_2 e^{-2\kappa d} e^{+\kappa z}) / (1-G) \end{aligned} \quad (3.10)$$

The dielectric frequency as a function of distance in the sample is given by (3.3) where $\frac{dI}{dz}$ is now given by the more general expression

$$\begin{aligned} \frac{dI}{dz} &= -\frac{dI_1}{dz} + \frac{dI_2}{dz} - \frac{dI_3}{dz} + \dots \\ &= \kappa (I_0 e^{-\kappa z} + I_1 e^{-\kappa(d-z)} + I_2 e^{-\kappa z} + \dots) \\ &= \kappa I(z) \end{aligned} \quad (3.11)$$

The reduced attenuation for the more general case

can then be written using (3.6) where $f(\xi)$ now takes the form

$$f(\xi) = x\zeta (e^{-\xi} + R_2 e^{-2x} e^{+\xi}) / (1-G)$$

The variables ξ , x and ζ have the same meanings as defined earlier.

The integral (3.6) with the above expression $f(\xi)$ can be solved numerically and plots of this function are shown in figure (3.c) by the dotted lines. These curves show clearly the effect of increased optical absorption due to reflections at the boundaries of the crystal. For the case where $x \gg 1$ the reflection of the light tends to hold the attenuation up. The region discussed earlier, where $y = \zeta$ when $x\zeta \ll 1$ is now seen to be extended to smaller values of x . Thus the actual attenuation for one round trip is

$$\alpha_T = \frac{2Bq}{\epsilon v_0} (\mu_n \tau_n + \mu_p \tau_p) \beta I_0$$

for $1 \lesssim x \ll \zeta^{-1}$.

For values of $x \ll 1$ the curves of figure (3.c) take on an asymptotic solution of the form

$$y = \left(\frac{1+R_2}{1-R_1 R_2} \right) x\zeta.$$

For the case shown in the figure (3.c) where
 $R = .16$ and $R = 1.0$ the asymptote is given by

$$y = 2.381 \times \zeta.$$

The actual attenuation for one round trip in the region where the above asymptotic solution is valid, becomes

$$\begin{aligned} \alpha_T &= \left(\frac{2B\omega d}{v_0} \right) \left(\frac{1+R_2}{1-R_1R_2} \right) \times \zeta \\ &= \left(\frac{2Bqd}{v_0 \epsilon} \right) \left(\frac{1+R_2}{1-R_1R_2} \right) (\mu_n \tau_n + \mu_p \tau_p) \beta \kappa I_0 \end{aligned}$$

The attenuation is seen to be independent of the ultrasonic frequency.

At this point it is instructive to look at numerical values for the various parameters to see the order of magnitude of the photosensitive attenuation effect in CdS. The attenuation measured for one round trip of the sample is given in terms of the reduced attenuation by equation (3.5)

$$\alpha_T = \left(\frac{2B\omega d}{v_0} \right) y$$

For CdS the values of the constants in the above expression are given in Appendix D for longitudinal waves propagating parallel to the c-axis as

$$v_0 = 4.3 \times 10^5 \text{ cm/sec}$$

$$B = e^2/2c\epsilon = .02$$

Thus $\alpha_T = (5.077 \text{ db sec cm}^{-1}) \nu d \quad (3.12)$

where ν is the frequency in mHz and d is the sample thickness in cm.

The maximum value that the reduced attenuation y can have is 0.5.* Hence the maximum photosensitive attenuation possible is

$$\alpha_{\max} = 2.54 \nu d$$

For $\nu = 10 \text{ mHz}$ and $d = 1 \text{ cm}$ the maximum attenuation is then

$$\alpha_{\max} \approx 25 \text{ db} .$$

* That the maximum value for y is 0.5 can be seen, simply by finding the maximum of equation (1.19)

i.e. $y = \alpha v_0/B\omega = \frac{(\omega_c/\omega)}{1+(\omega_c/\omega)^2}$ has a maximum

value of .5 when $\omega_c = \omega$.

CHAPTER 4

Experimental Details

1) Cryostat and Optical Arrangement

An optical cryostat was constructed to allow measurements of the ultrasonic attenuation to be made at temperatures below 300°K. Figure (4.a) illustrates a cross section of the cryostat showing the general layout of the sample holder, low temperature vacuum chamber, helium and nitrogen baths, and the optical arrangements. The sample holder is enclosed by copper radiation shields containing holes for the light to enter. The inner shield floats in temperature and can be heated above the bath temperature by a heater. A temperature controller is connected to the heater for regulating the temperature of the inner shield and sample holder. The outer shield is thermally grounded to the surrounding bath. The entire assembly is enclosed by a glass cylinder which is connected to a precisely tapered vacuum coupling by way of a copper-glass seal. This coupling, when properly coated with high vacuum silicone grease,

makes a good vacuum seal down to liquid helium temperatures. At room temperature it is quickly and easily demountable for simple access to the sample chamber.

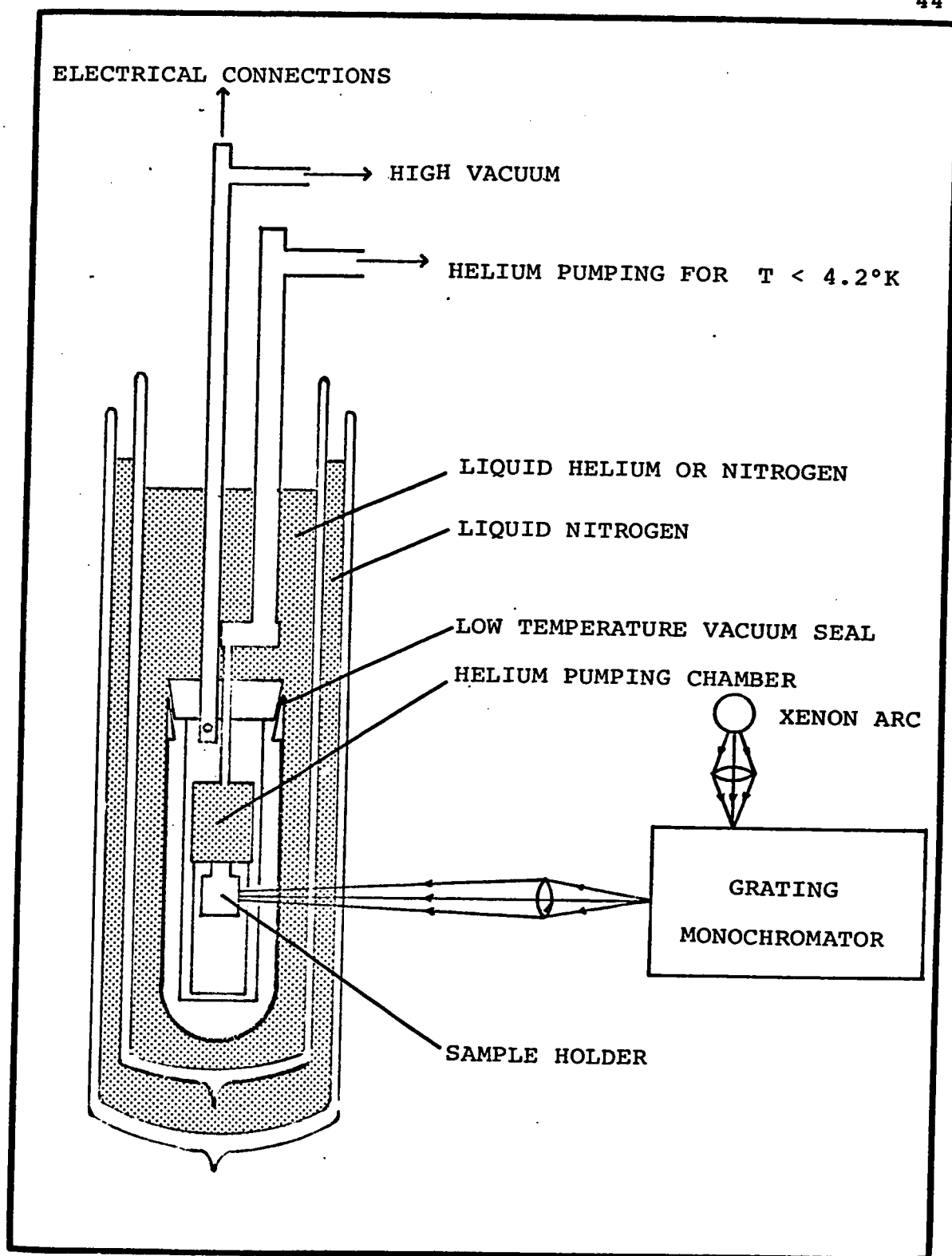
The temperature is measured with a calibrated germanium thermometer for temperatures below 100 °K and a copper-constantan thermocouple is used for temperatures above 100 °K. Both thermometers can be used with the temperature controller to maintain a constant temperature at the sample holder.

Electrical connections for the thermometers and heaters are taken down the high vacuum line using #38 copper wire with Formvar insulation. 50Ω impedance #UT-8 Micro Coax Cable* is used for the ultrasonic connections. All cables into the cryostat are thermally grounded on both the inner and outer sections of the low temperature vacuum chamber.

Room temperature measurements are made using the ultrasonic connections and sample holder of the cryostat, but without the dewars and vacuum system in place.

* Supplied by Uniform Tubes, Inc.

Figure 4.a : Cross-section of cryostat
showing location of sample holder with respect
to the optics, vacuum system and refrigerant.

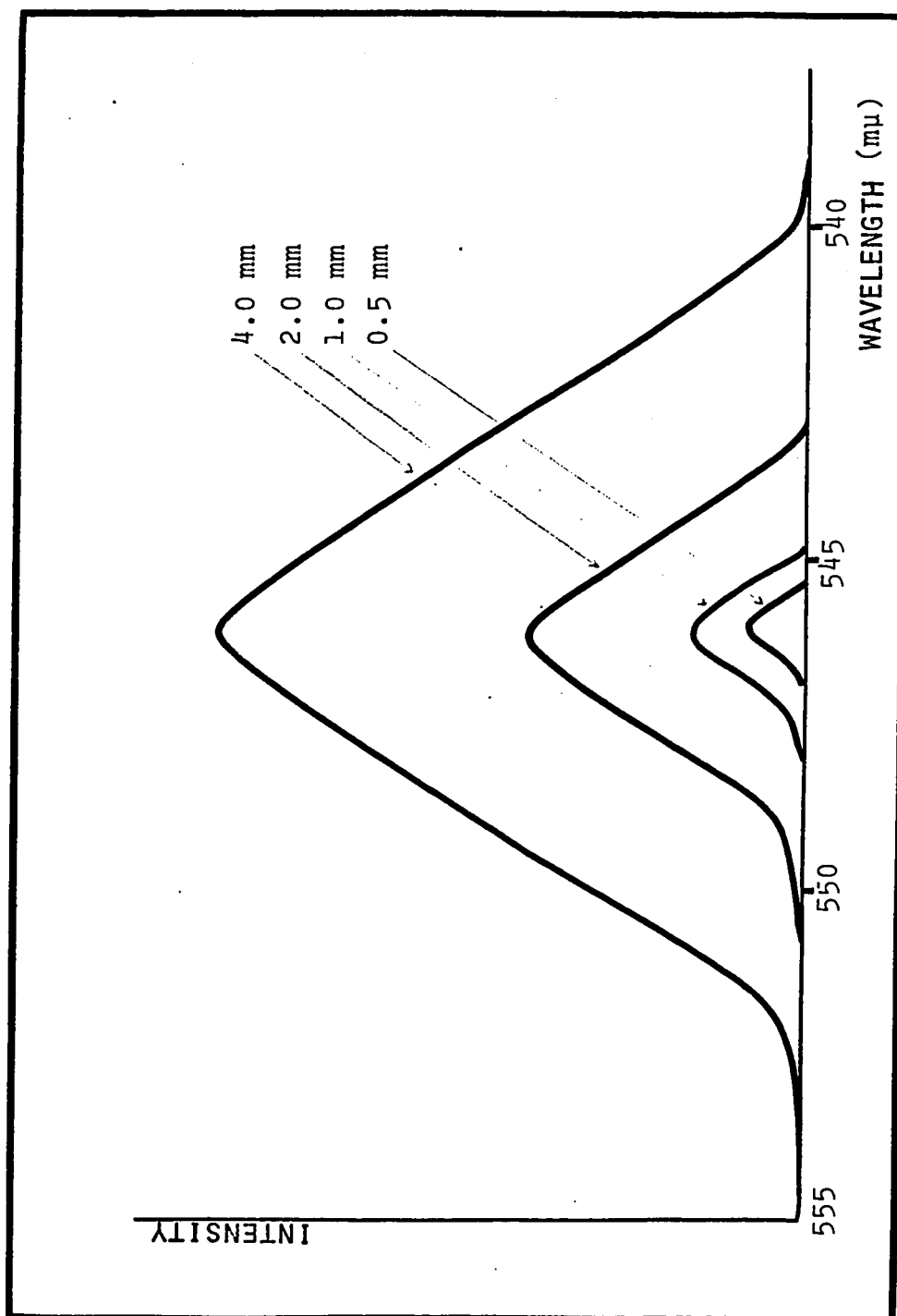


The light enters the cryostat through the glass walls of the dewars and the glass housing of the low temperature vacuum chamber. The light source is a high pressure Xenon arc lamp (#XBO 450) rated at 500 watts. The lamp is powered by a current regulated DC supply and, after a warm up period of about 30 minutes, is very stable over long periods of operation.

Light from the arc lamp is focused on the entrance slit of a Bausch and Lomb grating monochromator (500mm model; 1200 grooves/mm) to give a monochromatic beam that can be directed into the cryostat at the sample. Intensity of the light can be altered by introducing neutral density filters into the beam at the exit side of the monochromator and also by changing the width of the exit and entrance slits on the monochromator.

Changing the intensity of the lamp by altering the slit widths will also change the spectral width of the output beam from the monochromator. Figure (4.b) shows the line profile for slit widths of 4mm, 2mm, 1mm, and 0.5mm as obtained from the 5461 \AA mercury line. It is seen from figure (4.b) that the slit widths must be less than 1mm to obtain resolution below 10 \AA in the wavelength region of $550 \text{ m}\mu$.

FIGURE 4.B



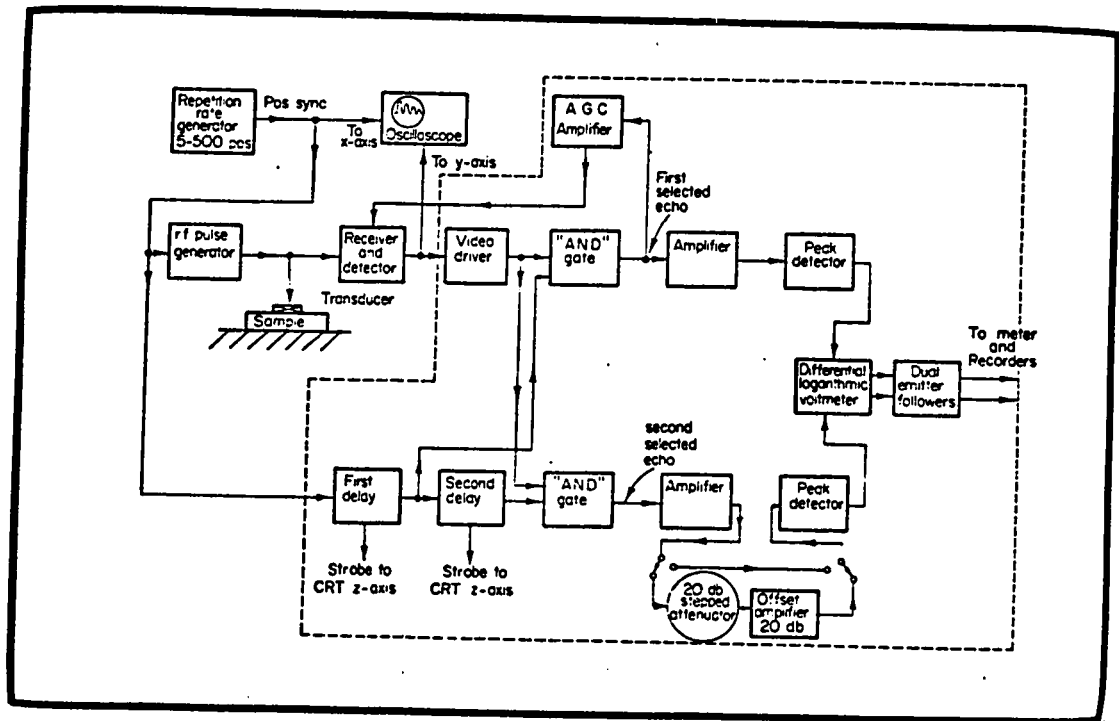
MONOCHROMATOR PROFILE OF 5461 Å Hg LINE
FOR DIFFERENT SLIT WIDTHS

2) Ultrasonics

The ultrasonic equipment used in the experiments was manufactured by Matec Inc. and forms the basis of the automatic attenuation measurement system illustrated in block form on figure (4.c). The essential components of this system are a) the synchronizer (Model 120) which supplies the basic timing pulses, b) the rf pulse generator and receiver (Model 6000 with #690 plug-in) which generates and detects the ultrasonics at a transducer, and c) an attenuation recorder (Model 2470) represented by the blocks contained within the dotted line in figure (4.c).

A pulsed high frequency electric field when applied to the quartz transducer, causes a vibrational pulse to enter the crystal. This ultrasonic pulse propagates through the crystal, is reflected back from the sample boundary and returns to the first surface. Here a small part of the acoustic energy leaves the sample and is converted to an electrical signal by the transducer, while the remaining acoustic energy is reflected back into the sample for a second round trip. The electrical signal produced at the transducer is

FIGURE 4.C



Automatic Attenuation Measurement System

picked up by the receiver and amplified. This signal is then rectified and displayed on an oscilloscope where a series of "echos" are seen as the acoustic pulse strikes the transducer sample interface on each round trip. Some typical echo patterns for a CdS sample are shown in figure (4.e).

The echo pattern is entered into the automatic attenuation recorder where time delay and gate circuits are used to look at only two individual pulses while the rest of the echo train is ignored. The output of the attenuation recorder is a DC signal representing the logarithm of the ratio of the heights of the two selected echos. This output is in the proper form for the attenuation coefficient and is calibrated in db or nepers.

Use of the automatic attenuation recorder thus allows the attenuation to be monitored continuously. Changes in the attenuation when some parameter is varied (e.g. the temperature or the wavelength of light incident on the sample) can then be displayed directly on an X-Y recorder.

One of the essential elements of ultrasonic

measurements using a transducer is in getting a good acoustic bond between the sample and the transducer. For the longitudinal waves used in the experiments, reasonable bonds can be made at room temperature by using a thin liquid layer between sample and transducer. Silicone fluids and alcohols can be used as bonding materials for temperatures from room temperature down to about 150°K. For temperatures below 150°K the bonds become a major problem and much time was spent during the project trying to overcome this difficulty for CdS.

It was found that a number of the common plastic cements would work quite well as low temperature bonds if they could be cooled quickly by immersion in liquid nitrogen, but when they were cooled more slowly, as is necessary in the cryostat, the bonds would break. Some success was obtained by using Dow Corning's High Vacuum Silicone grease. However, one of the problems with this grease is that good bonds were not easy to make at room temperature and a bond giving a poor echo pattern at room temperature would quite often give a good echo pattern when cooled. Therefore, it was not

possible to know if a bond would be adequate until the sample was cooled. Silicone grease seemed to be successful for about one in every three or four tries.

The silicone grease bond was used for many of the early measurements but in the latter stages of the project a technique for making bonds using indium metal was used. The indium bond proved to be so much more reliable and convenient compared to the silicone grease bond that the technique is outlined below.

The first step in making the indium bond is to evaporate a relatively thick layer (about 50μ) of indium metal on both the sample surface and transducer. This evaporation must be done under vacuum better than 10^{-5} torr and care must be exercised when opening the vacuum chamber not to expose the indium surfaces to oxygen until they have cooled completely to room temperature.

When the sample and transducer are removed from the evaporator (using extreme caution to avoid dust particles on the freshly coated

surfaces), the two surfaces are placed in contact. A small pressure applied to the transducer will then cause it to "stick" to the sample. The sample, transducer combination is then placed in a jig that allows a three kgm weight to apply pressure to the transducer inside a vacuum system. Pieces of clean teflon are placed under the sample and on top of the transducer to protect the polished surfaces.

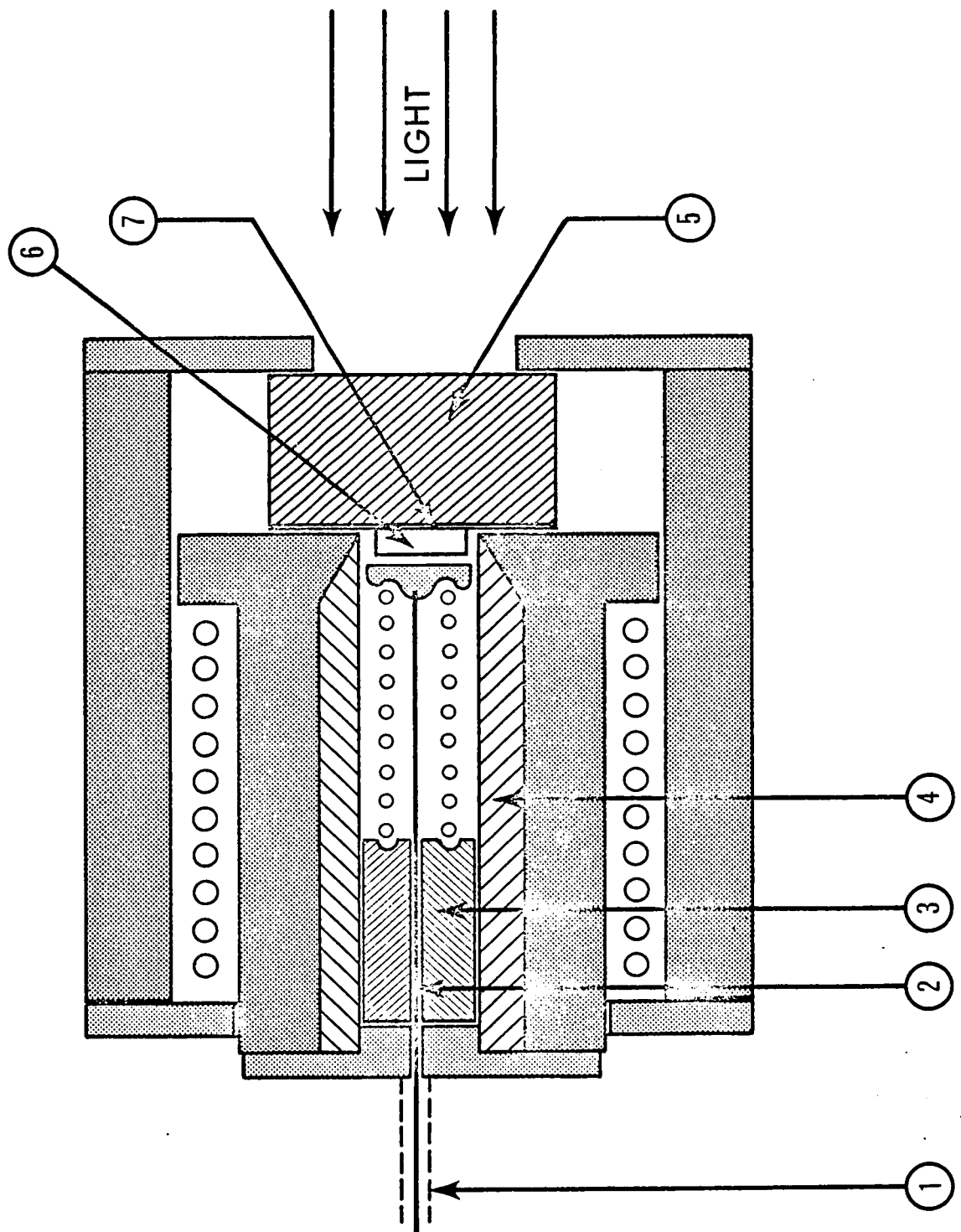
The pressure jig is then placed inside an oven where the temperature of the sample is slowly brought up to just under the melting point of indium, (i.e. $< 155^{\circ}\text{C}$) and then allowed to cool. If the temperature exceeds 155°C the bond does not appear to work well when used at liquid nitrogen temperatures.

The sample when cool can be removed from the vacuum system and pressure jig leaving the transducer solidly fixed to the sample. This bond has worked well for all temperatures from room temperature down to below liquid helium temperature.

Figure (4.d) shows the sample holder and the arrangement used to get electrical contacts

Figure 4.d : Cross-section of sample holder used to provide coaxial electrical connection to the quartz transducer. All shade portions are metal and dashed parts are teflon insulation.

- 1) coaxial cable to sample holder
- 2) teflon insulated wire makes contact to top of transducer
- 3) teflon piston
- 4) teflon cylinder
- 5) CdS sample
- 6) quartz transducer
- 7) evaporated indium layer provides contact to underside of transducer

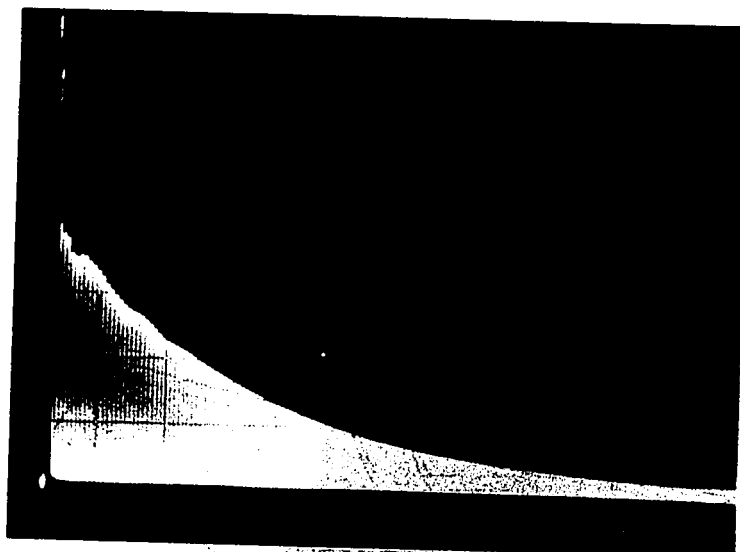


to the transducer. The indium layer on the sample that was used in making the bond provides the contact to the under side of the transducer. This contact becomes the outer conductor for the coaxial cable into the cryostat. The upper surface of the transducer makes electrical contact to the center wire of the coax cable by way of a spring loaded piston as shown in figure (4.d).

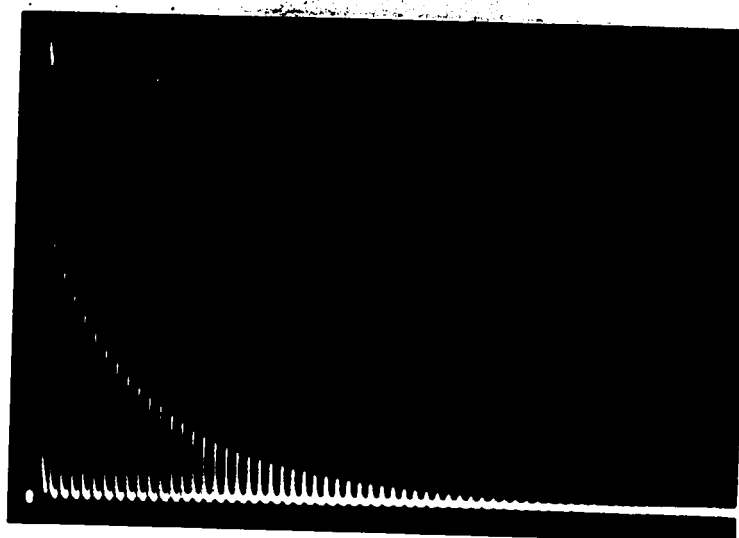
Samples that could be obtained for the experiments were rather limited in size. In fact the cross section was typically about a square centimeter. A cross section of this size makes it necessary to use small diameter transducers for the ultrasonic source which gives rise to diffraction problems at low frequencies. The transducers used in the experiments were 6mm in diameter and had fundamental frequencies between 7 MHz and 15 MHz. The photographs of figure (4.e), show typical echo patterns from a 15 MHz transducer tuned to 15 MHz, 45 MHz, 75 MHz, and 105 MHz. It is noticed that the decay pattern of the fundamental frequency is rather distorted whereas for the higher frequencies this distortion is much reduced. The disappearance of peaks and valleys

Figure 4.e Echo trains in sample SR-1 at room temperature.

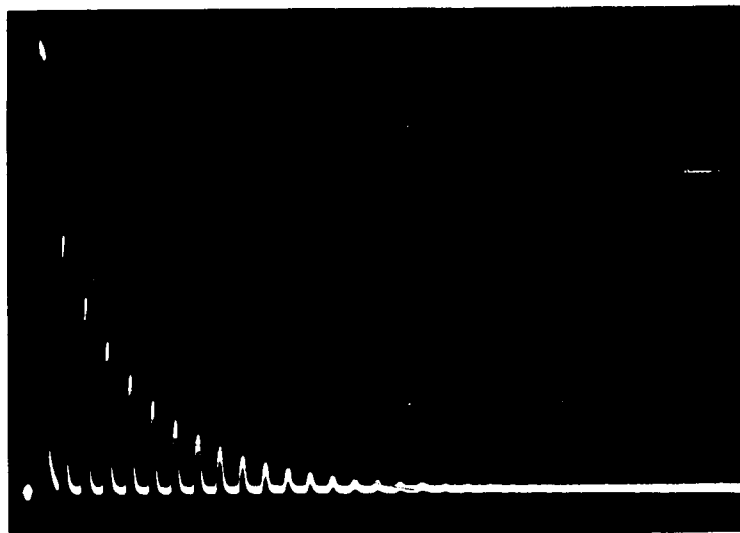
(i)	15 mHz	Sweep = 50 μ sec/cm
(ii)	45 mHz	Sweep = 20 μ sec/cm
(iii)	75 mHz	Sweep = 10 μ sec/cm
(iv)	105 mHz	Sweep = 5 μ sec/cm



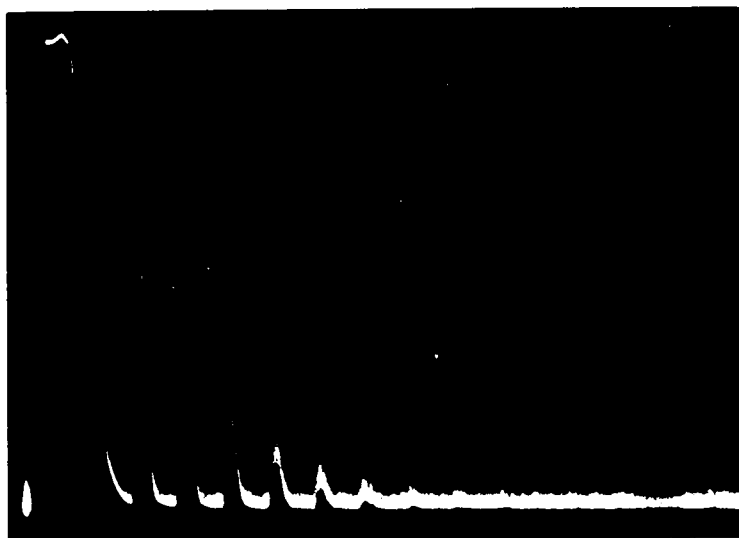
15 MHz



45 MHz



75 MHz



105 MHz

at the higher frequencies is typical of diffraction losses. This indicates that diffraction is probably the main source of non-exponential decay patterns rather than non-parallelism in the sample which would have the opposite effect with frequency. The transducers having 7 MHz fundamental frequency showed a more distorted decay at 7 MHz than that shown in figure (4.e) for 15 MHz, but at the higher harmonics the echo patterns became exponential as in figure (4.e).

When attenuation measurements are made, two echos from the echo pattern must be chosen for the attenuation recorder to look at. If two adjacent echoes are used then the maximum sensitivity allowed by the equipment enables measurements of attenuation changes $\sim .01$ db/round trip assuming noise levels can be kept sufficiently low. In order to facilitate the use of the sensitive scales when the background (or dark level attenuation in this case) is high, the equipment provides zero offset of up to 20 db.

For the case of low frequencies (i.e. 1st and 3rd harmonics) where the number of echoes is quite large, a further gain in the sensitivity

can be achieved by selecting two echoes for the attenuation recorder that are separated by 10 or 20 echoes. In this case the sensitivity can be increased to $\sim .001$ db/round trip in certain cases when the noise levels are small. When higher frequencies are used the background attenuation increases considerably reducing the number of echoes in the train and increasing the noise levels. In this case it is not possible to achieve sensitivities much better than .05 db/round trip.

3) CdS Samples and their Preparation

Samples for use with ultrasonic techniques must be oriented and cut along the proper crystallographic directions. The two surfaces perpendicular to the direction of wave propagation must be polished flat and parallel to within tolerances that will not effect the measurements. Further, since the pulse echo technique is being used, the samples themselves must be of sufficient thickness for the time of one acoustic round trip to be greater than the acoustic pulse length. This ensures that successive echoes will be distinguishable. For the case of longitudinal waves along the c-axis in

CdS, the sound velocity is 4.3×10^5 cm/sec and with a pulse width around 2 μ sec samples must have a thickness

$$d \geq 0.5 \times (4.3 \times 10^5 \text{ cm/sec}) \times (2 \times 10^{-6} \text{ sec}) \approx 0.4 \text{ cm}$$

Starting material for the samples are pieces of unoriented and uncut single crystal CdS having masses ranging from about 10 grams to 30 grams. Each of these pieces is encapsulated in "Crystalbond 509"* adhesive and mounted on a goniometer that fits on a diamond wire crystal saw. The "Crystalbond" provides the adhesive to hold the crystal to the goniometer and the encapsulation helps prevent chipping of the sample during the sawing operation. A cut is made close to one end to expose a fresh surface of CdS to be used for orienting with the X-ray machine. The goniometer could be moved from the saw to the X-ray machine and then back to the saw in such a way that the saw cut would be accurate to within 2° or 3° of the desired direction. The samples are then cut to thicknesses along the c-axis ranging from 4mm to

*Supplied by ARMECO Products, Inc.

10mm and with cross sections as large as possible, typically 10mm by 10mm.

Lapping and polishing of the crystals is carried out with equipment produced by Logitech Ltd. This equipment consists of a polishing machine (Model #PM2) which contains the lapping plate and drive mechanism and a precision polishing jig (#PP5) which rigidly holds the sample at the proper angle and controls the pressure of the sample against the lapping plates. The samples are fixed to the polishing jig's sample platform using "Crystalbond 509" adhesive.

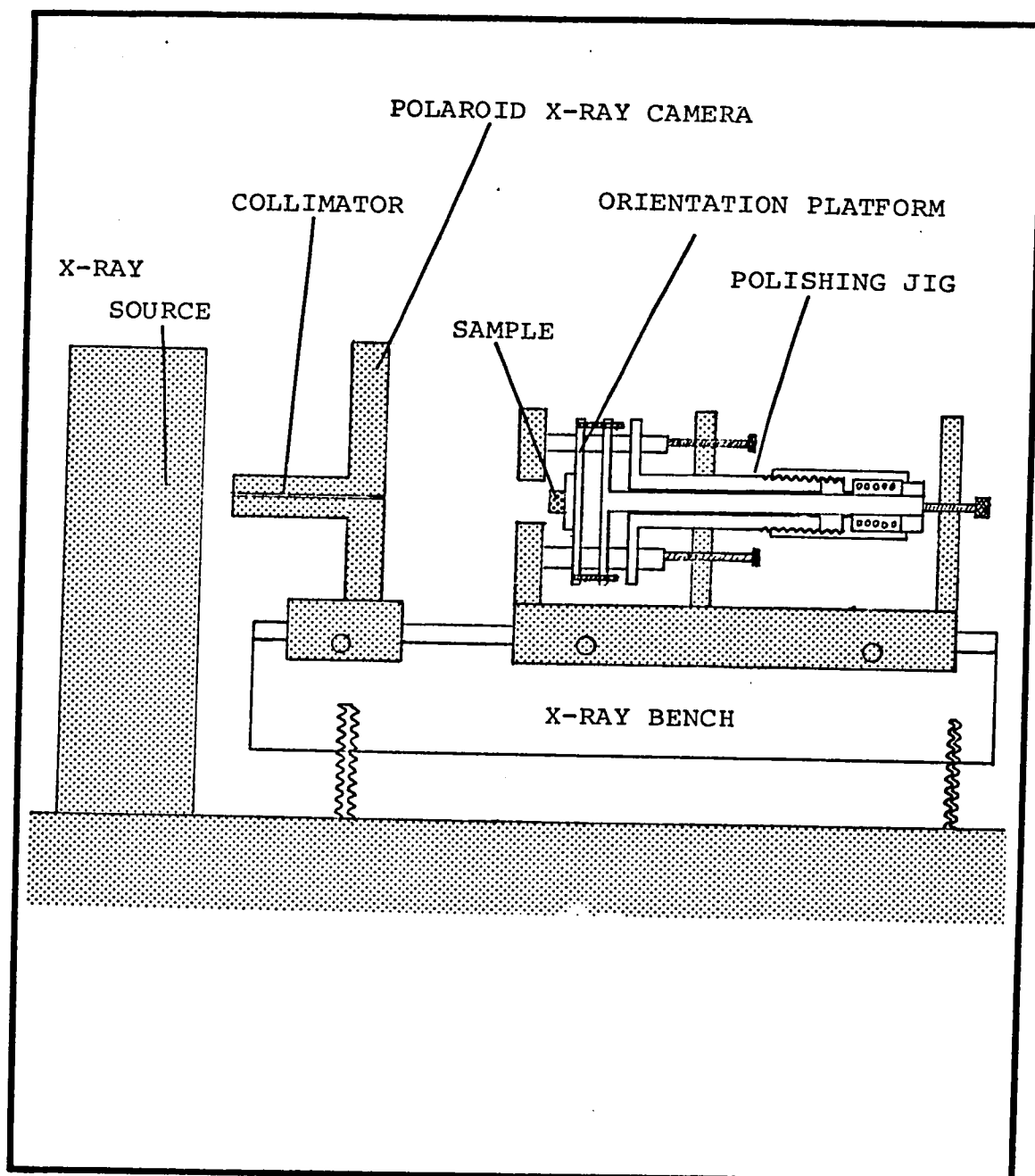
The lapping and polishing of CdS is carried out in two stages. The first stage consists of lapping the CdS sample against a brass plate using 5.0μ aluminum oxide abrasive suspended in oil. This lap produces a flat, matte surface. In the second stage the samples are polished against a 50% lead, 50% tin lapping plate using 1.0μ aluminum oxide powder suspended in a light silicone fluid. This final stage produced surfaces which were of optical quality where the mean height between hills and valleys on the surface was about $.01\mu$ according to manufactures specifications. Fringe patterns produced with an optical flat indicate that the surfaces have a very slight convex curvature where the

height at the center is less than $.2\mu$ above that of the sides of the crystal.

A final orientation is performed on the sample when the sample is mounted in the polishing jig so that the sample can be lapped in the "exact" position. Two methods can be employed for the final orientation. One method uses a device (figure 4.f) made up to hold the polishing jig on the X-ray bench such that the X-ray collimator tube can be accurately adjusted perpendicular to the lapping plane defined by the feet on the polishing jig. This initial alignment is carried out by having a freshly polished surface on the polishing jig and using this surface (which is exactly parallel to the feet on the jig) to reflect a HeNe laser beam back upon itself through the X-ray collimator tube. The accuracy with which samples could be oriented and then transferred back to the lapping machine is estimated to be better 1° .

Most of the samples were oriented using the above mentioned X-ray technique, however a second method which was quick and fairly reliable was used in a few cases. This method uses the pattern of a HeNe laser beam reflected off the

Figure 4.f : Diagram illustrating polishing jig mounted on X-ray table for precise sample orientation.

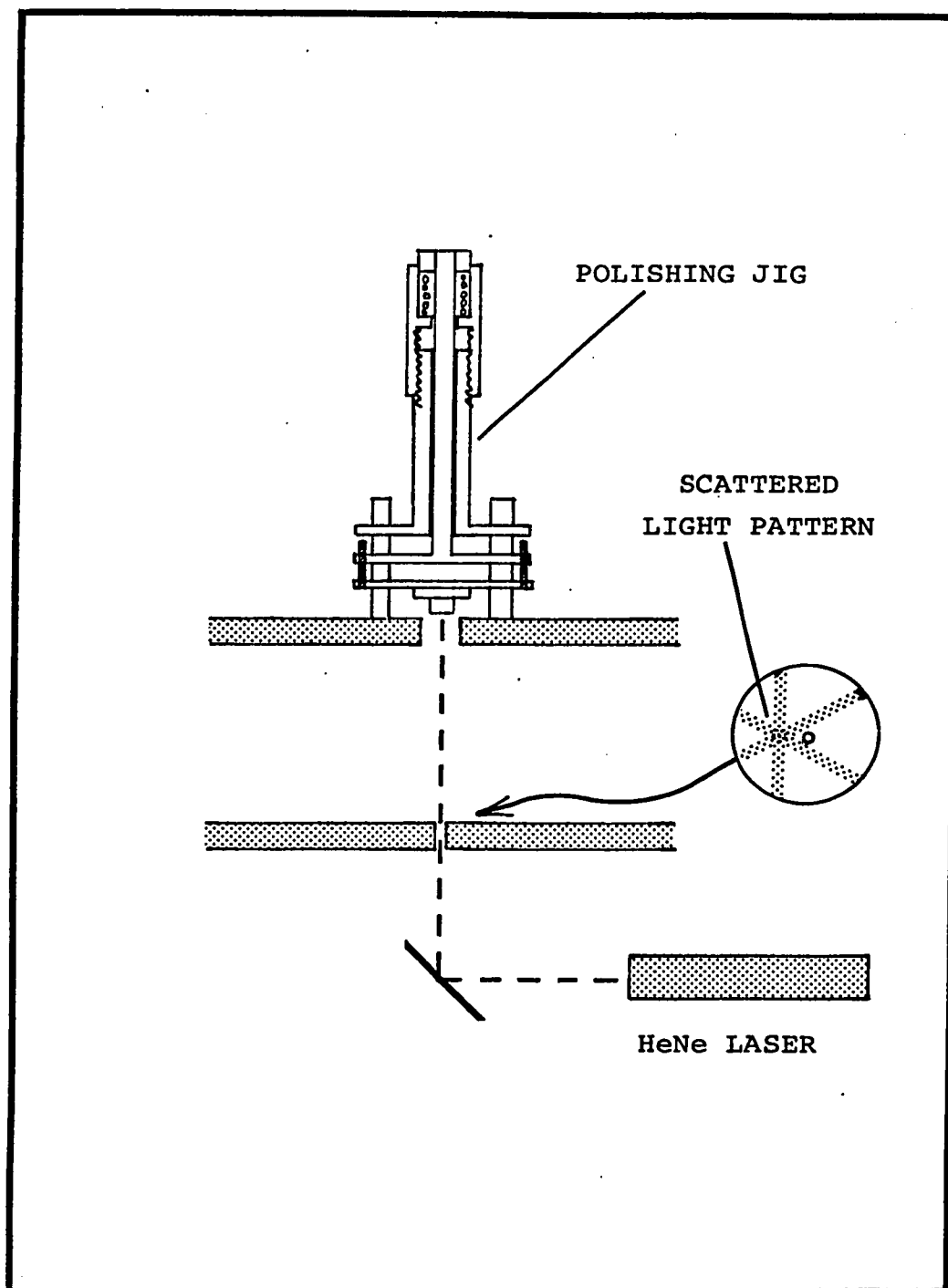


surface of a freshly polished and etched sample. Using the arrangement shown in figure (4.g) the jig is mounted on an optical table and adjusted so that the reflection of HeNe laser beam from the freshly polished surface is perpendicular to the laser beam and the jig is rigidly clamped in this position.

A freshly prepared etch (made from a mixture of 60% HCl and 40% of a saturated solution of CrO_3 dissolved in H_3PO_4 (c.f. Hemmat and Weinstein 1967) is repeatedly brushed on and then removed from the polished surface for a few minutes to produce etched pits on the face. The laser, when striking the CdS surface with the etch pits reflects back a pattern similar to a back reflection X-ray picture (c.f. figure 4.g). The center of this pattern represents the direction of the c-axis in the sample.

The attitude adjustments on the lapping jig are then set to bring the center of the reflected image back onto the incident laser beam. By using a transparent plastic sheet marked with three lines intersecting at 120° , the center of the reflected pattern can be determined

Figure 4.g : Diagram showing arrangement used for orienting CdS samples by scattering of a laser beam from etch pits on the sample surface.



accurately enough to give the sample orientation to about 0.5° .

The above procedures generate one surface on the sample which is flat and perpendicular to the c-axis. The sample platform is then removed from the lapping jig and the sample is removed by immersion in acetone for several hours. After removal and cleaning, the sample is again glued on the platform with the polished side down. The new surface can now be lapped and polished to obtain a reference surface to make parallelism tests.

The lapping jig with the two polished surfaces on the sample is placed on an optical bench with a HeNe laser directed at the front polished surface. Two light beams are now reflected back from the sample, one from the front and one from the back surface. The brightest reflected beam comes from the front surface and the jig must be oriented to reflect this beam back upon the incident laser beam. The jig is then clamped securely in this position and the attitude adjustment on the lapping jig is oriented to make the incident beam bisect the two

reflected beams. After adjustment the sample is relapped and polished. The above procedure is repeated until the two beams superimpose and fringe patterns start to appear. These fringes are then used to make further adjustments to the orientation platform on the lapping jig.

By careful use of this parallelism test the samples can be polished so that there will be about one fringe pattern across the width of the sample indicating that the wedge angle of non-parallelism is about

$$\theta \sim \frac{\lambda/2}{l_{cm}} \sim 3 \times 10^{-5} \text{ rad} \sim 6 \text{ sec of arc}$$

Parallelism in the samples of this order is reasonable for the ultrasonic measurements performed.

The samples used in the experiments can be divided into two broad categories. The first group consists of crystals that are strongly photosensitive, having dark conductivities of less than $10^{-10} \text{ (ohm cm)}^{-1}$ and under illumination the conductivity can be increased to $\leq 10^{-4} \text{ (ohm cm)}^{-1}$. The second group can be considered as weakly photosensitive where the conductivity under illumination will change much less than for the strong photoconductors.

Six samples were used in the observations reported in the thesis. Of these six, two crystals were considered strong and four were considered weak photoconductors. Table I gives a list of the six samples giving their source, size and their code name.

The two samples SB-00 and SE-1 had conductivities of about $10^{-1} \text{ (ohm cm)}^{-1}$ when they were first obtained and showed no significant photoconductance. These samples were annealed using a method described by White (1965). In this procedure the crystals were sealed in an evacuated quartz tube containing an appropriate amount of sulfur to provide a sulfur atmosphere of about .2 atms at 1000°C . The samples were then annealed at 1000°C for 24 hours, after which they were cooled very slowly at a rate of about 25°C per hour to avoid freezing in any unnecessary structural defects. The samples when removed from the sealed container were good insulators in the dark. SB-00 was weakly photosensitive and SE-1 was strongly photosensitive.

All samples used in the experiments showed a very strong optical quenching effect when exposed to $.9\mu$ infrared illumination.

TABLE I

Samples Used in Ultrasonic Experiments

Strong Photoconductors

Sample Code	Source	Anneal	Dark Conductivity	Light Conductivity*	Thickness
SB-3	Eagle-Pitcher Industries	no	$\sim 10^{-10} (\text{ohm cm})^{-1}$	$\sim 10^{-4}$.501cm
SE-1	"	yes	$\sim 10^{-10}$ "	$\sim 10^{-4}$.677cm

Weak Photoconductors

Sample Code	Source	Anneal	Dark Conductivity	Light Conductivity*	Thickness
SR-1	courtesy of Dr.D.C.Reynolds	no	$\sim 10^{-8} (\text{ohm cm})^{-1}$	$\sim 10^{-7}$.694cm
SR-2	"	no	$\sim 10^{-3}$ "	$\sim 10^{-2}$.745cm
SB-2	Eagle-Pitcher	no	$\sim 10^{-10}$ "	$\sim 10^{-6}$	1.000cm
SB-00	Harshaw	yes	$\sim 10^{-8}$ "	$\sim 10^{-6}$.309cm

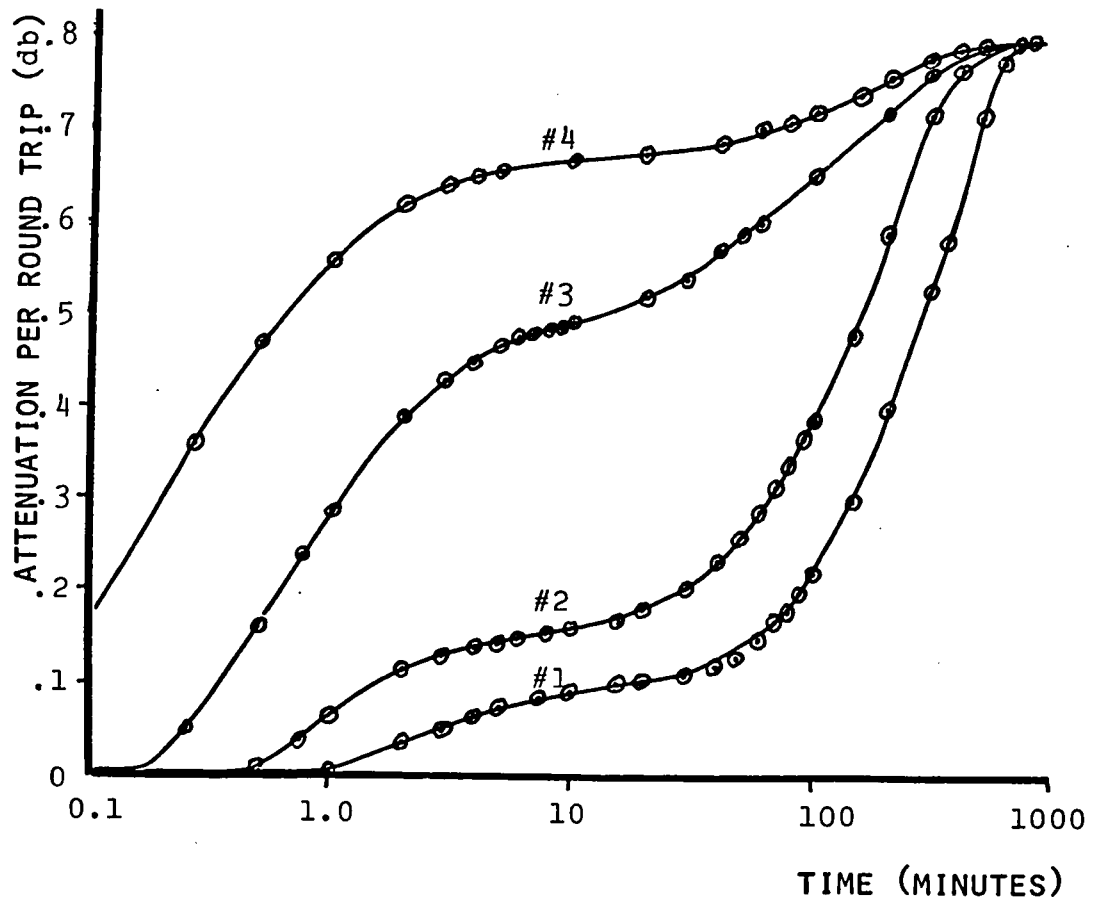
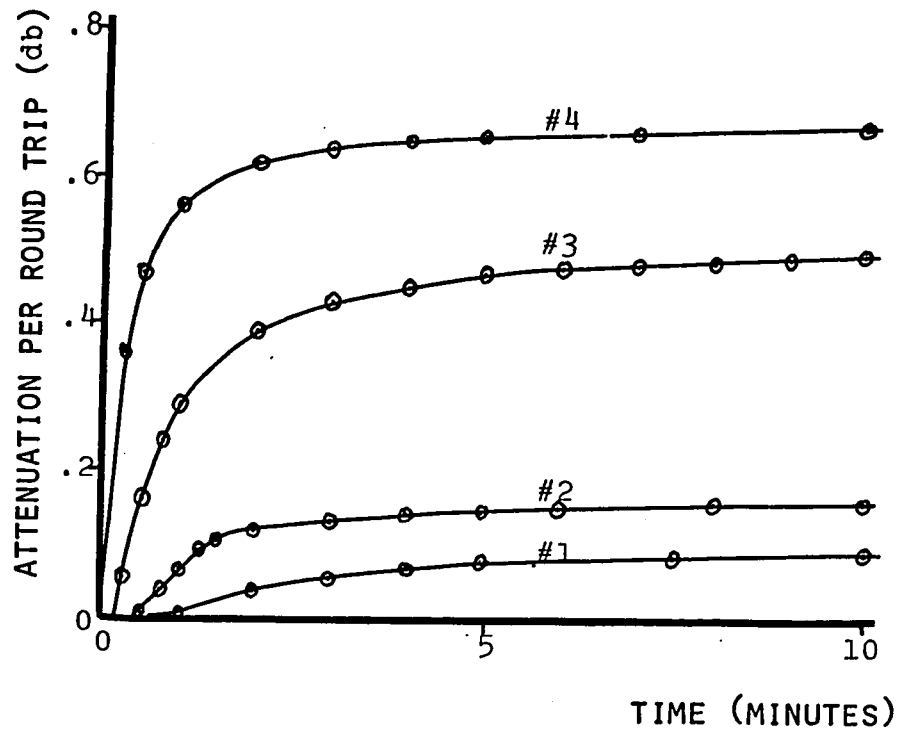
* Conduction measured when sample exposed to white light from a 100 watt light bulb.
(at a distance of 20cm)

CHAPTER 5

Experimental Results1) Observations on Strong Photoconductors

When the ultrasonic attenuation was measured on the strong photoconducting samples it was noticed that the times required to arrive at a steady state condition after exposure to light can be very long. For example figure (5.a) shows the time response of the ultrasonic attenuation at 15 mHz in sample SE-1. Curve number (1) shows the response of the sample to exposure with 550m μ light after it has been kept in the dark state for over 24 hours. Curve number (4) shows the response of the sample to the light when it has been kept in a dark state for only 5 minutes following a previous optical saturation with 550 m μ light. Curves (2) and (3) are intermediate cases where the sample has been kept in the dark for 6 hours and 1 hour respectively after saturation. It is noticed from these curves that about 10 hours are required to reach saturation at 550 m μ no matter what the previous conditions have been on the sample.

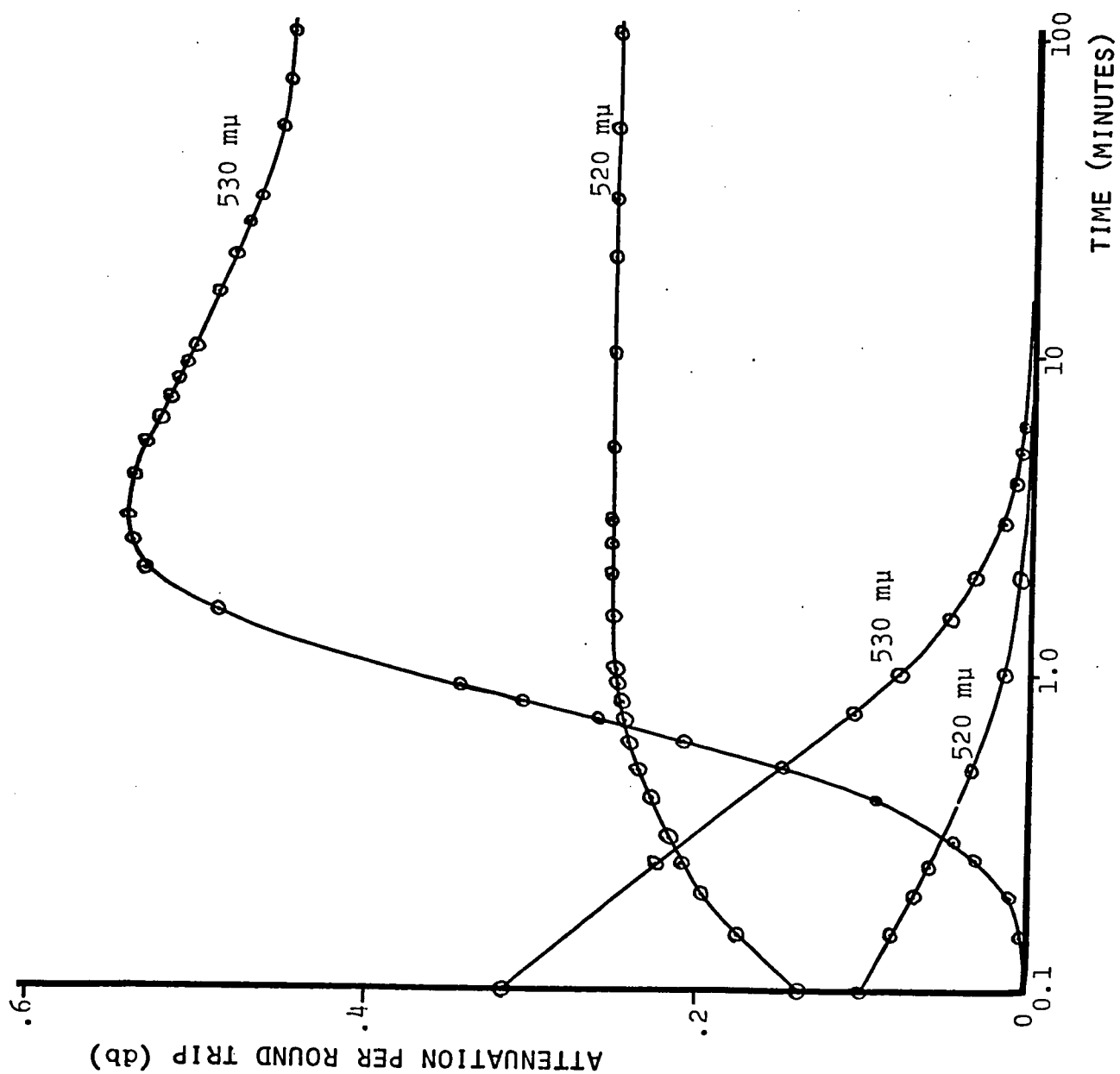
Figure 5.a : Time response curves for sample SE-1. Upper graph gives attenuation versus time on a linear scale, and lower graph gives attenuation versus time on a log scale. Curve #1 represents the case where the sample has reached an equilibrium condition in the dark state (i.e. ~ 24 hours). Curve #4 represents the case where the sample was kept in the dark state for only five minutes. Curves #3 and #2 are intermediate cases for dark state of one hour and six hours respectively.



Upon removing the illumination this sample in all cases returned to the dark level of attenuation in less than five minutes and no noticeable decay in the ultrasonic attenuation can be observed after this time even when the attenuation gain is increased 100 times. Although the dark level attenuation is reached after 5 minutes it is obvious from figure (5.a) that the history of any previous exposure to light is stored in the sample for many hours.

Of the two strong photoconductors, sample SE-1 took the longest times to reach a steady state. Time response curves for sample SB-3 are shown in figure (5.b). These curves show the rise and decay of the ultrasonic attenuation at 15 MHz from exposure to 530 m μ and 520 m μ light. It can be seen that for light which is highly absorbed (i.e. 520 m μ), a steady state condition is very quickly (\sim 2 min.) arrived at relative to the time required to reach steady state with the more weakly absorbed light at 530m μ . The same situation was observed in sample SE-1 for

Figure 5.b : Time response to an optical step function for sample SB-3 at two different wavelengths of light. The ultrasonic attenuation is plotted versus the time on a log scale.



the highly absorbed light, but here times in the order of 20 minutes were usually required for a steady state condition to set in.

The decay curves in sample SB-3 were observable for a longer period of time (i.e. up to 20 minutes) than for sample SE-1. However, there were no memory effects observed in SB-3 like those shown in figure (5.a) for sample SE-1. When the sample SB-3 had been in a dark state for 20 minutes it had returned to its equilibrium condition. Sample SB-3 was very susceptible to optical quenching and the decay back to the dark level could be reduced to about two minutes with exposure to 0.9μ infrared radiation. Optical quenching at $.9\mu$ did not, however, significantly reduce the memory effect shown in figure (5.a) for sample SE-1, although it did reduce considerably the steady state value for the ultrasonic attenuation in the wavelength region of low absorption.

Because of the relatively long time effects it was necessary, when measuring the attenuation as a function of the wavelength of illumination, to scan the spectrum with the

monochromator at a very slow rate. For example on sample SB-3 the wavelength range from 500 m μ to 600 m μ was usually scanned in about four hours. It was felt that sweeps of this duration would result in a steady state condition for each of the wavelengths of light with which the sample came in contact .

It is desirable to obtain the attenuation versus wavelength of light at a number of different ultrasonic frequencies. In order to do this, the α vs λ curves were traced sequentially for each ultrasonic frequency. The results were then superimposed to give a set of curves on one diagram. This procedure requires that the measurements be carried out over a period of about 20 hours, during which time it is essential that all conditions remain exactly the same for each frequency run. For example, long term stability in the lamp and in the ultrasonic equipment is very important.

Figure (5.c) shows the results of the attenuation versus wavelength of light for a number of different frequencies in sample SB-3 at room temperature. These curves were taken with the slits on the monochromator set at 0.5mm

Figure 5.c : The attenuation measured in db per one round trip at room temperature of sample SB-3 versus the wavelength of incident light. Curves are taken sequentially at different ultrasonic frequencies. Monochromator slits were set at 0.5mm.

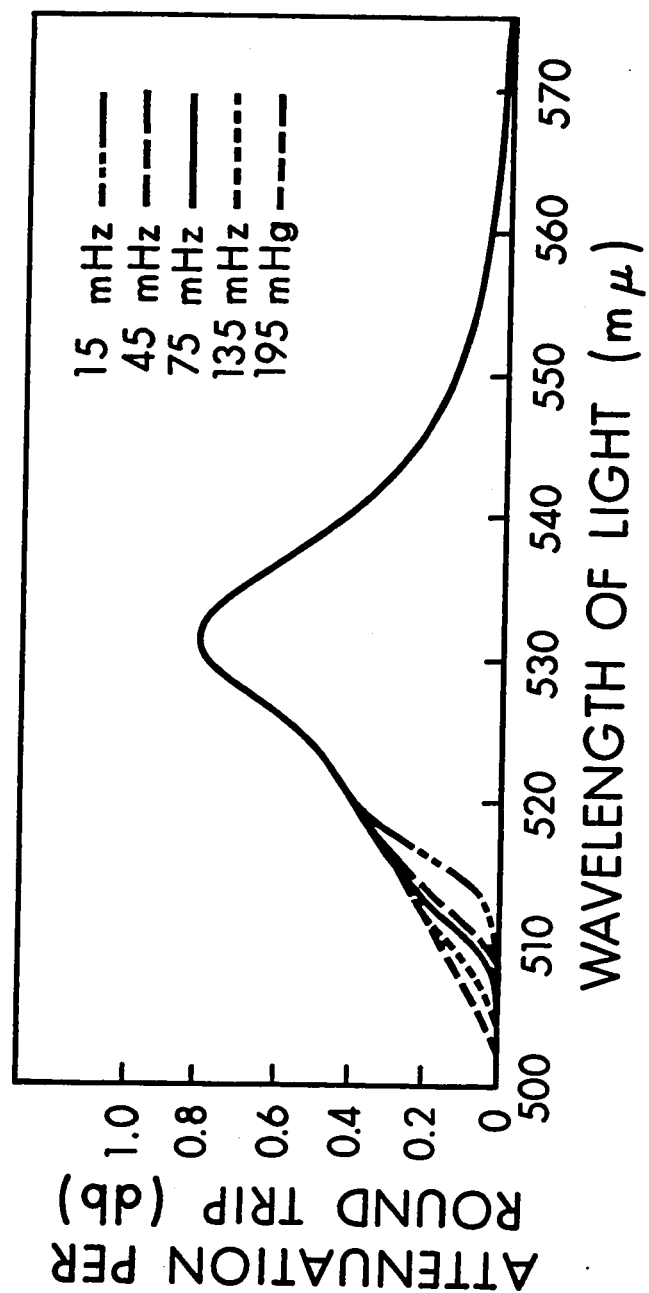


TABLE II

Actual attenuation in db per round trip for the
experimental curves of figure 5. .

λ (m μ)	15 mHz	45 mHz	75 mHz	135 mHz	195 mHz
504	0.000E00	0.000E00	0.000E00	0.000E00	2.000E ⁻⁰²
505	0.000E00	0.000E00	0.000E00	0.000E00	4.000E ⁻⁰²
506	0.000E00	0.000E00	0.000E00	2.000E ⁻⁰²	5.000E ⁻⁰²
507	0.000E00	0.000E00	0.000E00	4.000E ⁻⁰²	8.000E ⁻⁰²
508	0.000E00	0.000E00	1.000E ⁻⁰²	6.000E ⁻⁰²	1.000E ⁻⁰¹
509	0.000E00	0.000E00	3.000E ⁻⁰²	9.000E ⁻⁰²	1.200E ⁻⁰¹
510	0.000E00	2.000E ⁻⁰²	6.000E ⁻⁰²	1.200E ⁻⁰¹	1.400E ⁻⁰¹
511	1.000E ⁻⁰²	4.000E ⁻⁰²	1.000E ⁻⁰¹	1.600E ⁻⁰¹	1.700E ⁻⁰¹
512	2.000E ⁻⁰²	1.000E ⁻⁰¹	1.400E ⁻⁰¹	1.900E ⁻⁰¹	1.900E ⁻⁰¹
513	4.000E ⁻⁰²	1.400E ⁻⁰¹	1.900E ⁻⁰¹	2.100E ⁻⁰¹	2.100E ⁻⁰¹
514	8.000E ⁻⁰²	2.000E ⁻⁰¹	2.200E ⁻⁰¹	2.300E ⁻⁰¹	2.300E ⁻⁰¹
515	1.200E ⁻⁰¹	2.400E ⁻⁰¹	2.500E ⁻⁰¹	2.500E ⁻⁰¹	2.500E ⁻⁰¹
516	1.800E ⁻⁰¹	2.800E ⁻⁰¹	2.800E ⁻⁰¹	2.800E ⁻⁰¹	2.800E ⁻⁰¹
517	2.500E ⁻⁰¹	3.100E ⁻⁰¹	3.100E ⁻⁰¹	3.100E ⁻⁰¹	3.100E ⁻⁰¹
518	3.000E ⁻⁰¹	3.300E ⁻⁰¹	3.300E ⁻⁰¹	3.300E ⁻⁰¹	3.300E ⁻⁰¹
519	3.400E ⁻⁰¹	3.600E ⁻⁰¹	3.600E ⁻⁰¹	3.600E ⁻⁰¹	3.600E ⁻⁰¹
520	3.800E ⁻⁰¹	3.900E ⁻⁰¹	3.900E ⁻⁰¹	3.900E ⁻⁰¹	3.900E ⁻⁰¹

TABLE III

Reduced attenuation for the experimental curves
of figure 5.a .

λ (m μ)	15 mHz	45 mHz	75 mHz	135 mHz	195 mHz
504	0.000E00	0.000E00	0.000E00	0.000E00	4.032E ⁻⁰⁵
505	0.000E00	0.000E00	0.000E00	0.000E00	8.065E ⁻⁰⁵
506	0.000E00	0.000E00	0.000E00	5.825E ⁻⁰⁵	1.008E ⁻⁰⁴
507	0.000E00	0.000E00	0.000E00	1.165E ⁻⁰⁴	1.613E ⁻⁰⁴
508	0.000E00	0.000E00	5.242E ⁻⁰⁵	1.747E ⁻⁰⁴	2.016E ⁻⁰⁴
509	0.000E00	0.000E00	1.573E ⁻⁰⁴	2.621E ⁻⁰⁴	2.419E ⁻⁰⁴
510	0.000E00	1.747E ⁻⁰⁴	3.145E ⁻⁰⁴	3.495E ⁻⁰⁴	2.823E ⁻⁰⁴
511	2.621E ⁻⁰⁴	3.495E ⁻⁰⁴	5.242E ⁻⁰⁴	4.660E ⁻⁰⁴	3.428E ⁻⁰⁴
512	5.242E ⁻⁰⁴	8.737E ⁻⁰⁴	7.339E ⁻⁰⁴	5.533E ⁻⁰⁴	3.831E ⁻⁰⁴
513	1.048E ⁻⁰³	1.223E ⁻⁰³	9.960E ⁻⁰⁴	6.116E ⁻⁰⁴	4.234E ⁻⁰⁴
514	2.097E ⁻⁰³	1.747E ⁻⁰³	1.153E ⁻⁰³	6.698E ⁻⁰⁴	4.637E ⁻⁰⁴
515	3.145E ⁻⁰³	2.097E ⁻⁰³	1.311E ⁻⁰³	7.281E ⁻⁰⁴	5.041E ⁻⁰⁴
516	4.718E ⁻⁰³	2.446E ⁻⁰³	1.468E ⁻⁰³	8.154E ⁻⁰⁴	5.645E ⁻⁰⁴
517	6.553E ⁻⁰³	2.708E ⁻⁰³	1.625E ⁻⁰³	9.028E ⁻⁰⁴	6.250E ⁻⁰⁴
518	7.863E ⁻⁰³	2.883E ⁻⁰³	1.730E ⁻⁰³	9.611E ⁻⁰⁴	6.654E ⁻⁰⁴
519	8.912E ⁻⁰³	3.145E ⁻⁰³	1.887E ⁻⁰³	1.048E ⁻⁰³	7.258E ⁻⁰⁴
520	9.960E ⁻⁰³	3.407E ⁻⁰³	2.044E ⁻⁰³	1.136E ⁻⁰³	7.863E ⁻⁰⁴

giving a spectral line width of about 5 \AA in the wavelength region shown on the graph. The attenuation is given on the graph in db for one round trip of the sample.

Table II gives values taken from the original curves shown in figure (5.c) for the portion of the spectrum between 500 and 520 $\text{m}\mu$ where frequency effects are observed. Table III gives the values of the ultrasonic attenuation shown in Table II after they have been reduced according to equations (3.5) and (3.12). The values in these two tables will be used later for calculations.

To observe more closely the "blue edge" of the curves on figure (5.c) the gain was increased by an order of magnitude and traces for the spectrum between 505 $\text{m}\mu$ and 522 $\text{m}\mu$ were taken. Figure (5.d) shows these traces for 15 mHz and 45 mHz; all conditions are essentially the same as in figure (5.c) although a direct comparison of the two figures is probably not valid as they were done at different times. Table IV and Table V give numerical values for the actual measured attenuation and the reduced attenuation taken from the original traces of figure (5.d).

Figure 5.d : Magnified view of the blue edge at room temperature in sample SB-3. Monochromator slits are set at 0.5mm. Dashed curves are amplified $\times 2$ over scale factor.

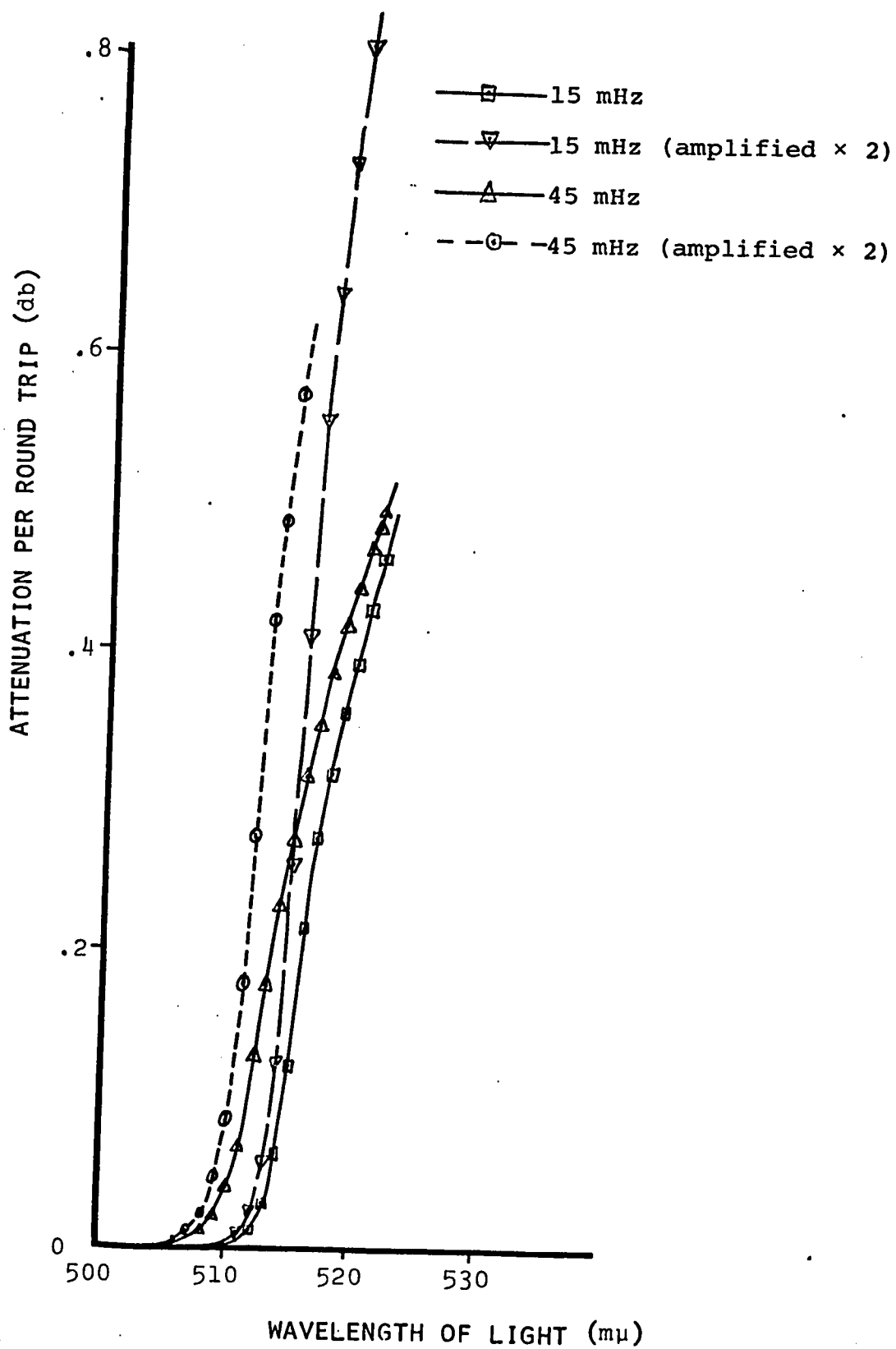


TABLE IV

Actual attenuation in db per round trip for
the experimental curves of figure 5.b .

λ (m μ)	15 mHz	15 mHz	45 mHz	45 mHz
506	0.000E00	0.000E00	3.000E-03	2.000E-03
507	0.000E00	0.000E00	5.000E-03	6.000E-03
508	0.000E00	0.000E00	1.100E-02	1.200E-02
509	0.000E00	0.000E00	2.400E-02	2.200E-02
510	0.000E00	0.000E00	4.200E-02	4.000E-02
511	5.000E-03	4.000E-03	8.800E-02	6.800E-02
512	1.200E-02	1.200E-02	1.380E-01	1.280E-01
513	2.800E-02	3.000E-02	2.100E-01	1.760E-01
514	6.200E-02	6.200E-02	2.440E-01	2.280E-01
515	1.280E-01	1.220E-01	2.860E-01	2.740E-01
516	2.060E-01	2.140E-01	0.000E00	3.160E-01
517	2.780E-01	2.740E-01	0.000E00	3.500E-01
518	3.200E-01	3.180E-01	0.000E00	3.840E-01
519	3.640E-01	3.580E-01	0.000E00	4.180E-01
520	4.020E-01	3.920E-01	0.000E00	4.420E-01
521	0.000E00	4.280E-01	0.000E00	4.680E-01
522	0.000E00	4.620E-01	0.000E00	4.920E-01

TABLE V

Reduced attenuation for the experimental
curves of figure 5.b .

λ (m μ)	15 mHz	15 mHz	45 mHz	45 mHz
506	0.000E00	0.000E00	2.621E ⁻⁰⁵	1.747E ⁻⁰⁵
507	0.000E00	0.000E00	4.368E ⁻⁰⁵	5.242E ⁻⁰⁵
508	0.000E00	0.000E00	9.611E ⁻⁰⁵	1.048E ⁻⁰⁴
509	0.000E00	0.000E00	2.097E ⁻⁰⁴	1.922E ⁻⁰⁴
510	0.000E00	0.000E00	3.670E ⁻⁰⁴	3.495E ⁻⁰⁴
511	1.311E ⁻⁰⁴	1.048E ⁻⁰⁴	7.688E ⁻⁰⁴	5.941E ⁻⁰⁴
512	3.145E ⁻⁰⁴	3.145E ⁻⁰⁴	1.206E ⁻⁰³	1.118E ⁻⁰³
513	7.339E ⁻⁰⁴	7.863E ⁻⁰⁴	1.835E ⁻⁰³	1.538E ⁻⁰³
514	1.625E ⁻⁰³	1.625E ⁻⁰³	2.132E ⁻⁰³	1.992E ⁻⁰³
515	3.355E ⁻⁰³	3.198E ⁻⁰³	2.499E ⁻⁰³	2.394E ⁻⁰³
516	5.399E ⁻⁰³	5.609E ⁻⁰³	0.000E00	2.761E ⁻⁰³
517	7.287E ⁻⁰³	7.182E ⁻⁰³	0.000E00	3.058E ⁻⁰³
518	8.387E ⁻⁰³	8.335E ⁻⁰³	0.000E00	3.355E ⁻⁰³
519	9.541E ⁻⁰³	9.383E ⁻⁰³	0.000E00	3.652E ⁻⁰³
520	1.054E ⁻⁰²	1.027E ⁻⁰²	0.000E00	3.862E ⁻⁰³
521	0.000E00	1.122E ⁻⁰²	0.000E00	4.089E ⁻⁰³
522	0.000E00	1.211E ⁻⁰²	0.000E00	4.299E ⁻⁰³

Curves like those of figure (5.c) were taken on sample SB-3 at a higher light intensity by opening the monochromator slits to 1.0mm. These are shown in figure (5.e). The procedure of widening the slits will increase the spectral line width to about 10 \AA and increase the overall light power in the beam by a factor of four. The curves of figure (5.e) show how the increased intensity puts the portion of the curve at $530 \text{ m}\mu$ into a region that is frequency dependent, whereas in figure (5.c) at the lower intensity this was not the case. Tables VI and VII give numerical values from figure (5.e) for the actual and reduced attenuation.

Altering the ultrasonic frequency changes the conductivity parameter ζ in the equations developed in Chapter 3. The conductivity parameter ζ can also be altered by changing the intensity of the light. If the conductivity is linear with intensity incident on the sample, then α vs λ curves at different light intensities will give curves that should satisfy the equations developed in Chapter 3.

Figure 5.e : The attenuation measured in db per round trip at room temperature of sample SB-3 versus the wavelength of incident light. Curves are taken sequentially at different frequencies. Monochromator slits were set at 1.0mm.

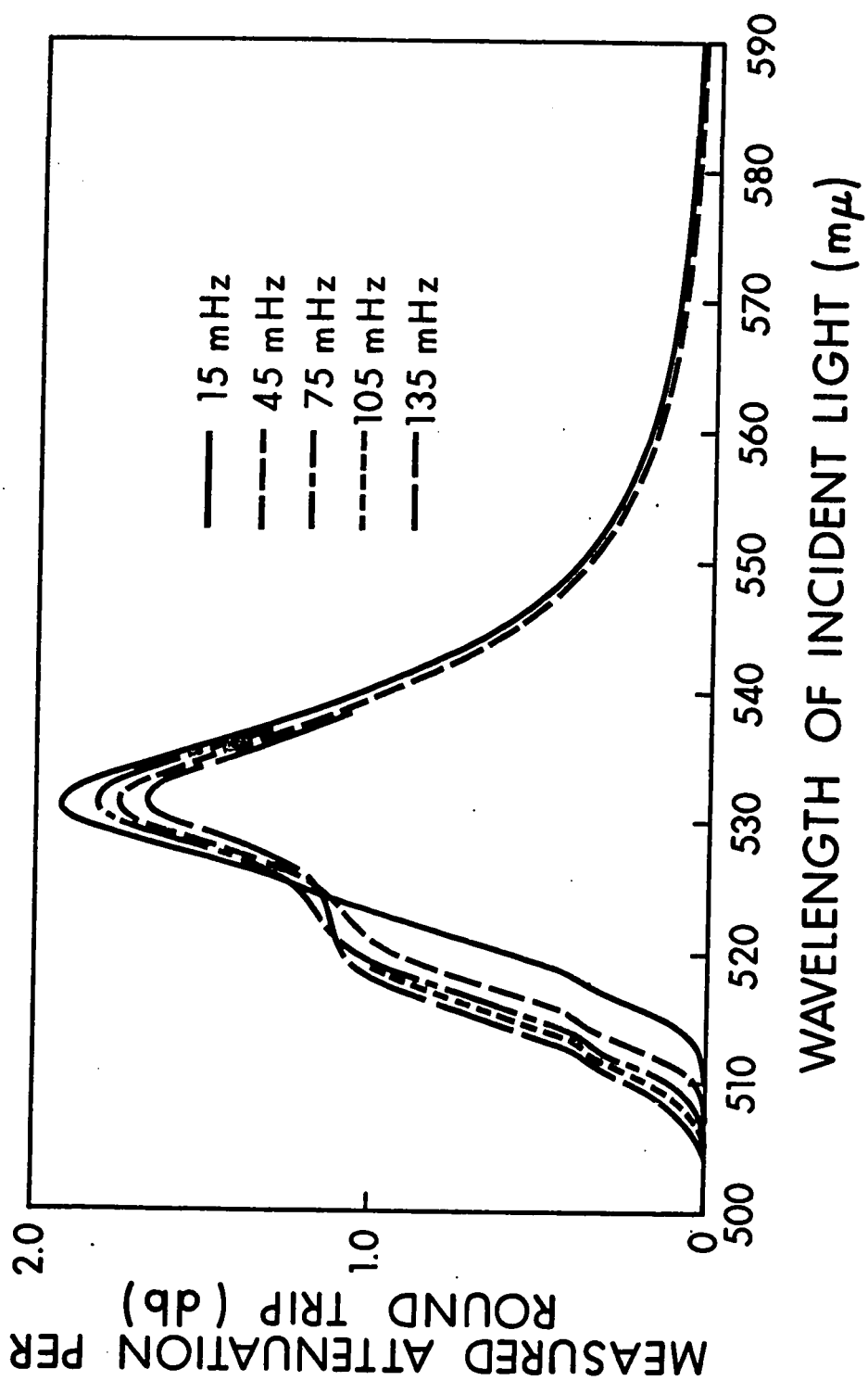


TABLE VI

Actual attenuation in db per round trip for the
experimental curves of figure 5.c .

λ (m μ)	15 mHz	45 mHz	75 mHz	105 mHz	135 mHz
506	0.000E00	0.000E00	1.000E-02	2.000E-02	3.000E-02
507	0.000E00	0.000E00	2.000E-02	4.000E-02	6.000E-02
508	0.000E00	1.000E-02	4.000E-02	7.000E-02	1.100E-01
509	0.000E00	2.000E-02	7.000E-02	1.100E-01	1.600E-01
510	0.000E00	4.000E-02	1.100E-01	1.700E-01	2.300E-01
511	1.000E-02	8.000E-02	1.900E-01	2.400E-01	3.000E-01
512	1.500E-02	1.600E-01	2.800E-01	3.100E-01	3.600E-01
513	3.500E-02	2.500E-01	3.400E-01	3.700E-01	4.600E-01
514	7.000E-02	3.200E-01	4.300E-01	4.800E-01	5.700E-01
515	1.500E-01	3.900E-01	5.200E-01	5.900E-01	6.700E-01
516	2.300E-01	4.800E-01	6.400E-01	7.100E-01	7.800E-01
517	3.200E-01	6.000E-01	7.600E-01	8.200E-01	9.000E-01
518	3.800E-01	7.200E-01	8.900E-01	9.100E-01	9.800E-01
519	4.700E-01	8.300E-01	9.800E-01	1.010E00	1.040E00
520	5.800E-01	9.200E-01	1.050E00	0.000E00	1.080E00
521	6.200E-01	9.900E-01	1.095E00	0.000E00	1.100E00
522	8.500E-01	1.040E00	1.130E00	0.000E00	1.110E00
523	9.800E-01	1.070E00	1.155E00	0.000E00	1.120E00
524	1.090E00	1.110E00	1.180E00	0.000E00	1.130E00
525	1.190E00	1.170E00	1.230E00	0.000E00	1.150E00
526	1.320E00	1.240E00	1.290E00	0.000E00	1.200E00
527	1.450E00	1.360E00	1.380E00	0.000E00	1.270E00
528	1.600E00	1.470E00	1.470E00	0.000E00	1.350E00
529	1.740E00	1.580E00	1.600E00	0.000E00	1.440E00
530	1.860E00	1.690E00	1.720E00	0.000E00	1.580E00
531	1.920E00	1.730E00	1.800E00	0.000E00	1.650E00
532	1.900E00	1.730E00	1.800E00	0.000E00	1.660E00
533	1.820E00	1.670E00	1.760E00	0.000E00	1.610E00
534	1.730E00	1.580E00	1.650E00	0.000E00	1.520E00
535	1.600E00	1.480E00	1.540E00	0.000E00	1.420E00

TABLE VI

Actual attenuation in db per round trip for the
experimental curves of figure 5.c .

λ (m μ)	15 mHz	45 mHz	75 mHz	105 mHz	135 mHz
506	0.000E00	0.000E00	1.000E-02	2.000E-02	3.000E-02
507	0.000E00	0.000E00	2.000E-02	4.000E-02	6.000E-02
508	0.000E00	1.000E-02	4.000E-02	7.000E-02	1.100E-01
509	0.000E00	2.000E-02	7.000E-02	1.100E-01	1.600E-01
510	0.000E00	4.000E-02	1.100E-01	1.700E-01	2.300E-01
511	1.000E-02	8.000E-02	1.900E-01	2.400E-01	3.000E-01
512	1.500E-02	1.600E-01	2.800E-01	3.100E-01	3.600E-01
513	3.500E-02	2.500E-01	3.400E-01	3.700E-01	4.600E-01
514	7.000E-02	3.200E-01	4.300E-01	4.800E-01	5.700E-01
515	1.500E-01	3.900E-01	5.200E-01	5.900E-01	6.700E-01
516	2.300E-01	4.800E-01	6.400E-01	7.100E-01	7.800E-01
517	3.200E-01	6.000E-01	7.600E-01	8.200E-01	9.000E-01
518	3.800E-01	7.200E-01	8.900E-01	9.100E-01	9.800E-01
519	4.700E-01	8.300E-01	9.800E-01	1.010E00	1.040E00
520	5.800E-01	9.200E-01	1.050E00	0.000E00	1.080E00
521	6.200E-01	9.900E-01	1.095E00	0.000E00	1.100E00
522	8.500E-01	1.040E00	1.130E00	0.000E00	1.110E00
523	9.800E-01	1.070E00	1.155E00	0.000E00	1.120E00
524	1.090E00	1.110E00	1.180E00	0.000E00	1.130E00
525	1.190E00	1.170E00	1.230E00	0.000E00	1.150E00
526	1.320E00	1.240E00	1.290E00	0.000E00	1.200E00
527	1.450E00	1.360E00	1.380E00	0.000E00	1.270E00
528	1.600E00	1.470E00	1.470E00	0.000E00	1.350E00
529	1.740E00	1.580E00	1.600E00	0.000E00	1.440E00
530	1.860E00	1.690E00	1.720E00	0.000E00	1.580E00
531	1.920E00	1.730E00	1.800E00	0.000E00	1.650E00
532	1.900E00	1.730E00	1.800E00	0.000E00	1.660E00
533	1.820E00	1.670E00	1.760E00	0.000E00	1.610E00
534	1.730E00	1.580E00	1.650E00	0.000E00	1.520E00
535	1.600E00	1.480E00	1.540E00	0.000E00	1.420E00

TABLE VII

Reduced attenuation for the experimental curves
of figure 5.c .

λ (m μ)	15 mHz	45 mHz	75 mHz	105 mHz	135 mHz
506	0.000E00	0.000E00	5.242E-05	7.489E-05	8.737E-05
507	0.000E00	0.000E00	1.048E-04	1.498E-04	1.747E-04
508	0.000E00	8.737E-05	2.097E-04	2.621E-04	3.204E-04
509	0.000E00	1.747E-04	3.670E-04	4.119E-04	4.660E-04
510	0.000E00	3.495E-04	5.766E-04	6.365E-04	6.698E-04
511	2.621E-04	6.990E-04	9.960E-04	8.987E-04	8.737E-04
512	3.932E-04	1.398E-03	1.468E-03	1.161E-03	1.048E-03
513	9.174E-04	2.184E-03	1.782E-03	1.385E-03	1.340E-03
514	1.835E-03	2.796E-03	2.254E-03	1.797E-03	1.660E-03
515	3.932E-03	3.407E-03	2.726E-03	2.209E-03	1.951E-03
516	6.028E-03	4.194E-03	3.355E-03	2.659E-03	2.272E-03
517	8.387E-03	5.242E-03	3.984E-03	3.070E-03	2.621E-03
518	9.960E-03	6.291E-03	4.666E-03	3.407E-03	2.854E-03
519	1.232E-02	7.252E-03	5.137E-03	3.782E-03	3.029E-03
520	1.520E-02	8.038E-03	5.504E-03	0.000E00	3.145E-03
521	1.625E-02	8.650E-03	5.740E-03	0.000E00	3.204E-03
522	2.228E-02	9.086E-03	5.924E-03	0.000E00	3.233E-03
523	2.569E-02	9.349E-03	6.055E-03	0.000E00	3.262E-03
524	2.857E-02	9.698E-03	6.186E-03	0.000E00	3.291E-03
525	3.119E-02	1.022E-02	6.448E-03	0.000E00	3.349E-03
526	3.460E-02	1.083E-02	6.762E-03	0.000E00	3.495E-03
527	3.801E-02	1.188E-02	7.234E-03	0.000E00	3.699E-03
528	4.194E-02	1.284E-02	7.706E-03	0.000E00	3.932E-03
529	4.561E-02	1.380E-02	8.387E-03	0.000E00	4.194E-03
530	4.875E-02	1.477E-02	9.017E-03	0.000E00	4.601E-03
531	5.032E-02	1.511E-02	9.436E-03	0.000E00	4.805E-03
532	4.980E-02	1.511E-02	9.436E-03	0.000E00	4.834E-03
533	4.770E-02	1.459E-02	9.226E-03	0.000E00	4.689E-03
534	4.534E-02	1.380E-02	8.650E-03	0.000E00	4.427E-03
535	4.194E-02	1.293E-02	8.073E-03	0.000E00	4.135E-03

Figure (5.f) gives the attenuation versus the wavelength of light for three different intensities. Neutral density filters were used to alter the intensity of the light without changing the monochromator settings. If the light intensity for curve (1) is taken as I_0 , then curves (2) and (3) will have incident light intensities of $.31 I_0$ and $.10 I_0$ respectively.

Some measurements on sample SB-3 were carried out at low temperatures. For the room temperature measurements the attenuation versus wavelength curves were made over a period of about four hours in order to ensure that a steady state condition was established for each wavelength. However, the long times required for these runs are not convenient for low temperature measurements because long term temperature stability is difficult to achieve except at the temperatures of the surrounding bath. As a result a number of curves were made only in a small part of the spectrum which we will term the "blue edge". This region at room temperature is between about 505 $m\mu$ and 515 $m\mu$. A steady state condition in this blue edge region is attained in about two minutes as

Figure 5.f : The attenuation measured in db per round trip at room temperature of sample SB-3 versus the wavelength of incident light. Curves represent three different intensities of light, i.e. I_0 , $I_0 10^{-0.5} = .31 I_0$ and $I_0 10^{-1.0} = 0.10 I_0$. Curves #1, #2, and #3 are taken on the more sensitive scale shown in the diagram. Ultrasonic frequency used for measurements was 10 MHz with monochromator slits set at 1.0mm.

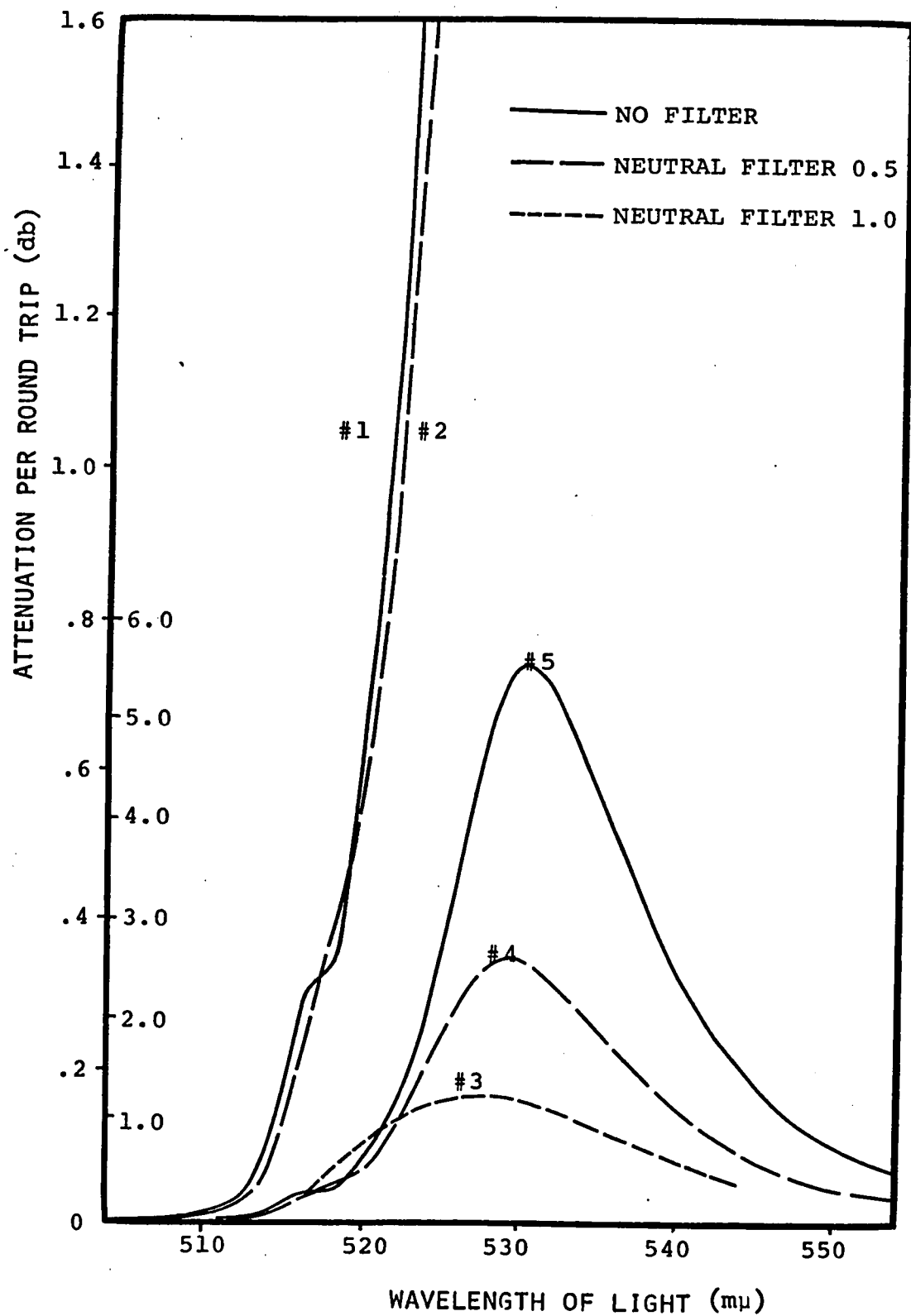


TABLE VIII

Actual attenuation for the experimental curves
in figure 5.f taken at different intensities.

λ (m μ)	I_0	$0.31 I_0$	$0.10 I_0$	I_0	$0.31 I_0$
510	$5.000E^{-03}$	$5.000E^{-03}$	$0.000E00$	$0.000E00$	$0.000E00$
511	$1.000E^{-02}$	$1.000E^{-02}$	$0.000E00$	$0.000E00$	$0.000E00$
512	$2.400E^{-02}$	$1.600E^{-02}$	$0.000E00$	$0.000E00$	$0.000E00$
513	$4.800E^{-02}$	$3.000E^{-02}$	$0.000E00$	$0.000E00$	$0.000E00$
514	$1.000E^{-01}$	$6.000E^{-02}$	$0.000E00$	$0.000E00$	$0.000E00$
515	$1.800E^{-01}$	$1.300E^{-01}$	$1.200E^{-02}$	$0.000E00$	$0.000E00$
516	$2.700E^{-01}$	$2.100E^{-01}$	$2.400E^{-02}$	$0.000E00$	$0.000E00$
517	$3.250E^{-01}$	$3.120E^{-01}$	$4.000E^{-02}$	$0.000E00$	$0.000E00$
518	$3.340E^{-01}$	$3.850E^{-01}$	$6.400E^{-02}$	$0.000E00$	$0.000E00$
519	$4.320E^{-01}$	$4.650E^{-01}$	$8.400E^{-02}$	$0.000E00$	$0.000E00$
520	$6.400E^{-01}$	$5.900E^{-01}$	$1.060E^{-01}$	$0.000E00$	$0.000E00$
521	$8.700E^{-01}$	$8.000E^{-01}$	$1.240E^{-01}$	$0.000E00$	$0.000E00$
522	$1.180E00$	$1.000E00$	$1.360E^{-01}$	$0.000E00$	$0.000E00$
523	$1.600E00$	$1.200E00$	$1.440E^{-01}$	$0.000E00$	$0.000E00$
524	$0.000E00$	$0.000E00$	$0.000E00$	$2.010E00$	$1.510E00$
526	$0.000E00$	$0.000E00$	$0.000E00$	$3.300E00$	$2.100E00$
528	$0.000E00$	$0.000E00$	$0.000E00$	$4.700E00$	$2.500E00$
530	$0.000E00$	$0.000E00$	$0.000E00$	$5.450E00$	$2.800E00$
532	$0.000E00$	$0.000E00$	$0.000E00$	$5.200E00$	$2.400E00$
534	$0.000E00$	$0.000E00$	$0.000E00$	$4.600E00$	$2.020E00$
536	$0.000E00$	$0.000E00$	$0.000E00$	$3.800E00$	$1.680E00$
538	$0.000E00$	$0.000E00$	$0.000E00$	$3.140E00$	$1.360E00$
540	$0.000E00$	$0.000E00$	$0.000E00$	$2.400E00$	$1.100E00$
542	$0.000E00$	$0.000E00$	$0.000E00$	$1.900E00$	$8.900E^{-01}$
544	$0.000E00$	$0.000E00$	$0.000E00$	$1.540E00$	$6.800E^{-01}$

TABLE IX

Reduced attenuation for the experimental curves
in figure 5.f taken at different intensities.

λ (m μ)	I_0	$0.31 I_0$	$0.10 I_0$	I_0	$0.31 I_0$
510	$2.188E^{-05}$	$2.188E^{-05}$	$0.000E00$	$0.000E00$	$0.000E00$
511	$4.376E^{-05}$	$4.376E^{-05}$	$0.000E00$	$0.000E00$	$0.000E00$
512	$1.050E^{-04}$	$7.002E^{-05}$	$0.000E00$	$0.000E00$	$0.000E00$
513	$2.101E^{-04}$	$1.313E^{-04}$	$0.000E00$	$0.000E00$	$0.000E00$
514	$4.376E^{-04}$	$2.626E^{-04}$	$0.000E00$	$0.000E00$	$0.000E00$
515	$7.877E^{-04}$	$5.689E^{-04}$	$5.251E^{-05}$	$0.000E00$	$0.000E00$
516	$1.182E^{-03}$	$9.190E^{-04}$	$1.050E^{-04}$	$0.000E00$	$0.000E00$
517	$1.422E^{-03}$	$1.365E^{-03}$	$1.750E^{-04}$	$0.000E00$	$0.000E00$
518	$1.462E^{-03}$	$1.685E^{-03}$	$2.801E^{-04}$	$0.000E00$	$0.000E00$
519	$1.891E^{-03}$	$2.035E^{-03}$	$3.676E^{-04}$	$0.000E00$	$0.000E00$
520	$2.801E^{-03}$	$2.582E^{-03}$	$4.639E^{-04}$	$0.000E00$	$0.000E00$
521	$3.807E^{-03}$	$3.501E^{-03}$	$5.427E^{-04}$	$0.000E00$	$0.000E00$
522	$5.164E^{-03}$	$4.376E^{-03}$	$5.952E^{-04}$	$0.000E00$	$0.000E00$
523	$7.002E^{-03}$	$5.251E^{-03}$	$6.302E^{-04}$	$0.000E00$	$0.000E00$
524	$0.000E00$	$0.000E00$	$0.000E00$	$8.796E^{-03}$	$6.608E^{-03}$
526	$0.000E00$	$0.000E00$	$0.000E00$	$1.444E^{-02}$	$9.190E^{-03}$
528	$0.000E00$	$0.000E00$	$0.000E00$	$2.057E^{-02}$	$1.094E^{-02}$
530	$0.000E00$	$0.000E00$	$0.000E00$	$2.385E^{-02}$	$1.225E^{-02}$
532	$0.000E00$	$0.000E00$	$0.000E00$	$2.276E^{-02}$	$1.050E^{-02}$
534	$0.000E00$	$0.000E00$	$0.000E00$	$2.013E^{-02}$	$8.840E^{-03}$
536	$0.000E00$	$0.000E00$	$0.000E00$	$1.663E^{-02}$	$7.352E^{-03}$
538	$0.000E00$	$0.000E00$	$0.000E00$	$1.374E^{-02}$	$5.952E^{-03}$
540	$0.000E00$	$0.000E00$	$0.000E00$	$1.050E^{-02}$	$4.814E^{-03}$
542	$0.000E00$	$0.000E00$	$0.000E00$	$8.315E^{-03}$	$3.895E^{-03}$
544	$0.000E00$	$0.000E00$	$0.000E00$	$6.739E^{-03}$	$2.976E^{-03}$

shown by figure (5.b) and hence it was felt that steady state conditions would be displayed in the blue edge region if this portion of the spectrum was scanned in about 15 minutes. Temperature stability over a period of 15 minutes in the temperature range 300°K to 77°K did not prove to be a problem.

Measurements were thus made of the attenuation versus optical wavelength of the blue edge in a 15 minute sweep at a fixed temperature. After the blue edge was scanned, the sample was brought back to the dark level by optical quenching with 0.9μ infrared radiation. The temperature was then changed and the process repeated. Figure (5.g) shows the blue edge as a function of optical wavelengths for a number of temperatures between 300°K and 77°K .

As the sample is cooled, the illumination has its maximum effect on the attenuation at about 250°K . Below this temperature the attenuation due to optical generation of carriers diminishes steadily. Just above liquid nitrogen temperature the photosensitive attenuation starts to drop off significantly, as can be seen in figure (5.g) from

Figure 5.g : Ultrasonic attenuation versus the wavelength of light, showing the shift in the blue edge with temperature measurements, were done using 1.0mm slits on the monochromator and at an ultrasonic frequency of 15 mHz.

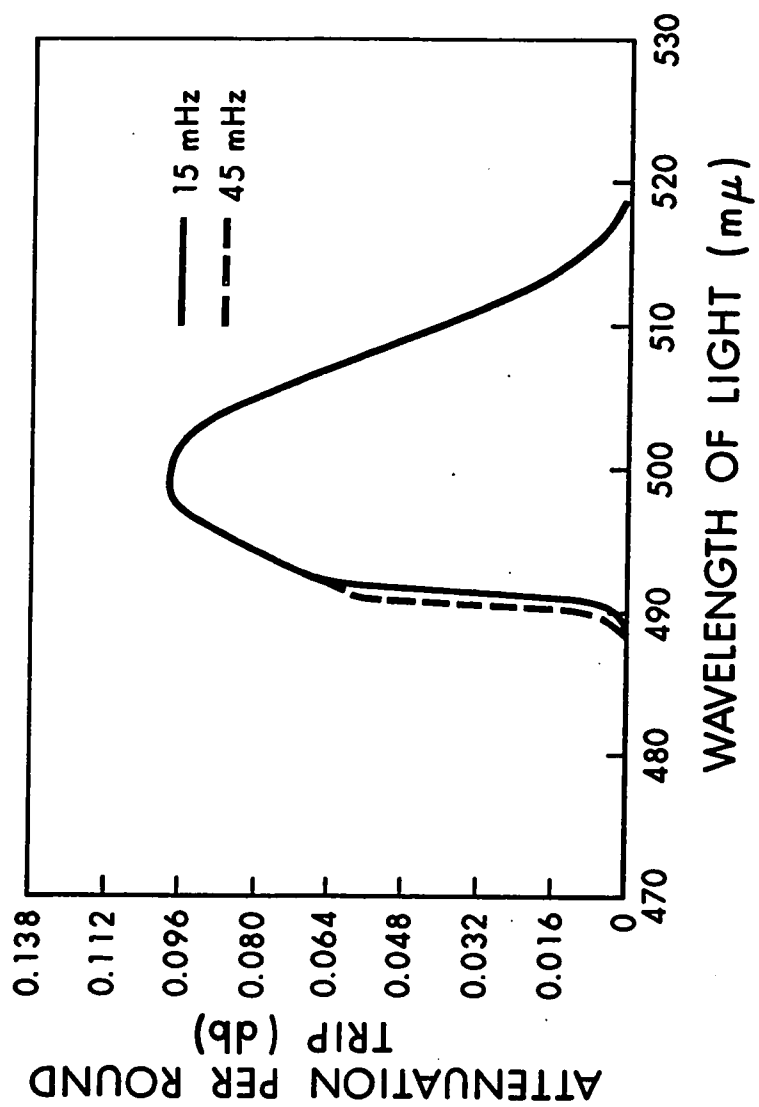
- (1) 297°K
- (2) 285°K
- (3) 274°K
- (4) 262°K
- (5) 253°K
- (6) 230°K
- (7) 205°K
- (8) 180°K
- (9) 166°K
- (10) 138°K
- (11) 131°K
- (12) 103°K
- (13) 96°K
- (14) 92°K
- (15) 80°K

the last two traces shown by #14 and #15.

At liquid nitrogen temperatures the photosensitive ultrasonic attenuation is about one order of magnitude reduced from the room temperature value. Figure (5.h) shows attenuation versus optical wavelength for 15 mHz and 45 mHz at 77°K. Because the photosensitive attenuation is much smaller at liquid nitrogen temperature than at room temperature, noise problems become significant, especially at higher frequencies. Thus in figure (5.h) measurements for 15 mHz and 45 mHz only are shown.

When sample SB-3 was cooled below 77°K the photosensitive attenuation was observed to increase slightly as the temperature changed from 77°K down to 50°K. From 50°K down to liquid helium temperature the photo attenuation dropped off rapidly. At 4.2°K the maximum change that could be observed in the attenuation with light conditions similar to those used to obtain the curves of figure (5.h) was about .002 db at 15 mHz. Under these conditions measurements of the spectral response are nearly impossible with the equipment available

Figure 5.h : Ultrasonic attenuation versus the wavelength of light for 15 mHz and 45 mHz at 77°K. Slits on monochromator are set at 0.5mm.

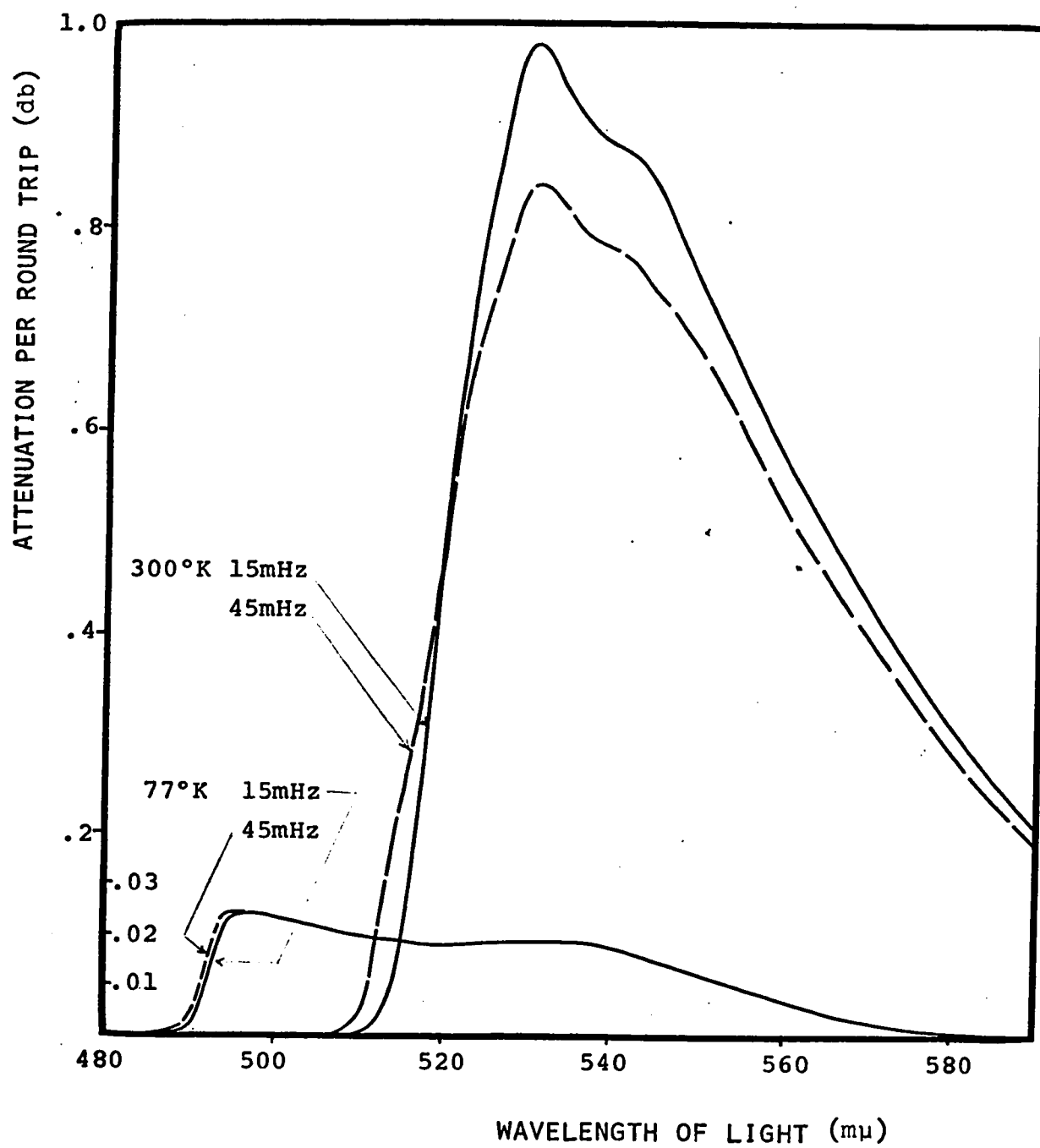


and at the intensities of light that can be obtained. By increasing the slits of the monochromator to 4mm it is possible to get a more intense light beam. In this case the attenuation change due to the light has a maximum of nearly .1 db, but the broad line width of over 100 Å makes the α vs λ curves more difficult to interpret.

Also at low temperatures (i.e. below 200°K) the time response of sample SB-3 becomes much longer and steady state conditions require many hours for weakly absorbed light.

Measurements similar to those carried out on sample SB-3 were also performed on sample SE-1. In this case the much longer response times and the memory effect shown in figure (5.a) can be a problem. Figure (5.i) shows the results of α vs λ curves taken at room temperature and at liquid nitrogen temperature. These traces were taken at the slowest speeds available for sweeping λ with the monochromator, namely about four hours for a sweep of the wavelength region shown in figure (5.i). Because of the long memory effects and times required to reach a steady state, these

Figure 5.i : Ultrasonic attenuation in sample SE-1 versus wavelength of incident light. Curves are shown for ultrasonic frequencies of 15 mHz and 45 mHz. Both room temperature results and liquid nitrogen results are shown. Monochromator slits were set at 1.0mm.



curves are probably only valid in the blue edge region. However, they do show a wavelength region of photosensitivity which is much broader than in sample SB-3. At 77°K the photosensitive attenuation is reduced by nearly two orders of magnitude compared with the room temperature results.

2) Observations on Weak Photoconductors

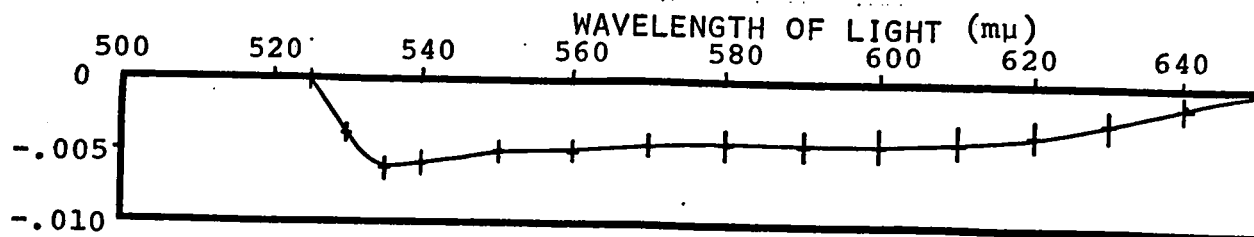
The weak photoconductors had in general faster response times than was the case with the strong photoconductors. However, the lower photosensitive ultrasonic attenuation observed meant that the measurements had to be made on the most sensitive scales of the equipment where noise levels can be a problem.

Figure (5.j) shows α vs λ traces for three of the weak samples. In these traces, the light intensity was made as high as possible by widening the slit widths to 4mm. The photosensitive attenuation in samples SR-1 and SR-2 was just measureable at the high optical intensities used. Sample SB-2 showed a much stronger effect, although when the monochromator slits were reduced to give a narrower line width, the attenuation

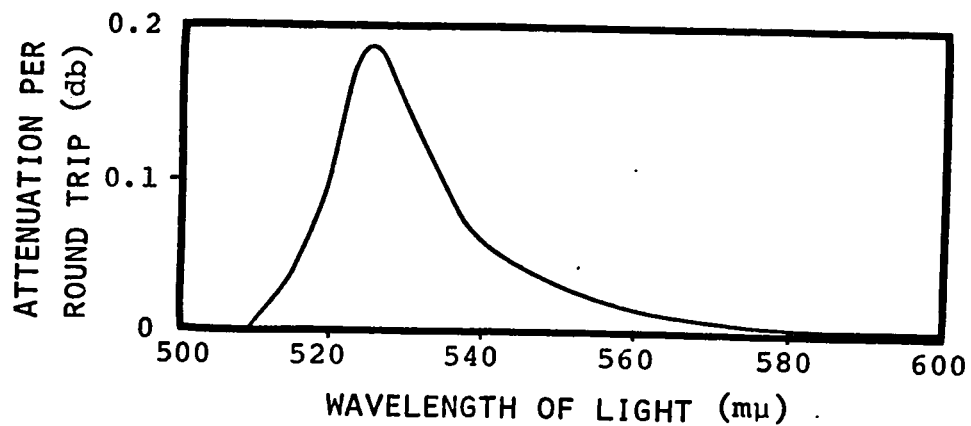
Figure 5.j : The ultrasonic attenuation measured for one round trip of the sample versus wavelength of incident light is shown for three weakly photoconducting samples at room temperature.

- 1) Sample SR-2 with monochromator slits set at 4.0mm. Measurements were the same at both 7 mHz and 21 mHz. Dark conductivity in SR-2 is about $10^{-3}(\text{ohm cm})^{-1}$ and the small increase in conductivity due to light causes the attenuation relative to the dark level to be negative.
- 2) Sample SB-2 with monochromator slits set at 4.0mm. Measurement done at 10 mHz.
- 3) Sample SR-1 with monochromator slits set at 4.0mm. Results are the same within experimental error for both 15 mHz and 45 mHz.

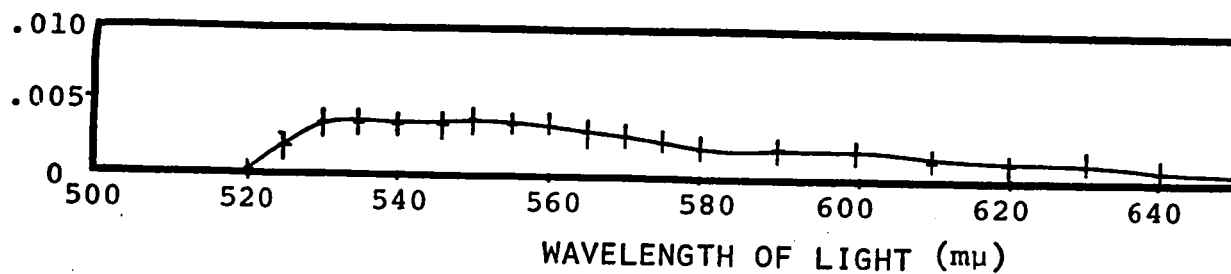
(1)



(2)



(3)



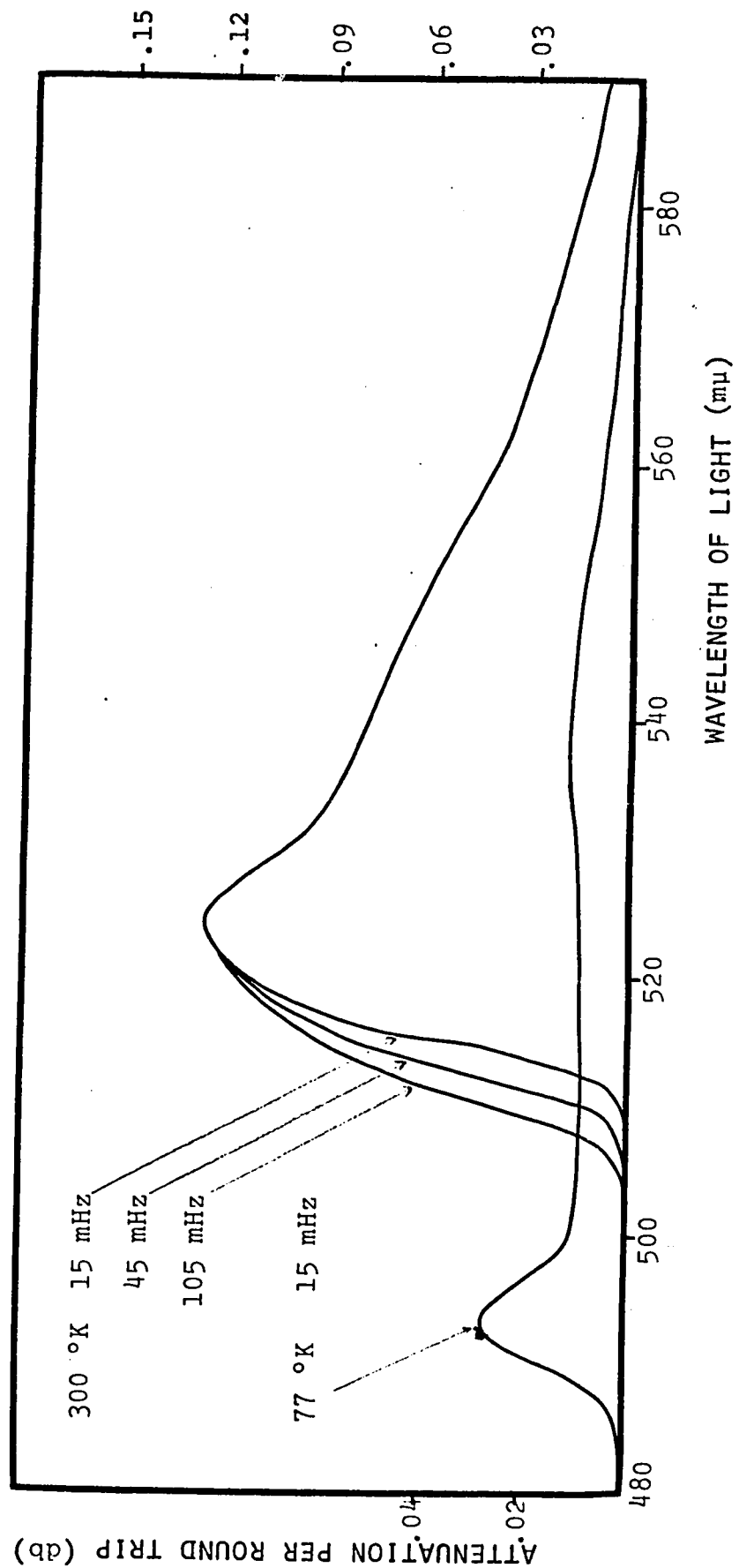
changes that had to be measured were in the .001 db to .01 db range where noise is a problem.

Each of the curves of figure (5.j) were measured at the fundamental frequency and first harmonic frequency of the transducer and no difference was found in the two traces. The fact no frequency dependence was observed on the blue edge was probably due to the broad line width of the monochromator when the slits were wide.

Sample SB-00 showed a more significant photosensitive attenuation than the other weak samples. Room temperature measurements of the α vs λ curves are shown in figure (5.k) for three different ultrasonic frequencies. The monochromator slits were set at 1.0mm for these curves so that the resolution is of the order 10 \AA .

When sample SB-00 was cooled to liquid nitrogen temperature the photosensitive attenuation decreased considerably as was the case with other samples. Figure (5.k) also shows the α vs λ curve for sample SB-00 at 77°K where the monochromator slits were set at 4mm to increase the beam intensity.

Figure 5.k : Ultrasonic attenuation versus wavelength of incident light in sample SB-00. Monochromator slits are set at 1.0mm for the three room temperature curves and at 77°K the slits were set at 4.0mm.



3) Intensity Profile of Monochromator

The Xenon lamp used for the light source was only regulated with respect to the current flowing through the lamp. Therefore, the intensity that will emerge from the monochromator will not necessarily be constant with the wavelength. In order that corrections can be made to the calculations, the intensity profile of the monochromator output was measured. Figure (5.1) shows this profile, where the number of photons per unit time are plotted versus the wavelength. Table X gives numerical values for the curve on figure (5.1).

Figure 5.1 : Profile of the light output in number of photons per unit time from the monochromator at different wavelengths.

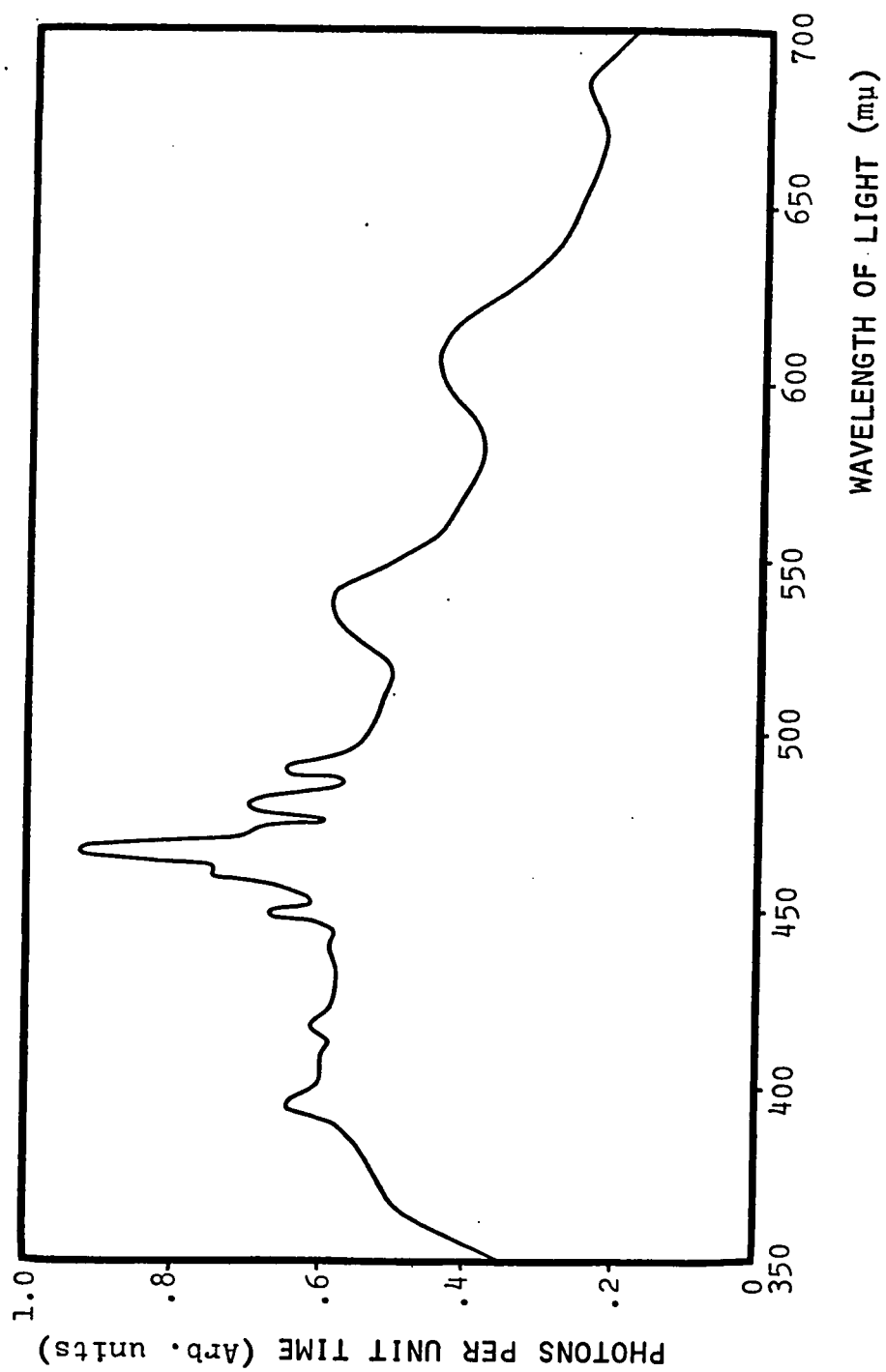


TABLE X
Intensity Normalization

λ (m μ)	Normalization Factor
500	.918
505	.895
510	.884
511	.879
512	.876
513	.871
514	.864
515	.857
516	.852
517	.850
518	.849
519	.849
520	.850
521	.857
522	.864
523	.884
524	.898
525	.912
526	.925
527	.939
528	.949
529	.961
530	.973
531	.980
532	.986
533	.993
534	.997
535	1.000
540	.993
545	.908
550	.833

CHAPTER 6

Calculations and Discussions

Of the CdS samples available for measuring the photosensitive ultrasonic attenuation, sample SB-3 was by far the most useful. That is to say, sample SB-3 had a relatively large photosensitive attenuation effect combined with response times that could be tolerated experimentally. As a result most of the measurements were carried out on this sample. The process of polishing and mounting the transducer was repeated several times in order to insure that the results obtained did not originate with errors in sample preparation. It was felt therefore, that the results obtained on SB-3 would be most suitable for calculations and an attempt was made to fit the data to the theory outlined in Chapter 3.

Experimental measurements of the reduced attenuation y at two different frequencies will give two equations in the two unknowns x (the modified absorption parameter) and ζ (the conductivity parameter). If these two equations can be simultaneously solved, the values of both x and

ζ can be obtained. A number of computer programs (c.f. Appendix E) were written to solve these two equations by numerical iterative techniques.

The experimental data presented in figures 5.c, 5.d, and 5.e were used for computations of x and ζ . These data are presented in their most useful form as the reduced attenuation in the tables of III, V and VII. Two of the tables give values of the reduced attenuation for five different frequencies and it is therefore possible to enter many combinations of two frequencies for computation. The results for the optical absorption coefficient $\kappa = x/d$ are given in the tables XI, XII and XIII. Blank spots occur in the tables when no unique solution for x and ζ could be found. As was discussed in Chapter 3, unique solutions for both x and ζ are only possible when the values of the reduced attenuations do not lie on the asymptotes of the theoretical curves in figure 3.d. The results for optical wavelengths longer than 520 m μ (for the case of table XI) or 525 m μ (for the case of table XIII) fall into this category.

Experimental values of the reduced attenuation are subject to a 20% to 30% error

TABLE XI

The optical absorption coefficient $\kappa(\text{cm}^{-1})$ calculated from the reduced attenuation in table III.

$\lambda(\text{m}\mu)$	$h\nu(\text{eV})$	15,45	15,75	15,135	15,195	45,75	45,135	45,195	75,135	75,195
511	2.426								5190	4590
512	2.421					2790	2790	2790	2990	2600
513	2.417		2990			2000	1640	1640	1300	1160
514	2.412	1370	1300	1260	1260	757	735	735	759	639
515	2.407	818	778	759	757	419	339	339		
516	2.403	459	439	419	419					
517	2.398	240	240	220	220					
518	2.393	138	140	132	131					
519	2.389	95	94	92	92					
520	2.384	60	56	56	56					

TABLE XII

The optical absorption coefficient $\kappa(\text{cm}^{-1})$ calculated from the reduced attenuation in table V.

$\lambda(\text{m}\mu)$	$h\nu(\text{eV})$	$\kappa(\text{cm}^{-1})$
515	2.407	858
516	2.403	359
517	2.398	240
518	2.393	182
519	2.389	146
520	2.384	120
521	2.380	95
522	2.375	74

TABLE XIII

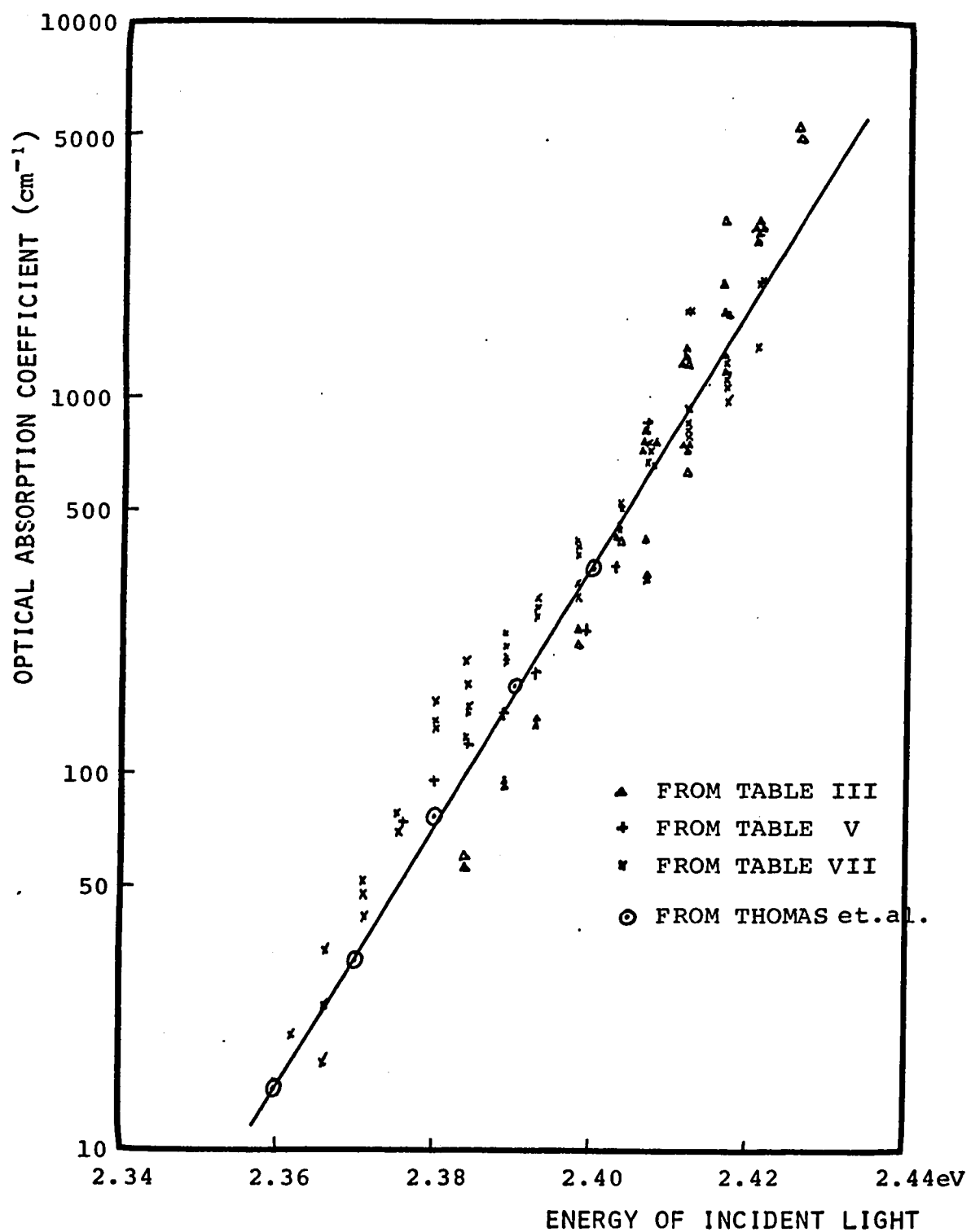
The optical absorption coefficient $\kappa(\text{cm}^{-1})$ calculated from the reduced attenuation in table VII.

$\lambda(\text{m}\mu)$	$h\nu(\text{eV})$	15,45	15,75	15,105	15,135	45,75	45,105	45,135	75,135
512	2.421						2000	2000	1360
513	2.417					1060	998	1120	1220
514	2.412			1700	1700	818	798	858	934
515	2.407	739	739	739	739	659	660	679	737
516	2.403	439	460	460	459	535	519	535	531
517	2.398	299	299	319	320	399	377	399	419
518	2.393	260	260	260	260	299	279	299	260
519	2.389	200	200	200	200	240	220	220	200
520	2.384	146	150		150	200		174	120
521	2.380	136	138		136	156		133	
522	2.375	70	78		74				
523	2.371	42	52		48				
524	2.366	17	34		24				

due to the method used to obtain the curves at different frequencies. Also the computer programs, that were used to solve the equations, can introduce an error in the results as high as 20% since it was only possible to carry out the search for x and ζ to about two significant figures without consuming excessive amounts of computer time. Furthermore, the values of x and ζ for the input data that are being considered lie in a sensitive region where the reduced attenuations are near the theoretical asymptotes and hence any error in the input data is magnified. As a result the calculated values for the absorption coefficient κ can be subject to rather large errors.

The optical absorption coefficients in tables XI, XII and XIII are presented in graphic form on figure 6.a as a function of the incident photon energy. Superimposed on this figure are five points taken from the room temperature results published by Thomas, Hopfield and Power (1960) of the optical absorption coefficient in CdS. A straight line is placed through these points which shows that the results calculated from the ultrasonic measurements are consistent with the

Figure 6.a : The calculated values for the optical absorption coefficient taken from tables XI, XII and XIII and plotted against energy of incident light. Points enclosed by circles are taken from results of Thomas (1960).



results of Thomas et. al. even though they fluctuate about their results considerably. It is also of interest to note that the results shown in figure 6.a give values for κ which extend up the band edge by nearly one order of magnitude compared with the results obtained from the more conventional optical methods used by Thomas.

The conductivity parameter ζ was also obtained from the calculations. These results are presented in tables XIV, XV and XVI and correspond respectively to the experimental results presented in figure 5.c, 5.d and 5.e. The values of ζ are taken from table XVI and plotted against wavelength of the incident light in figure 6.b. The computed values for ζ only go out in wavelength to 524 m μ , after that unique solutions for x and ζ do not occur since the reduced attenuations lie in the asymptotic regions. However, it is in this region that $y \approx \zeta$ if the condition is satisfied that $1 < x \ll \zeta^{-1}$. The results for the optical absorption coefficient κ for CdS quoted by Thomas give κ to be greater than one for $\lambda < 534$ m μ hence it should be reasonable to take $\zeta = y$ in the range 524 m μ to 534 m μ . This range is represented on figure 6.b by the values of y at 15mHz in table VII.

TABLE XV

Calculated values for the conductivity parameter ζ using the reduced attenuations from table V. All are normalized for constant intensity of light and 15 mHz ultrasonic frequency.

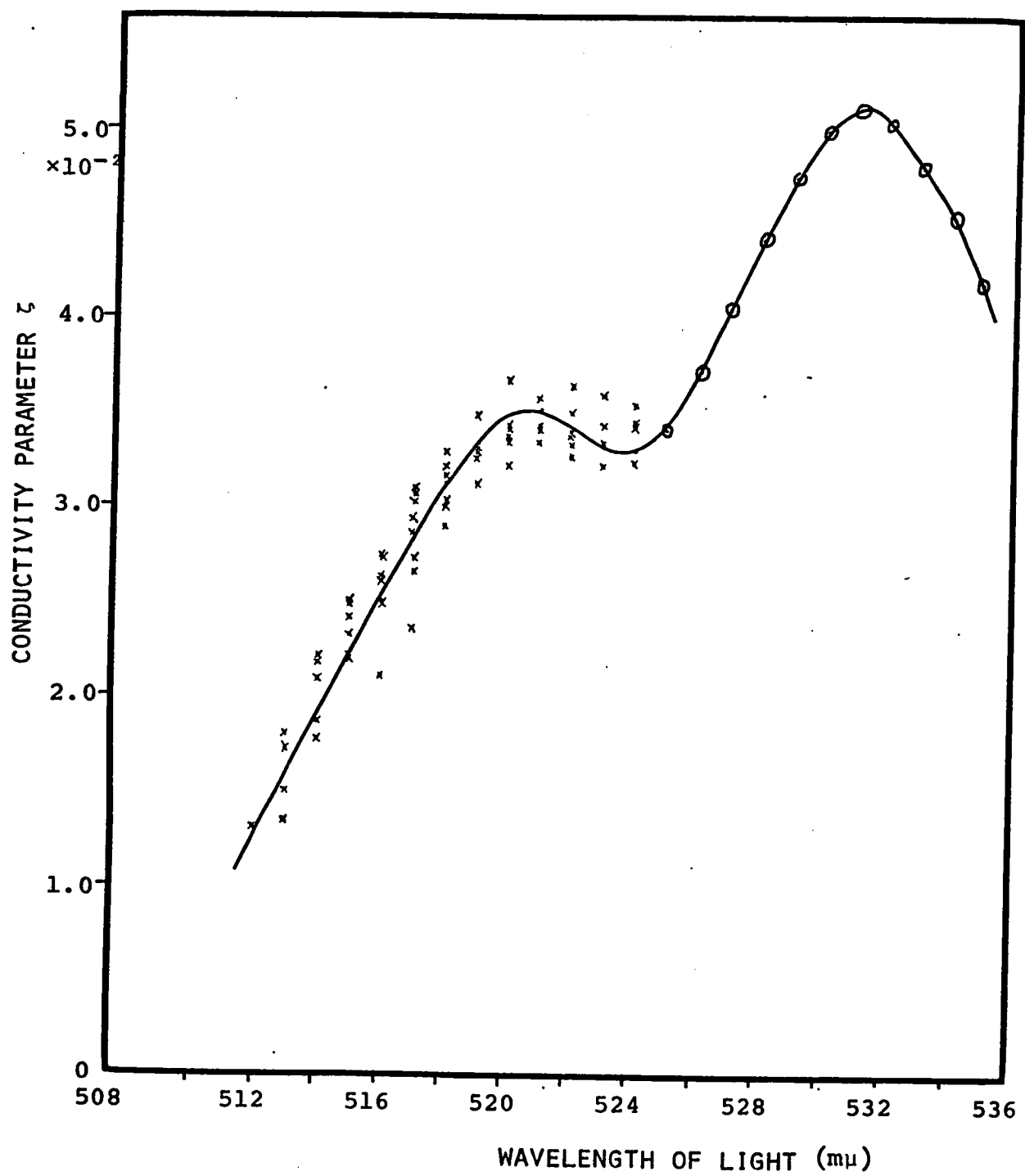
$\lambda(\text{m}\mu)$	$\zeta(\times 10^{-2})$
515	1.36
516	1.06
517	1.13
518	1.23
519	1.32
520	1.41
521	1.45
522	1.51

TABLE XVI

Calculated values for the conductivity parameter $\zeta (\times 10^{-2})$ using different pairs of frequencies from table VII. All ζ are normalized for constant intensity of light and 15 mHz ultrasonic frequency.

$\lambda(\text{m}\mu)$	15,45	15,75	15,105	15,135	45,75	45,105	45,135	75,135	Average ζ
512								1.31	1.31
513					1.50	1.33	1.72	1.81	1.59
514			2.21		1.87	1.77	2.10	2.19	2.03
515		2.49	2.35	2.50	2.22	2.21	2.41	2.49	2.38
516	2.11	2.48	2.50	2.64	2.75	2.61	2.75	2.74	2.57
517	2.36	2.67	2.74	2.95	3.04	2.85	3.06	3.10	2.85
518	2.90	3.13	3.00	3.17	3.29	3.04	3.22	3.17	3.12
519	3.13	3.31	3.27	3.31	3.49	3.29	3.33	3.31	3.31
520	3.21	3.43		3.38	3.67		3.41	3.37	3.41
521	3.43	3.52		3.41	3.59		3.43	3.35	3.46
522	3.27	3.50		3.39	3.62		3.40	3.33	3.42
523	3.22	3.43		3.32	3.59		3.34	3.43	3.39
524	3.24	3.45		3.30	3.55		3.30	3.44	3.38

Figure 6.b : Calculated values for the conductivity parameter ζ taken at 15 MHz and normalized for constant incident intensity. Values for ζ when $\lambda < 524 \text{ m}\mu$ are taken from table XVI and for $524 \text{ m}\mu < \lambda < 534 \text{ m}\mu$, ζ is obtained directly from the reduced attenuation at 15 MHz in table VII .



It is interesting to make a comparison between the ultrasonic measurements and a photoconduction measurement made by using electrodes attached to the sample. Consider the situation presented in figure 6.c. The conductivity of the sample as measured by the external circuit is given by

$$\sigma_{\text{total}} = \int_0^d \sigma(z) dz .$$

If the same conditions used in Chapter 3 are taken, then

$$\sigma(z) dz = q(\mu_n \tau_n + \mu_p \tau_p) \beta I_0 \kappa e^{-\kappa z} dz$$

and the measured conductivity becomes

$$\sigma_{\text{total}} = q(\mu_n \tau_n + \mu_p \tau_p) \beta I_0$$

where the case of $\kappa d \gg 1$ is taken.

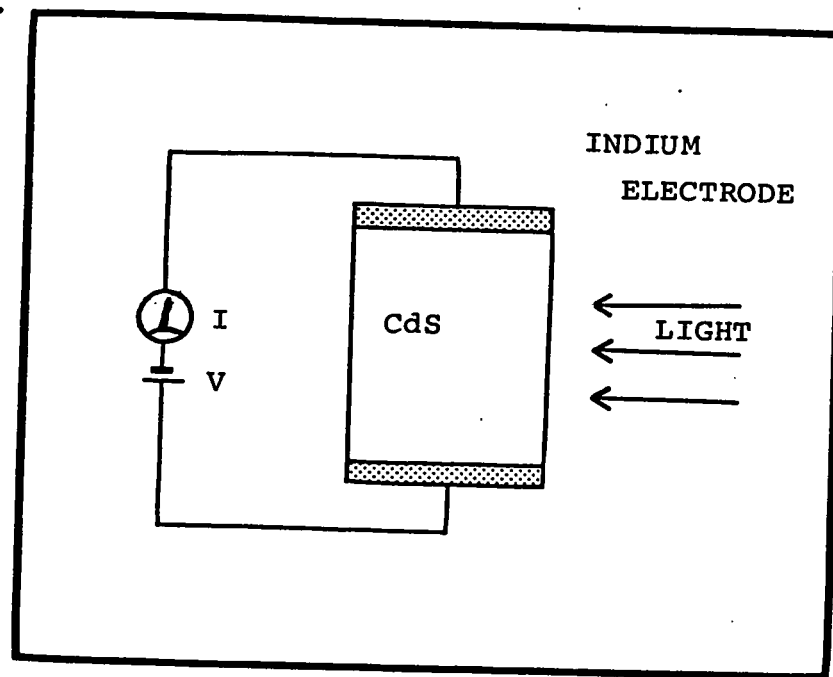
From the above equation it is immediately seen that the conductivity parameter used in connection with the ultrasonic measurements is given by

$$\zeta = (\epsilon \omega d)^{-1} \times \sigma_{\text{total}} = \text{constant} \times \sigma_{\text{total}}$$

Measurements of the photoconduction on sample SB-3 were made using an arrangement similar

FIGURE 6.c

SAMPLE GEOMETRY FOR PHOTOCONDUCTION MEASUREMENT



to that of figure 6.c. The results of one of these measurements is shown in figure 6.d. It can be seen that a reasonable degree of similarity exists between figure 6.d and the calculated conductivity parameter ζ shown in figure 6.b.

The data used for the calculations seen in the previous six tables originated by taking measurements of the attenuation at different frequencies. This in effect merely changes the value of ζ in the expression for the reduced attenuation y . The parameter ζ can also be changed by using different light intensities on the sample. Thus it is possible to get a value of the reduced attenuation for each intensity used and in so doing, it should be possible to do a simultaneous solution of two equations representing two values of y at two different intensities.

The results of attenuation measurements at different intensities are given in table VIII with the reduced form given in table IX. By entering the data from table IX into the computer programs, it is possible to get solutions for κ and ζ . The results of these computations are presented in

Figure 6.d : The photoconduction versus the wavelength of incident light using the experimental configuration of figure 6.c.

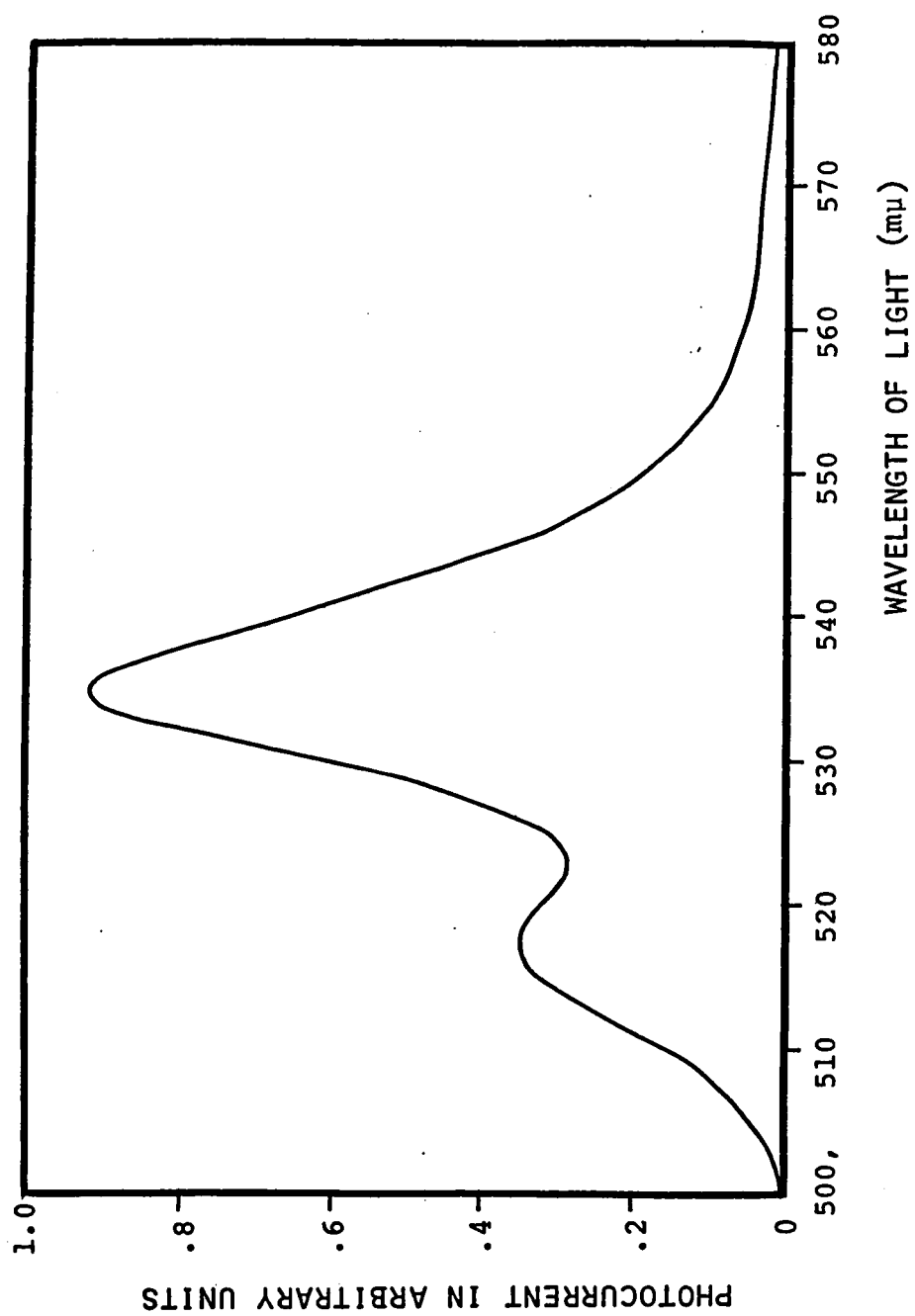


table XVII. It is seen that the values obtained for the optical absorption coefficient κ agree reasonably well with the values plotted on the graph of figure 6.a.

The theory presented in Chapter 3 is based on the assumption that the steady state conductivity varies linearly in the intensity of incident light. This assumption leads to the conclusion that the reduced attenuation is given by

$$y \propto \zeta(1 - e^{-x})$$

in the region where $x\zeta \ll 1$ and hence

$$y \propto I_0$$

This would indicate that the ratio of the reduced attenuations, measured at two different intensities, should be equal to the ratio of intensities. In the data of tables IX, the ratio of the intensities is $(0.31)^{-1}$, however, for the case of long wavelengths, table XVII shows values of the ratio of the two reduced attenuations to be about 2.2. This would indicate that the assumption of linearity between steady state conduction and light intensity may not be valid.

As an alternative to the linear case,

TABLE XVII

The optical absorption coefficient calculated from the reduced attenuations in table IX for two different frequencies.

$\lambda(\text{m}\mu)$	$\kappa(\text{cm}^{-1})$	y_1	y_2	y_1/y_2
512	2790			
513	1350			
514	639			
515	379			
516	260			
517	240			
518				
519				
520	120			
521	88			
522	64			
523	44			
524	36			
526	20	.130	.0826	1.57
528	12	.185	.0983	1.88
530		.214	.110	1.94
532		.204	.0944	2.16
534		.181	.0794	2.28
536		.149	.0661	2.26
538		.124	.0535	2.32
540		.0944	.0433	2.18
542		.0747	.0350	2.13
544		.0606	.0267	2.27
546		.0472	.0212	2.23
548		.0373	.0165	2.26
550		.0295	.0130	2.27
552		.0236	.0106	2.22
554		.0195	.0086	2.27

consider the conductivity to be proportional to a power of the light intensity i.e. $\sigma \propto I^Q$. Then if one follows through a derivation similar to that in Chapter 3, an expression can be obtained for the reduced attenuation as

$$y = \frac{1}{Qx} \tan^{-1} \left\{ \frac{(x\zeta')^Q (1-e^{-Qx})}{1 + (x\zeta')^{2Q} e^{-Qx}} \right\}$$

where $(\zeta')^Q = (q(\mu_n \tau_n + \mu_p \tau_p) \beta / \epsilon \omega) (I_0/d)^Q$.

In the limit as $x\zeta' \ll 1$, the above expression reduces to

$$y \approx (\zeta')^Q (1-e^{-Qx})/Q$$

The ratio of the reduced attenuations measured at two different intensities of light is

$$(y_1/y_2) = (I_1/I_2)^Q$$

For the case where $(y_1/y_2) = 2.2$ and $I_1/I_0 = 1/0.31$ a value for Q can be obtained as

$$Q = -(\ln 2.2)/(\ln .31) \approx .67$$

If the reduced attenuation data from table IX are entered into the computer programs when the non-linear function is used for the reduced attenuation, values for κ that result are much too high in the high optical absorption region.

For example

λ (m μ)	κ (cm $^{-1}$)
513	14,000
514	6,400
515	4,400
516	3,200

It appears therefore, that a simple non-linear case where $\sigma \propto I^Q$ does not work, in the region where κ is large, although it satisfies the observed data in the asymptotic parts.

The computations that were done using the linear model give results for the value of the optical absorption coefficient κ , that are consistent with results obtained by other methods. However, it is readily noticed that the model fails to fit the observed data in the short wavelength tail of figures 5.c, 5.d and 5.e. The theory of Chapter 3 predicts that in the high optical absorption region the reciprocal of the modified absorption parameter (i.e. $y = \pi/2x$) and hence y is independent of the frequency. However, when the reduced attenuation as given in table III and VII is plotted as a function of

frequency (c.f. figures 6.e and 6.f) it is seen that the reduced attenuation does not become independent of the frequency for the case of high optical absorption and in fact the frequency dependence changes direction. The fact that this occurs indicates that the assumption that the carrier density decays exponentially within the bulk is not true.

Figure 6.e : The reduced attenuation is plotted against the reciprocal of the ultrasonic frequency for different wavelengths of light. Both x and y axis are logarithmic scales. Data are taken from table III.

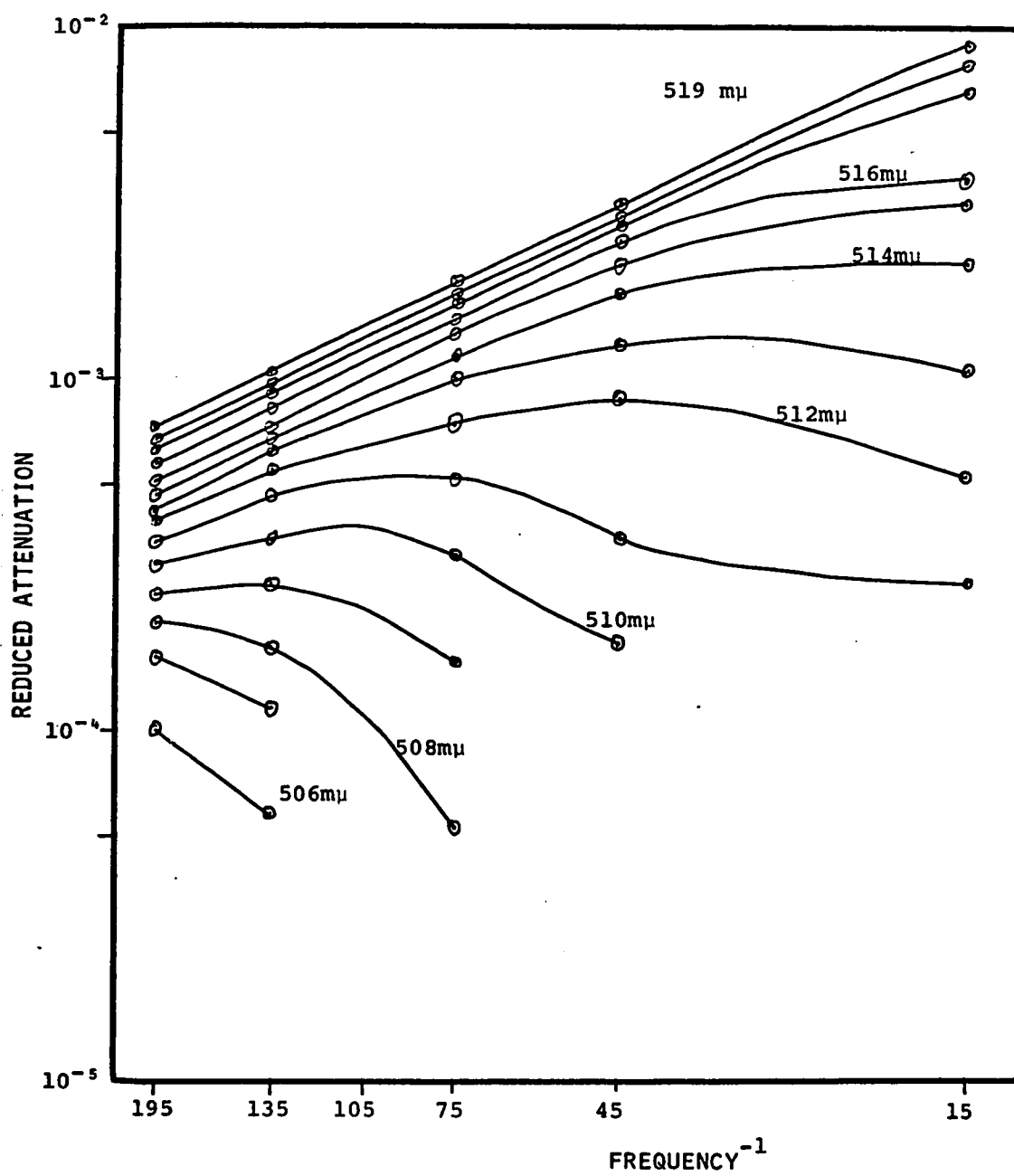


Figure 6.f : The reduced attenuation versus the reciprocal of the ultrasonic frequency for different wavelengths of light. Data are taken from table VII. Both x and y axis are logarithmic scales.

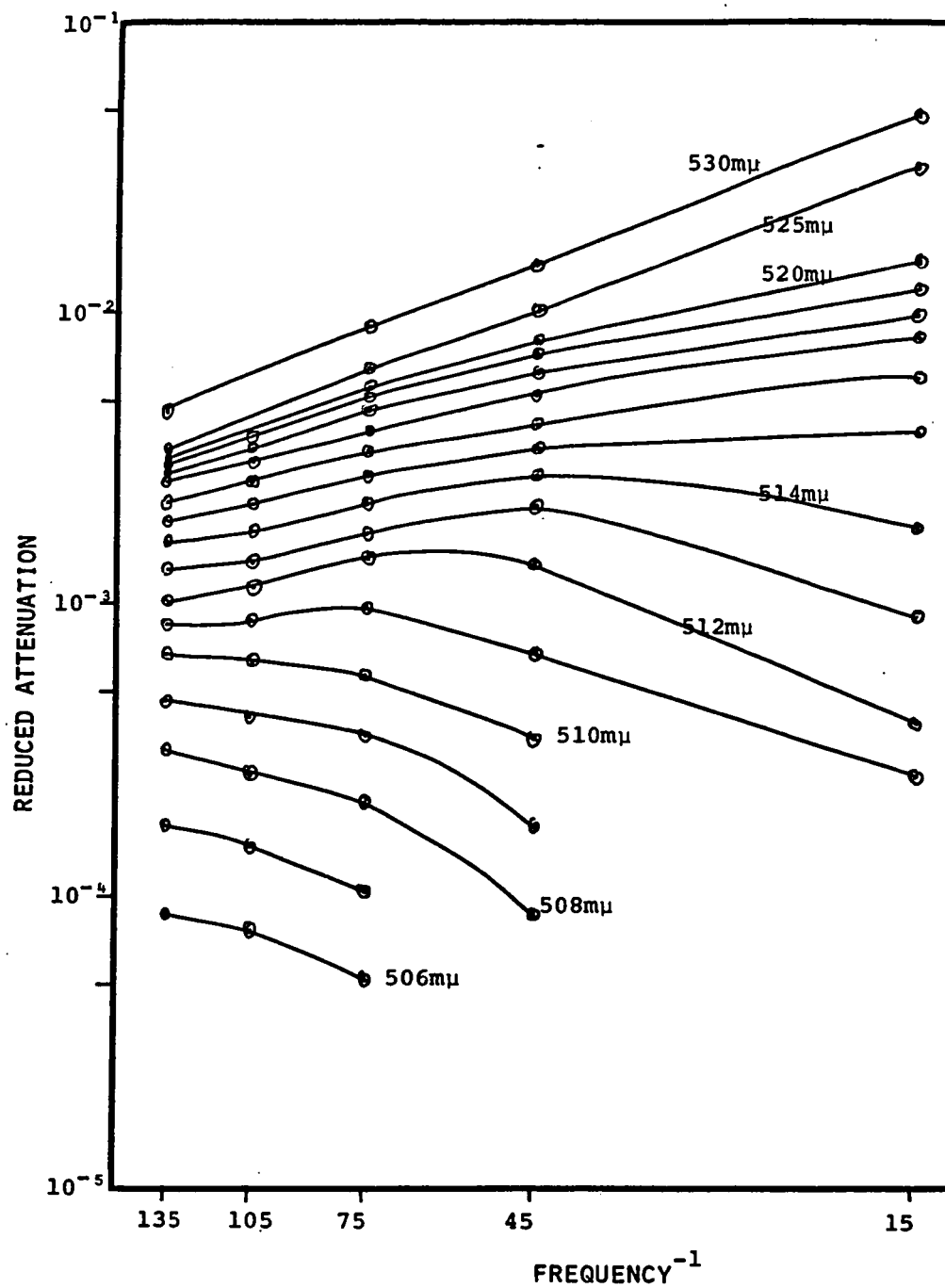
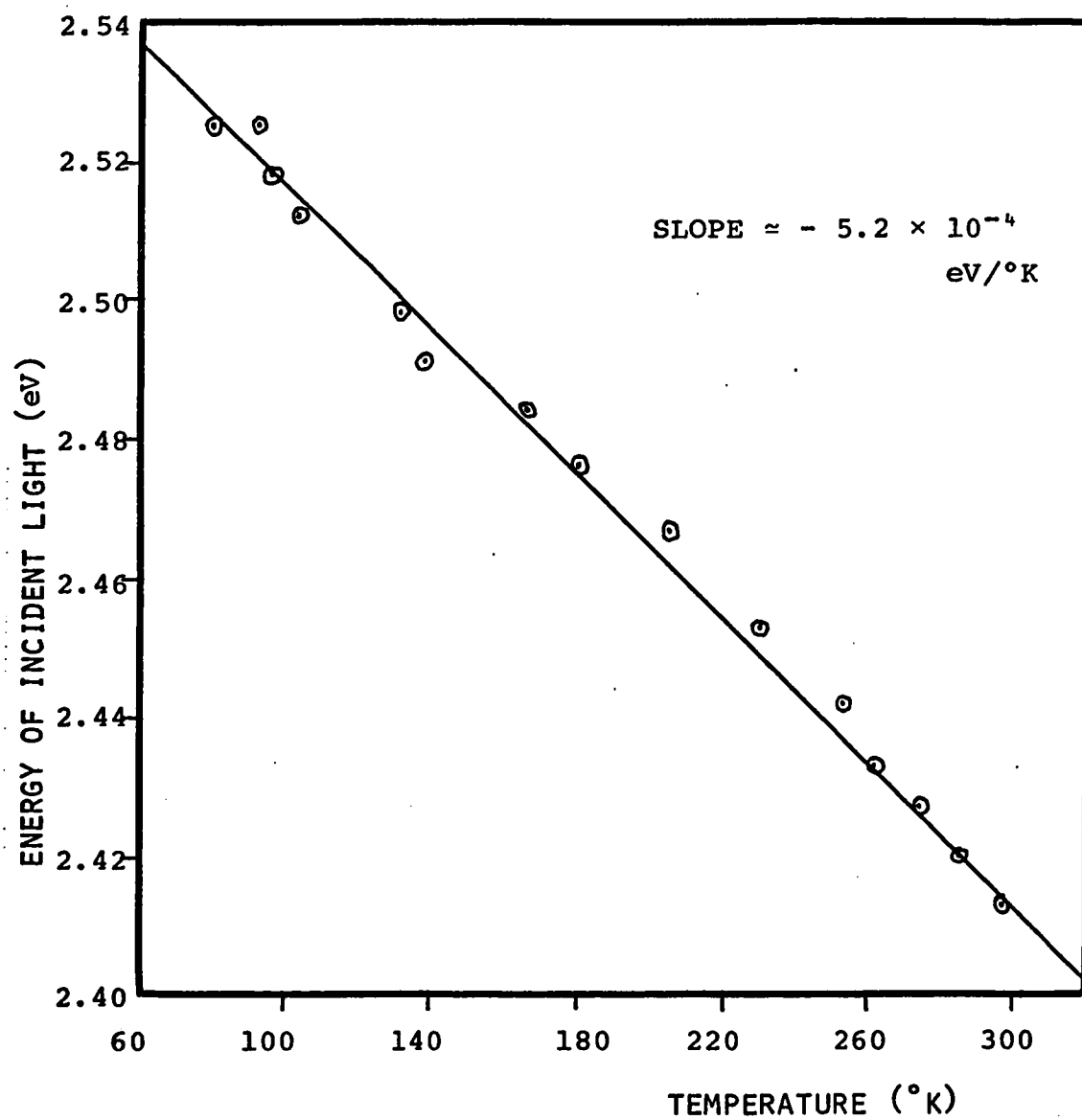


Figure 5.g gives the attenuation on the blue edge at various temperatures from 300°K to 77°K. From these curves it should be possible to get a measure of the shift of the band edge with temperature. At points where the attenuation is small but measurable (e.g. .05db), the attenuation is predominantly determined by the optical absorption coefficient κ and hence if the wavelength is taken as the point where the attenuation is the same for each temperature, a plot of the incident photon energy against temperature should show the shift in the band edge with temperature. This plot is presented in figure 6.g and from it it is seen that the points lie fairly well on a straight line. If the slope of this line is measured we get a value for the shift in band edge of -5.2×10^{-4} eV/°K. This value for the slope agrees with published values for the band edge shift; for example the Handbook of Chemistry and Physics quotes the band shift as -5×10^{-4} eV/°K.

There are many improvements that could be made to the experiments to increase their reliability and accuracy. For example, the experiment required that attenuation measurements be made at

Figure 6.g : The energy of incident light is plotted against temperature for a constant ultrasonic attenuation of .05 db per round trip. The slope of the straight line is 5.2×10^{-4} eV/°K.



different frequencies and in the method that was used these measurements were made at different times which means that there is a basic uncertainty that all the experimental conditions are exactly the same for each measurement. An obvious improvement in the method would be a system that allows measurements of the attenuation at different frequencies to be made at the same time. This is probably a very difficult requirement to achieve in practice, especially in a low noise system, however attempts might be tried along the line of using a burst pulse generator to excite the transducer at all the odd harmonics. That is to say if the transducer is connected to a generator that gives out an envelope of square pulses, with the repetition rate of the square wave corresponding to the fundamental frequency of the transducer, then the frequency components of the square wave will be that of the odd harmonics of the transducer. Impedance matching between the pulse generator and the transducer could be achieved with stubbed transmission lines which will allow proper matching for $(2n-1) (\lambda/4)$ where $n = 1, 2, 3, \dots$

and hence each of the odd harmonics of the transducer can propagate freely to and from the transducer. At the receiver end the odd harmonics must be filtered out and each fed into a separate attenuation recorder.

In regard to the work done at low temperatures, there is one area in particular where an improvement would be beneficial. The optical arrangement required that the light pass through the nitrogen and helium baths. This introduced into the system a fair amount of unnecessary noise because of fluctuations in the light intensity due to turbulence in the liquids. A better optical cryostat that allows light to enter the cold chamber unhindered by liquids and layers of glass would give higher light intensities at the sample and reduce noise levels to allow much more reliable measurements at low temperatures.

The experiments carried out were all performed using longitudinal waves. An obvious extension to this work would be to make measurements using transverse ultrasonic waves. In this experiment the sample would have to be oriented to allow propagation of the acoustic wave

perpendicular to the c-axis with polarization direction parallel to the c-axis. For this arrangement the value of $B = e^2/2c\epsilon$ is about the same as for the longitudinal case but since the transverse acoustic wave velocity is lower (i.e. $v_0 = 1.75 \times 10^{-5}$ cm/sec) the photosensitive attenuation is increased by a factor of about 2.5. The slower velocity also allows the use of thinner samples which could be very helpful particularly at high frequencies since the ratio of the photosensitive attenuation to the background attenuation will be increased giving a higher signal to noise level.

Also the use of transverse waves puts the sample into an orientation where the polarization of the incident light should have an effect on the results (i.e. $\vec{E} \perp \vec{c}$ and $\vec{E} \parallel \vec{c}$). For the case where longitudinal waves are used only $\vec{E} \perp \vec{c}$ is possible for the geometry of the experiments.

In addition to the work already mentioned there are several areas where effects were observed but no detailed measurements were undertaken. These observations may be of interest as possible future work. For example when the ultrasonic attenuation was recorded as a function of time various over shoots and spikes were seen when light of different wavelengths was turned off and on at different times. For example if the sample was allowed to reach a steady state with exposure to light at $530\text{m}\mu$ and then suddenly exposed to $.9\mu$ infrared light, the attenuation was observed to increase momentarily before decaying down to a value lower than before. Observations of a spike similar to this were reported by Michenaud (1964) from photoconduction measurements on CdS. Michenaud goes on in his paper to use these observations to propose a model for a distribution of energy levels within the forbidden gap.

Observations of ultrasonic attenuation time effects of the above nature were observed in most of the weakly photoconducting samples and at low temperatures some of these effects became more significant. The frequency dependence for ultrasonic attenuation measurements of these time effects may

prove to be of some use in providing a better understanding of interband energy levels in CdS.

Also some observations that may be of interest were seen on sample SB-3 in the near ultraviolet and far visible region between 400m μ and 500m μ . When the slits on the monochromator were increased to 4mm, to get as intense a light as possible on the sample, and the sensitivity of the ultrasonic equipment turned up to maximum, long term drifts in the attenuation were observed. The changes in the attenuation due to the light were in the order of .005 db per round trip of the sample and were quite reproduceable. The effect appeared to be the same for all light wavelengths between 410m μ and 500m μ and was seen at both 15 mHz and 45 mHz. However in a narrow wavelength region around 400m μ the time response increased considerably and a change of .008 db would take place in about five minutes, where as at longer wavelengths a period of up to an hour would be required to show the same change in attenuation. This ultraviolet effect was not observed in the other strongly photoconducting sample SE-1 nor on any of the weak photconductors.

In some of the earlier work a series of measurements were made on one CdS crystal that showed a rather significant decrease in the attenuation below the dark level when the sample was exposed to very intense and highly absorbed light in the wavelengths between 510m μ and 520m μ . At longer wavelengths the attenuation would increase with the light as occurs normally in high dark resistive and strongly photoconducting material. Although these results were reproduceable at the time subsequent polishing and treatment on the sample removed the effects. It is thought that this effect must have resulted from some irregularities at the surface of the sample however it is not known what this might be at the present time.

CHAPTER 7

Conclusion

The work reported in this thesis is intended to give a preliminary look into the use of ultrasonic attenuation measurements as a tool for studying photoconduction and optical properties in piezoelectric crystals. Data that were collected from CdS samples agree in part with an adaptation of the theory of Hutson to describe the photo-sensitive attenuation effects at different values of the optical absorption coefficient. However, discrepancies between theory and experiment at high values of the optical absorption coefficient (i.e. $\kappa > 10^3 \text{ cm}^{-1}$) indicate that a more elaborate model is required.

Calculations on the experimental data give numerical values for the optical absorption coefficient at the band edge that agree within experimental error with measurements of the absorption coefficient made by others. In fact the ultrasonic measurements extend the values of κ by an order of magnitude up the band edge compared to the results of Thomas, where the

measurements were made using direct methods of studying the light attenuation in very thin samples. With the aid of a better model to describe the ultrasonic attenuation at high frequencies and high optical absorption, it should be possible to obtain values for the optical absorption coefficient up to $\sim 10^5 \text{ cm}^{-1}$.

The sensitivity of the ultrasonic method when the photoconductivity is very small (i.e. $\omega_c \ll \omega$) is rather limited when compared with the sensitivity of direct measurements on the photocurrent. However, in crystals where the photoconduction can be made reasonably large, the method of ultrasonic probing should prove to be quite useful. By making careful measurements at different frequencies, the crystal is essentially probed in different ways while the photo conditions are held constant. The resulting frequency dependence of the attenuation gives additional information over and above a typical photocurrent measurement. Therefore, with measurements done at different light intensities and with measurements of the attenuation time response to optical step functions, a much better model for describing the photo-

conduction process should be possible.

The observed frequency dependence of the ultrasonic attenuation at very high optical absorption coefficient indicates that this method may prove interesting in studying the surface region of CdS crystals. Charge at surface states caused by such things as mechanical damage to the crystal from polishing, absorbed gases and termination of the periodic lattice , can give rise to space charge regions at the surface with the resulting band bending. Photo generated carriers then see different conditions at the surface than in the bulk (for example different lifetimes and mobilities will result). Ultrasonic attenuation may therefore prove to be an interesting tool in studying this region. The unique aspect of the ultrasonic method is that the surface is probed from the bulk side and not from the vacuum side. A possible disadvantage to this method of probing is that the surfaces must be polished flat. Mechanical polishing is known to introduce changes in observed structure related to the surface (for example see Gross 1961)

Improvements to studying the surface at

high optical absorptions could be made by using higher ultrasonic frequencies. The higher frequencies, however, have larger background attenuations, therefore, thinner samples are necessary. This can introduce complications with instrumentation. The use of transverse waves may solve these problems to some extent because of the slower velocity. The smaller velocity results in a larger photosensitive attenuation and also allows use of thinner samples which in turn increases the ratio of photo attenuation to background attenuation and also allows higher ultrasonic frequencies.

APPENDIX A

General Wave Motion in a Piezoelectric Medium

To obtain the conditions for propagation of plane waves through a piezoelectric medium, it is necessary to simultaneously solve the Maxwells field equations and the equations of motion for the lattice. These are

$$\nabla \times \vec{H} = \frac{\partial \vec{D}}{\partial t} + \vec{J} \quad (A.1)$$

$$\nabla \times \vec{E} = - \frac{\partial \vec{B}}{\partial t} \quad (A.2)$$

$$\nabla \cdot \vec{B} = 0 \quad (A.3)$$

$$\nabla \cdot \vec{D} = Q \quad (A.4)$$

$$T_{ij,j} = \rho \ddot{u}_i \quad (A.5)$$

where ρ is the average mass density and u_i is the material displacement. The notation assumes summation over repeated indicies and

$$\ddot{u}_i = \frac{\partial^2 u_i}{\partial t^2}$$

$$T_{ij,j} = \sum_{j=1}^3 \frac{\partial T_{ij}}{\partial x_j}$$

Substitution of equation (1.1) into the equation (A.5) gives

$$\rho \ddot{u}_i = c_{ijkl} S_{kl,j} - e_{lij} E_{l,j}.$$

The strain for small displacements can be defined in terms of the material displacement as

$$S_{kl} = (u_{l,k} + u_{k,l})/2$$

and then

$$c_{ijkl} S_{kl,j} = c_{ijkl} u_{l,kj}$$

since $c_{ijkl} = c_{ijlk}$. The equation of motion, therefore, becomes

$$\rho \ddot{u}_i = c_{ijkl} u_{l,kj} - e_{lij} E_{l,j} \quad (A.6)$$

Assume that the material of interest has no magnetic properties and that

$$\vec{B} = \mu_0 \vec{H} \quad (A.7)$$

Then take the curl of equation (A.2) and substitute (A.1) and (A.7) to get

$$\begin{aligned} \nabla \times (\nabla \times \vec{E}) &= -\frac{\partial}{\partial t} (\nabla \times \vec{B}) \\ &= \mu_0 \frac{\partial}{\partial t} \left(\frac{\partial \vec{D}}{\partial t} + \vec{J} \right) \end{aligned} \quad (A.8)$$

An expression for the dielectric displacement can be obtained from the second equation of state (1.2)

$$\begin{aligned} D_k &= e_{klm} S_{lm} + \epsilon_{ik} E_i \\ &= e_{klm} u_{l,m} + \epsilon_{ik} E_i \end{aligned} \quad (A.9)$$

where use was made of the symmetry $e_{klm} = e_{kml}$.

Now take the time derivative of equation (A.9)

and substitute into equation (A.8) to get

$$[\nabla \times (\nabla \times \vec{E})]_k = -\mu_0 e_{klm} \ddot{u}_{l,m} - \mu_0 \epsilon_{ik} E_i - \dot{J}_k \quad (\text{A.10})$$

Since only propagation of plane waves is of interest, no generality is lost by restricting the propagation direction of the waves to the x_3 direction. The derivatives of the field variables with respect to the x_1 and x_2 directions are then zero. Thus

$$[\nabla \times (\nabla \times \vec{E})]_p = -E_{p,33} \quad \text{where } p = 1, 2$$

$$[\nabla \times (\nabla \times \vec{E})]_3 = 0$$

Equation (A.10) can then be written

$$E_{p,33} = \mu_0 (e_{pj3} u_{j,3} + \epsilon_{jp} \ddot{E}_j - J_p) \quad (\text{A.11})$$

$$0 = \mu_0 (e_{3j3} u_{j,3} + \epsilon_{j3} \ddot{E}_j - J_p) \quad (\text{A.12})$$

The medium is considered to be insulating such that

$$\vec{J} = \sigma \vec{E} = 0$$

Hence (A.11) and (A.12) reduce to

$$E_{p,33} = \mu_0 (e_{pj3} u_{j,3} + \epsilon_{jp} \ddot{E}_j) \quad (\text{A.13})$$

$$0 = e_{3j3} u_{j,3} + \epsilon_{j3} \ddot{E}_j \quad (\text{A.14})$$

Equation (A.14) gives E_3 in terms of E_1 and E_2

$$\ddot{E}_3 = -(e_{3j3} u_{j,3} + \epsilon_{p3} \ddot{E}_p) / \epsilon_{33} \quad (\text{A.15})$$

(A.15) can be substituted into (A.13) and (A.6)

to get

$$E_{p,33} = \mu_0 (e'_{pj3} u_{j,3} + \epsilon'_{pq} \ddot{E}_q) \quad (A.16)$$

$$\rho \ddot{u}_i = c'_{i33j} u_{j,33} - e'_{pi3} E_{p,3} \quad (A.17)$$

Where $e'_{pj3} = e_{pj3} - e_{3j3} \epsilon_{3p} / \epsilon_{33}$

$$\epsilon'_{pq} = \epsilon_{pq} - \epsilon_{p3} \epsilon_{q3} / \epsilon_{33}$$

$$c'_{i33j} = c_{i33j} + e_{3i3} e_{3j3} / \epsilon_{33}$$

Take plane wave solutions for the equation

(A.16) and (A.17)

$$u_i = u'_i e^{i(kx_3 - \omega t)}$$

$$E_i = E'_i e^{i(kx_3 - \omega t)}$$

then equations (A.16) and (A.17) become

$$-k^2 E_p = \mu_0 e'_{pj3} i k u_j - \omega^2 \mu_0 \epsilon'_{pq} E_q \quad (A.18)$$

$$-\omega^2 \rho u_i = -c'_{i33j} k^2 u_j - i k e'_{pi3} E_p \quad (A.19)$$

Equations (A.18) and (A.19) give five equations in the five unknowns u_i and E_p where $i = 1, 2, 3$ and $p = 1, 2$.

A non-trivial solution of the above equations exists if the determinant of the coefficients vanishes. The secular determinant is then given by

$$\begin{vmatrix}
 (c'_{1331}k^2 - \omega^2\rho) & c'_{1332}k^2 & c'_{1333}k^2 & ike'_{113} & ike'_{213} \\
 c'_{2331}k^2 & (c'_{2332}k^2 - \omega^2\rho) & c'_{2333}k^2 & ike'_{123} & ike'_{223} \\
 c'_{3331}k^2 & c'_{3332}k^2 & (c'_{3333}k^2 - \omega^2\rho) & ike'_{133} & ike'_{233} \\
 ik\mu_0 e'_{113} & ik\mu_0 e'_{123} & ik\mu_0 e'_{133} & (k^2 - \omega^2\mu_0 \epsilon'_{11}) & -\omega^2\mu_0 \epsilon'_{12} \\
 ik\mu_0 e'_{213} & ik\mu_0 e'_{223} & ik\mu_0 e'_{233} & -\omega^2\mu_0 \epsilon'_{21} & (k^2 - \omega^2\mu_0 \epsilon'_{22})
 \end{vmatrix} = 0$$

The equation from the above determinant is of fifth degree in $(k/\omega)^2$. Thus there are five possible phase velocities for the waves propagated. The piezoelectric medium is therefore pentrefrangent both elastically and electrically since the propagation constant satisfies all wave equations.

APPENDIX B

Tensor Properties of CdS1) Rank two tensors

Any rank two tensor that describes a property of a crystal is symmetric. Thus in an arbitrary coordinate system there will be a maximum of six different components, however not all of these are independent. In the most general case there can be at most three independent components which can be displayed in a principal coordinate system as a 3×3 diagonal matrix. The symmetry properties of the crystal can reduce the number of independent components. For CdS the symmetry requires that there be two independent components for any rank two tensor and these can be displayed in a coordinate system with the c-axis parallel to the X_3 axis as

$$\begin{pmatrix} \epsilon_{11} & 0 & 0 \\ 0 & \epsilon_{11} & 0 \\ 0 & 0 & \epsilon_{33} \end{pmatrix}$$

2) Rank three tensors

Rank three tensors describing properties of any crystal have a maximum of eighteen different

coefficients because of the basic symmetry requirement that $e_{ijk} = e_{ikj}$. The eighteen components can be reduced to nine independent components by using a coordinate system in which the contracted tensor is diagonal. The symmetry properties of CdS reduce the number of independent components to three. In a coordinate system with the c-axis parallel to the x_3 direction, the contracted rank three tensor for CdS has the form

$$\begin{pmatrix} 0 & 0 & 0 & 0 & e_{15} & 0 \\ 0 & 0 & 0 & e_{15} & 0 & 0 \\ e_{31} & e_{31} & e_{33} & 0 & 0 & 0 \end{pmatrix}$$

where the tensor is contracted in to a 3×6 matrix using the notation

$$e_{ijk} = e_{iv} \quad i = 1, 2, 3 \quad \text{and} \quad v = 1, 2, 3, 4, 5, 6$$

such that

v	jk = kj
1	11
2	22
3	33
4	23 = 32
5	13 = 31
6	12 = 21

3) Rank four tensor properties

Rank four tensors are characterized by $3^4 = 81$ components. For any rank four tensor describing properties of a solid there exist the basic symmetry properties

$$c_{ijkl} = c_{ijlk}$$

$$c_{ijkl} = c_{jikl}$$

$$c_{ijkl} = c_{klij}$$

These symmetries reduce the number of different components to 21 of which only 18 are independent. The symmetry properties of CdS reduce the number of independent components from 18 to 7. Using the notation defined for the rank three tensor, the rank four tensor can be contracted into a 6×6 matrix. For a coordinate system with the c-axis parallel to the x_3 direction rank four tensors for CdS have the form

$$\begin{pmatrix} c_{11} & c_{12} & c_{13} & 0 & 0 & 0 \\ c_{12} & c_{11} & c_{13} & 0 & 0 & 0 \\ c_{13} & c_{13} & c_{33} & 0 & 0 & 0 \\ 0 & 0 & 0 & c_{44} & 0 & 0 \\ 0 & 0 & 0 & 0 & c_{44} & 0 \\ 0 & 0 & 0 & 0 & 0 & (c_{11}-c_{12})/2 \end{pmatrix}$$

where $c_{ijkl} = c_{\nu\gamma}$ and $\nu, \gamma = 1, 2, 3, 4, 5, 6$.

APPENDIX C

Derivation of Complex Elastic Stiffness Constant.

For the case of an extrinsic semiconductor, the relevant equations are:

$$\frac{\partial^2 u}{\partial t^2} = \frac{c}{\rho} \frac{\partial^2 u}{\partial z^2} - \frac{e}{\rho} \frac{\partial E}{\partial z} \quad (1.7)$$

$$D = e \frac{\partial u}{\partial z} + \epsilon E \quad (1.8)$$

$$\frac{\partial D}{\partial z} = Q \quad (1.9)$$

$$\frac{\partial Q}{\partial t} + \frac{\partial J}{\partial z} = 0 \quad (1.10)$$

$$Q = -qn \quad (1.11)$$

$$J = q(n_0 + fn)\mu E + qD_n f \frac{dn}{dz} \quad (1.12)$$

Take the spatial derivative of equation (1.12) and the time derivative of equation (1.9) and combine with equation (1.10) to get

$$\begin{aligned} \frac{\partial^2 D}{\partial z \partial t} &= - \frac{\partial J}{\partial z} = -[q(n_0 + fn)\mu \frac{\partial E}{\partial z} + qf\mu E \frac{\partial n}{\partial z} + qn f \frac{\partial^2 n}{\partial z^2}] \\ &= - q\mu n_0 \frac{\partial E}{\partial z} + f \frac{\partial D}{\partial z} \frac{\partial E}{\partial z} + \mu f E \frac{\partial^2 D}{\partial z^2} + D_n f \frac{\partial^2 D}{\partial z^3} \end{aligned} \quad (c.1)$$

where equations (1.11) and (1.9) were used to eliminate n from the above equation.

Taking plane wave solutions of the form

$$\begin{aligned} D &= D_0 \exp(ikz - i\omega t) \\ E &= E_0 \exp(ikz - i\omega t) \end{aligned} \quad (c.2)$$

equation (c.1) becomes

$$\omega k D = -iq\mu n_0 k E - 2\mu f k^2 D E, -i D_n f k^3 D$$

and solving for D gives

$$D = \frac{-i(\frac{\sigma}{\omega}) E}{[1 + 2(\frac{k}{\omega}) f \mu E + i\omega(\frac{k}{\omega}) D_n f]}$$

where $\sigma = q\mu n_0$.

It will be assumed that the modulation in n_0 due to the wave is small (i.e. $f n \ll n_0$) and hence the drift velocity due to the piezoelectric field is small. Thus

$$2\frac{k}{\omega} f \mu E \sim \frac{v_d}{v_s} \ll 1$$

and this term may be neglected in equation (c.3) to give

$$D = \frac{-i(\frac{\sigma}{\omega}) E}{[1 + i\omega(\frac{k}{\omega})^2 f D_n]} \quad (c.4)$$

Now combine equations (c.4) and (1.8) to get

$$E = \left\{ \frac{1 + i\omega(\frac{k}{\omega})^2 f D_n}{1 + i[\frac{\sigma}{\epsilon\omega} + (\frac{k}{\omega})^2 \omega f D_n]} \right\} \left\{ \left(\frac{e}{\epsilon} \right) \frac{\partial u}{\partial z} \right\} \quad (c.5)$$

Define the frequencies

$$\omega_c = \frac{\sigma}{\epsilon} = \text{dielectric relaxation frequency}$$

$$\omega_D = v_0 / f D_n = \text{diffusion frequency.}$$

In the definition of ω_D the dispersion in the the acoustic wave is neglected and $(\omega/k)^2 \approx v_0$ so that ω_D is considered a constant. Equation (c.5) then becomes

$$E = \left[\frac{1 + i \frac{\omega}{\omega_D}}{1 + i \left(\frac{\omega_c}{\omega} + \frac{\omega}{\omega_D} \right)} \right] \left(\frac{e}{\epsilon} \right) \frac{\partial u}{\partial z}$$

which can be substituted into the wave equation (1.7) to give

$$\frac{\partial^2 u}{\partial t^2} = \frac{c'}{\rho} \frac{\partial^2 u}{\partial z^2}$$

where

$$\begin{aligned} c' &= c \left\{ 1 + \frac{e^2}{\epsilon c} \left(\frac{1 + i \frac{\omega}{\omega_D}}{1 + i \left[\frac{\omega_c}{\omega} + \frac{\omega}{\omega_D} \right]} \right) \right\} \\ &= c \left\{ 1 + \frac{e^2}{\epsilon c} \left[\frac{1 + \frac{\omega_c}{\omega_D} + \left(\frac{\omega}{\omega_D} \right)^2 - i \left(\frac{\omega_c}{\omega} \right)}{1 + 2 \frac{\omega_c}{\omega_D} + \left(\frac{\omega}{\omega_D} \right)^2 + \left(\frac{\omega_c}{\omega} \right)^2} \right] \right\} \end{aligned}$$

(c.6)

For the case of an intrinsic semiconductor where the recombination time is long compared with the period of the acoustic wave, there will be separate continuity equations for each of the charge carriers.

Thus equation (1.9) will become

$$\frac{\partial D_p}{\partial z} = Q_p \quad (c.7)$$

and

$$\frac{\partial D_n}{\partial z} = Q_n \quad (c.8)$$

where the total dielectric displacement is given by

$$D = D_p + D_n$$

Equation (1.10), (1.11) and (1.12) will become equations (1.20), (1.21), (1.22), (1.23), (1.24), (1.25)

$$\frac{\partial J_p}{\partial z} + \frac{\partial Q_p}{\partial t} = 0 \quad (1.20)$$

$$\frac{\partial J_n}{\partial z} + \frac{\partial Q_n}{\partial t} = 0 \quad (1.21)$$

$$Q_p = qp \quad (1.22)$$

$$Q_n = -qn \quad (1.23)$$

$$J_p = q(p_0 + p)\mu_p E - qD_p \frac{dp}{dz} \quad (1.24)$$

$$J_n = -q(n_0 + n)\mu_n E + qD_n \frac{dn}{dz} \quad (1.25)$$

Take the spatial derivative of (1.24) and the time derivative of equation (c.7) and combine with (1.20) to get

$$\frac{\partial^2 D_p}{\partial z \partial t} = -q\mu_p p_0 \frac{\partial E}{\partial z} - \mu_p \frac{\partial D_p}{\partial z} \frac{\partial E}{\partial z} - \mu_p E \frac{\partial^2 D_p}{\partial z^2} + D_p \frac{\partial^3 D_p}{\partial z^3}$$

A similar expression can be obtained for the electron contribution

$$\frac{\partial^2 D_n}{\partial z \partial t} = -q\mu_n n_0 \frac{\partial E}{\partial z} + \mu_n \frac{\partial D_n}{\partial z} \frac{\partial E}{\partial z} + \mu_n E \frac{\partial^2 D_n}{\partial z^2} + D_n \frac{\partial^3 D_n}{\partial z^3}$$

Now using plane wave solutions of the form (c.2) gives

$$\begin{aligned} \omega k D_p &= -iq\mu_p p_0 k E - 2\mu_p k^2 D_p E - i \frac{D_p}{q} k^3 \\ \text{and} \quad \omega k D_n &= -iq\mu_n n_0 k E + 2\mu_n k^2 D_n E - i \frac{D_n}{q} k^3 \end{aligned}$$

Then solve for D_p and D_n and take the small signal case where $2 \frac{k}{\omega} \mu E \ll 1$ to get

$$\begin{aligned} D &= D_p + D_n \\ &= - \frac{iqE}{\omega} \left\{ \frac{\mu_p p_0}{1 + i\omega \left(\frac{k}{\omega}\right)^2 D_p} + \frac{\mu_n n_0}{1 + i\omega \left(\frac{k}{\omega}\right)^2 D_n} \right\} \quad (c.9) \end{aligned}$$

Substitute (c.9) into (1.8) and solve for E in terms of $\frac{\partial u}{\partial z}$

$$E = -e \frac{\partial u}{\partial z} \left\{ \epsilon + \frac{iq}{\omega} \left[\frac{\mu_p p_0}{1+i(\omega/\omega_{D_p})} + \frac{\mu_n n_0}{1+i(\omega/\omega_{D_n})} \right] \right\}^{-1} \quad (c.10)$$

Substitution of (c.10) into the wave equation (1.7) will now give c'

$$c' = c \left\{ 1 + \left(\frac{e^2}{ce} \right) \left\{ 1 + i \left[\frac{\omega_{c_p}/\omega}{1+i(\omega/\omega_{D_p})} + \frac{\omega_{c_n}/\omega}{1+i(\omega/\omega_{D_n})} \right] \right\} \right\}^{-1}$$

where

$$\omega_{c_p} = q\mu_p p_0 / \epsilon$$

$$\omega_{c_n} = q\mu_n n_0 / \epsilon$$

$$\omega_{D_n} = v_0^2 / D_n$$

$$\omega_{D_p} = v_0^2 / D_p$$

ω_{c_p} and ω_{c_n} are the dielectric relaxation frequency for holes and electrons respectively; and ω_{D_p} and ω_{D_n} are the diffusion frequencies for holes and electrons respectively.

APPENDIX D

Miscellaneous Properties of CdS

The data presented here have been taken from tables given in the following references:

- 1) Handbook of Chemistry and Physics (1969)
- 2) Hutson (1962)
- 3) Reynolds, Litton and Collins (1965)
- 4) Mort and Spear (1962)
- 5) Collins, Ewema and DeWitt
- 6) Hutson (1960)
- 7) Pado, Kobayakov and Sysoev (1969)
- 8) Wolf (1969)

Band gap 2.58eV at T = 0°K (3)

$$2.42\text{eV at } T = 300^\circ\text{K} \quad (1)$$

Dielectric Constant

$$\epsilon_{33}^T/\epsilon_0 = 10.33 \quad (3)$$

$$\epsilon_{11}^T/\epsilon_0 = 9.35 \quad (3)$$

$$\epsilon_{11}/\epsilon_0 = 9.02 \quad (3)$$

$$\epsilon_{\infty} / \epsilon_0 = 5.24 \quad (3)$$

also see (7) for temperature dependence.

Refractive Index

$$n = \sqrt{\epsilon_{\infty}} = \sqrt{5.24} = 2.29$$

Effective Masses

$$m_n/m_0 \sim .21 \quad (8)$$

$$\sim .18 \quad (5)$$

$$(m_p/m_0)_\perp \sim .7 \quad (5)$$

$$\sim .8 \quad (8)$$

$$(m_p/m_0)_\parallel \sim 5.0 \quad (5)$$

Mobility $\mu_n \sim 340 \text{ cm}^2/\text{volt sec} \quad (8)$

$$\mu_p \sim 10 - 18 \text{ cm}^2/\text{volt sec} \quad (4)$$

Lattice Constant

$$\bar{c} = 5.83\text{\AA} \quad (8)$$

Density $= 4.84 \quad (8)$

Melting Point $1750^\circ\text{C} \quad (8)$

Velocity of Sound

$$v_{\text{long}} = 4.3 \times 10^5 \text{ cm/sec} \quad (2)$$

$$v_{\text{trans}} = 1.75 \times 10^5 \text{ cm/sec} \quad (2)$$

Piezoelectric Properties

$$B_{\text{long}} = e^2/2c\epsilon \sim .02 \quad (2)$$

$$B_{\text{trans}} = e^2/2c\epsilon \sim .018$$

$$d_{33} = 3.2 \times 10^{-7} \text{ stat coul/dyne} \quad (6)$$

$$d_{31} = -1.1 \times 10^{-7} \text{ stat coul/dyne} \quad (6)$$

$$d_{15} = -4.3 \times 10^{-7} \text{ stat coul/dyne} \quad (6)$$

also see (7) for temperature dependence.

From Landolt-Börstein (1966) or Beyer (1969) p.46

$$d_{33} = 10.3 \times 10^{-12} \text{ coul/nt}$$

$$d_{31} = -5.2 \times 10^{-12} \text{ coul/nt}$$

$$d_{15} = -14.0 \times 10^{-12} \text{ coul/nt}$$

$$e_{33} = 0.49 \text{ coul/m}^2$$

$$e_{31} = 0.25 \text{ coul/m}^2$$

$$e_{15} = 0.21 \text{ coul/m}^2$$

APPENDIX E

A.P.L. Computer Programs

"RUNI" is the program that accepts the input data and initiates execution of the set of programs "CONTROL", "TWXA", "TWXB", "EXCHANGE", "PRINT" and "FUNCTION". Input data is entered as "RUNI V" where V is a vector whose six components have the following meaning:

$V_1 = \lambda$ = wavelength of light

$V_2 = \alpha_1$ = attenuation #1 in db per round trip

$V_3 = \alpha_2$ = attenuation #2 in db per round trip

$V_4 = d$ = thickness of sample in cm

$V_5 = \nu_1$ = frequency of α_1 in mHz

$V_6 = \nu_2$ = frequency of α_2 in mHz

After execution of the above set of programs, a vector W is printed whose components are:

$W_1 = \lambda$

$W_2 = y_1$ = reduced attenuation for α_1

$W_3 = y_2$ = reduced attenuation for α_2

$W_4 = (\nu_1 \zeta)^{-1}$

$W_5 = (x/d)$

W_6 = least squares error in the calculated data.

VRUN1[]V

```

V RUN1 DA
[1]  +(6=ρDA)/4
[2]  'INPUT VECTOR ERROR'
[3]  →0
[4]  THICK←DA[4]
[5]  B←4×08.686×DA[4]×0.02÷430000
[6]  FREQ←DA[5 6]×1000000
[7]  →3
[8]  ρ0
[9]  'INPUT DATA IS  WL,AT1,AT2,D,F1,F2 = ' ; 4 EFT DA
[10] ρ0
[11] CONTROL Y,FREQ
V

```

VFUNCTION[]V

```

V Y←X FUNCTION A
[1]  Y←÷((A÷X)*2)+*-X
[2]  Y←(A×Y×1--X)÷X
[3]  Y←((-3)○Y)÷X
V

```

VEXCHANGE[]V

```

V EXCHANGE
[1]  G←÷G
[2]  A←Y1
[3]  Y1←Y2
[4]  Y2←A
[5]  FREQ[2 1]←FREQ[1 2]
V

```

VPRINT[]V

```

V PRINT P
[1]  4 EFT P[1 2 3 4],(P[5]÷FREQ[1]),(P[6]÷THICK),P[7]
V

```

▽CONTROL[]▽

```

▽ CONTROL DAT
[1]  Y1←DAT[1]
[2]  Y2←DAT[2]
[3]  G←DAT[4]÷DAT[3]
[4]  FREQ←DAT[3 4]
[5]  →(Y1=Y2)/E6
[6]  →(G>1)/E1
[7]  →(Y1>Y2)/E2
[8]  EXCHANGE
[9]  →E4
[10] E2:→(Y2>Y1×G)/E3
[11] →(Y2<Y1×G÷10)/EN
[12] 'A < 1 AND X < 30'
[13] PRINT Y1,Y2, 0 0 0 0 0
[14] →0
[15] E3:'TWXA'
[16] PRINT TWXA Y1,Y2,FREQ
[17] EXCHANGE
[18] 'TWXA'
[19] PRINT TWXA Y1,Y2,FREQ
[20] →0
[21] E1:→(Y1>Y2)/E4
[22] EXCHANGE
[23] →E2
[24] E4:→(Y2>Y1÷G)/E5
[25] →(Y2<Y1÷G×10)/EN
[26] 'X < A = ' ;÷Y1
[27] PRINT Y1,Y2, 0 0 ,(÷Y1), 0 0
[28] →0
[29] E5:'TWXB'
[30] PRINT TWXB Y1,Y2,FREQ
[31] EXCHANGE
[32] 'TWXB'
[33] PRINT TWXB Y1,Y2,FREQ
[34] →0
[35] E6:PRINT Y1,Y2, 0 0 0 ,(0÷2×Y1),0
[36] →0
[37] EN:'NO SOLUTION'
[38] PRINT Y1,Y2, 0 0 0 0 0

```

▽

▽TWXA[□]▽

```

▽ R←TWXA DATA
[1]  Y1←DATA[1]
[2]  Y2←DATA[2]
[3]  G←DATA[4]÷DATA[3]
[4]  C←10*(112)-9
[5]  D←10*7-112
[6]  SIGA←3
[7]  SIGX←3
[8]  DYT←1000
[9]  FF← 1 0
[10] J←2
[11] A←FL2←SAV1←SAV2←SCX←IC←CTX←Y1P←Y2P←0
[12] SAV2← 0 0 0 0
[13] SW2←1
[14] XS←0÷2×Y1[Y2
[15] X←D[J-1]
[16] E0:→(10>CTX←CTX+1)/EOA
[17] CTX←1
[18] →((ρD)>J+J+1)/EOA
[19] 'ERROR-XS'
[20] →END
[21] EOA:X←X-D[J]
[22] →(X>XS)/EO
[23] X←X+D[J]
[24] →(0<CTX←CTX-1)/X1
[25] CTX←9
[26] J←J-1
[27] X1:→(10>CTX←CTX+1)/X4
[28] X2:→((ρD)>J+J+1)/X2+3
[29] 'ERROR-J'
[30] →END
[31] X3:CTX←1
[32] X4:→(FF[1]=1)/X4+3
[33] X←X+D[J]
[34] →A0
[35] X←X-D[J]
[36] →A0
[37] X5:→(FL1^SW1)/X5+3
[38] →(SW1≠FF[1])/X6
[39] →X1
[40] Y2P←X FUNCTION A×G
[41] SAV1←((|⊙Y2P÷Y2)+|⊙Y1P÷Y1)÷|⊙Y2×Y1
[42] →(DYT≤SAV1)/X6
[43] DYT←SAV1
[44] SW2←0
[45] SAV2←Y1P,Y2P,A,X
[46] →X1

```

```

[47] X6:X←SAV2[4]
[48] →(SIGX≤SCX+SCX+1)/END
[49] →(1≠SW2+SW2+1)/X6+5
[50] →(CTX=1)/X3
[51] →X2
[52] →(2≠SW2)/X7
[53] FF[2 1]←FF[1 2]
[54] →X3
[55] X7:SW2←1
[56] →X2
[57] END:R←Y1,Y2,SAV2,DYT
[58] →0
[59] A0:SAV4←SCA←YT←CT←FL1←0
[60] I←SIGA
[61] A←C[I-1]
[62] □←X
[63] A1:→(10>CT←CT+1)/A3
[64] A2:CT←1
[65] →((pC)≥I←I+1)/A3
[66] SW1←0
[67] →AE
[68] A3:→(1000>IC←IC+1)/A3+3
[69] 'ERROR+IC'
[70] →END
[71] A←A+C[I]
[72] Y1P←X FUNCTION A
[73] →(Y1P≠Y1)/A4
[74] SW1←FL1←1
[75] →AE
[76] A4:→(Y1P>Y1)/A6
[77] FL1←1
[78] →(Y1P>YT)/A5
[79] SW1←0
[80] →AE
[81] A5:YT←Y1P
[82] SAV4←A
[83] →A1
[84] A6:SW1←1
[85] A←SAV4
[86] →(SIGA≤SCA←SCA+1)/AE
[87] I←I-2
[88] →A2
[89] AE:→X5

```

▽

VTWXB[] ▽

```

▽ R←TWXB DATA
[1]  Y1←DATA[1]
[2]  Y2←DATA[2]
[3]  G←DATA[4]÷DATA[3]
[4]  C←10*5-18
[5]  D←10*7-112
[6]  SIGA←3
[7]  SIGX←3
[8]  DYT←1000
[9]  FF← 1 0
[10] J←2
[11] A←FL2+SAV1+SAV2+SCX+IC+CTX+Y1P+Y2P+0
[12] SAV2← 0 0 0 0
[13] SW2←1
[14] XS←0÷2×Y1[Y2
[15] X←D[J-1]
[16] EO:→(10>CTX+CTX+1)/EOA
[17] CTX←1
[18] →((ρD)>J+J+1)/EOA
[19] 'ERROR-XS'
[20] →END
[21] EOA:X←X-D[J]
[22] →(X>XS)/EO
[23] X←X+D[J]
[24] →(0<CTX+CTX-1)/X1
[25] CTX←9
[26] J←J-1
[27] X1:→(10>CTX+CTX+1)/X4
[28] X2:→((ρD)>J+J+1)/X2+3
[29] 'ERROR-J'
[30] →END
[31] X3:CTX←1
[32] X4:→(FF[1]=1)/X4+3
[33] X←X+D[J]
[34] →A0
[35] X←X-D[J]
[36] →A0
[37] X5:→(FL1^SW1)/X5+3
[38] →(SW1*FF[1])/X6
[39] →X1
[40] Y2P←X FUNCTION A×G
[41] SAV1←((|⊗Y2P÷Y2)+|⊗Y1P÷Y1)÷|⊗Y2×Y1
[42] →(DYT≤SAV1)/X6
[43] DYT←SAV1
[44] SW2←0
[45] SAV2←Y1P,Y2P,A,X
[46] →X1

```

```

[47] X6: X+SAV2[4]
[48] →(SIGA≤SCX+SCX+1)/END
[49] →(1≠SW2+SW2+1)/X6+5
[50] →(CTX=1)/X3
[51] →X2
[52] →(2≠SW2)/X7
[53] FF[2 1]←FF[1 2]
[54] →X3
[55] X7: SW2←1
[56] →X2
[57] END: R←Y1, Y2, SAV2, DYT
[58] →0
[59] A0: SAV4←SCA+YT←CT←FL1←0
[60] I←2
[61] A←C[I-1]
[62] □←X
[63] A1: →(10>CT+CT+1)/A3
[64] A2: CT←1
[65] →((pC)≥I←I+1)/A3
[66] SW1←0
[67] →AE
[68] A3: →(1000>IC+IC+1)/A3+3
[69] 'ERROR+IC'
[70] →END
[71] A←A-C[I]
[72] Y1P←X FUNCTION A
[73] →(Y1P≠Y1)/A4
[74] SW1←FL1←1
[75] →AE
[76] A4: →(Y1P>Y1)/A6
[77] FL1←1
[78] →(Y1P>YT)/A5
[79] SW1←0
[80] →AE
[81] A5: YT←Y1P
[82] SAV4←A
[83] →A1
[84] A6: SW1←1
[85] A←SAV4
[86] →(SIGA≤SCA+SCA+1)/AE
[87] →A2
[88] AE: →X5

```

BIBLIOGRAPHY

1. Astrov, D. N., Baibakov, V.I., Pado, G.S. and Sysoev, L. A. (1964) Soviet Physics - Solid State 7, 524.
2. Beyer, R. T. and Letcher, S. V. (1969) "Physical Ultrasonics" (Academic Press, New York).
3. Carleton, H. R., Kroger, H. and Prohofsky, E. W. (1965) Proceedings of the IEEE 53, 1452
4. Collins, T. C., Euwema, R. N. and DeWitt, J. S. 1966 Proc. Int. Conference on Phys. of Semiconductors (KYOTO 1966) p. 15.
5. Crandall, R. (1967) J. Appl. Phys. 38, 5425
6. Eckstein S. G. (1964) J. Appl. Phys. 35, 2702
7. Greebe, C. A. A. J. (1963) Physics Letters 4, 45
8. Gross, E. F., Bancie-Grillot, M., Grillot, E. and Rasbirin, B. S. (1961) Optics and Spectroscopy (USA) 11, 43.
9. Hutson, A. R. (1960) Phys. Rev. Letters 4, 505.
10. Hutson, A. R. and White, D. L. (1961) J. Appl. Phys. 33, 40.
11. Hutson A. R., McFee, J. H. and White, D. L. (1961) Phys. Rev. Letters 7, 237.

12. Kikuchi, Y., Chubachi, N. and Iinuma, K.
(1967) Jap. J. Appl. Phys. 6, 1251.
13. Kumar, C. S. and Hutchinson, W. G. (1969)
J. Appl. Phys. 40, 4687.
14. Kyame, J. J. (1948) J. Acoust. Soc. Am. 21, 159.
15. Kyame, J. J. (1954) J. Acoust. Soc. Am. 26, 990
16. Many, A., Goldstein, Y. and Grover, N. B. (1965)
"Semiconductor Surfaces" (North-Holland
Publishing Co. Amsterdam)
17. McFee, J. H. (1962) J. Appl. Phys. 34, 1548
18. McFee, J. H. (1966) "Physical Acoustics" Vol. IVA
(Academic Press, New York)
19. Michenand, J. P. and Luyckx, A. (1964)
"Proceedings of the 7th Int. Conf. on the Phys.
of Semiconductors Paris 1964" (DUNOD, Paris).
20. Mikoshiba, N. (1960) J. Phys. Soc. Jap. 15, 982.
21. Mort, J. and Spear, W. E. (1962) Phys. Rev.
Letters 5, 32.
22. Nine, H. D. (1960) Phys. Rev. Letters 4, 359
23. Nine, H. D. and Truell, R. (1961) Phys. Rev.
123, 799.
24. Pado, G. S., Kobayakov, I. B. and Sysoev, L. A.
(1969) Soviet Phys. - Solid State 11, 376.

25. Paranjape, B. V. (1963) Physics Letters 5, 32.
26. Parmenter, R. H. (1952) Phys. Rev. 89, 990.
27. Pippard, A. B. (1963) Phil. Mag. (GB) 8, 161.
28. Pomerantz, M. (1965) Proceedings of the IEEE 53, 1438.
29. Ray, B. (1969) "II-VI Compounds" (Pergamon Press)
30. Reynolds, D. C., Litton, C. W. and Collins, T. C. (1965) Phys. Stat. Sol. 9, 645 and phys. stat. sol. 12, 3.
31. Rose, A. (1963) "Concepts in Photoconductivity and Allied Problems" (Interscience Publishers, John Wiley & Sons, New York).
32. Ryvkin, S. M. (1964) "Photoelectric Effects in Semiconductors" (Consultants Bureau, New York).
33. Sandomirskii, V. B. and Kogan, Sh. M. (1963) Soviet Physics - Solid State 5, 1383.
34. Smith, R. W. (1962) Phys. Rev. Letters 9, 87.
35. Southgate, P. D. and Spector, H. N. (1965) J. Appl. Phys. 36, 3728.
36. Spector, H. N. (1962) Phys. Rev. 127, 1962.
37. Spector, H. N. (1964) Phil. Mag. (GB) 9, 1057.
38. Thomas, D. G., Hopfield, J. J. and Power, M. (1960) Phys. Rev. 119, 570.
39. Truell, R., Elbaum, C. and Granato, A. (1964) J. Appl. Phys. 35, 1483.

40. Truett, R., Elbaum, C. and Chick, B. B. (1969)
"Ultrasonic Methods in Solid State Physics"
(Academic Press, New York).
41. Uchida, I., Ishiguro, T., Sasaki, Y. and
Suzuki, T. (1964) J. of the Physical Soc. of
Jap. 19, 674.
42. Wang, W. (1962) Phys. Rev. Letters 9, 443.
43. Weinreich, G. (1956) Phys. Rev. 104, 321.
44. Weinreich, G., Sanders, T. M. and White H. G.
(1958) Phys. Rev. 114, 33.
45. White, D. L. (1962) J. Appl. Phys. 33, 2547.
46. Wolf, Helmut, F. (1969) "Silicon Semiconductor
Data" (Pergamon Press) p.6.
47. Zemon, S., Wasko, J. H., Hope, L. L., and
Zucker, J. (1967) Appl. Phys. Letters 11, 40.
48. Hutson, A. R. (1962) Phys. Rev. Letters 9, 296.
49. Hemmat, N. and Weinstein, M. (1967) J. Electro-
chem. Soc. - Solid State Sci. 114, 851.
50. Landolt-Börnstein (1966) "Elastic, Piezoelectric
Piezo-Optic and Electro-Optic constants" New Ser. B,
Group III, Vol. 1 Springer Berlin